MULTIUSER DETECTION FOR MULTICARRIER COMMUNICATION SYSTEMS

by

SAMER L HIJAZI

B.S., The University of Jordan, 2000

M.S., South Dakota State University, 2002

AN ABSTRACT OF A DISSERTATION

Submitted in partial fulfillment of the

requirements for the degree

DOCTOR OF PHILOSOPHY

Department of Electrical and Computer Engineering

College of Engineering

KANSAS STATE UNIVERSITY

Manhattan, Kansas

2006

ABSTRACT

Wireless broadband communications is a rapidly growing industry. New enabling technologies such as multi-carrier code division multiple access (MC-CDMA) are shaping the future of wireless systems. However, research efforts in improving MC-CDMA receiver performance have received limited attention and there is a need for innovative receiver designs for next generation MC-CDMA. In this thesis, we propose novel multi-user detection (MUD) schemes to enhance the performance of both synchronous and asynchronous MC-CDMA. First, we adapt the ant colony optimization (ACO) approach to solve the optimal MUD problem in MC-CDMA systems. Our simulations indicate that the ACO based MUD converges to the optimal BER performance in relatively few iterations providing more that 95% savings in computational complexity.

Second, we propose a new MUD structure specifically for asynchronous MC-CDMA. Previously proposed MUDs for asynchronous MC-CDMA perform the detection for one user (desired user) at a time, mandating multiple runs of the algorithm to detect all users' symbols. In this thesis, for the first time we present a MUD structure that detects all users' symbols simultaneously in one run by extending the receiver's integration window to capture the energy scattered in two consecutive symbol durations. We derive the optimal, decorrelator and minimum mean square error (MMSE) MUD for the extended window case. Our simulations demonstrate that the proposed MUD structures not only perform similar to a MUD that detects one user at a time, but its computational complexity is significantly lower. Finally, we extend the MUD ideas to multicarrier implementation of single carrier systems. Specifically, we employ the novel MUD structure as a multi-symbol detection scheme in CI-CDMA and illustrate the resulting performance gain via simulations.

MULTIUSER DETECTION FOR MULTICARRIER COMMUNICATION SYSTEMS

by

SAMER L HIJAZI

B.S., The University of Jordan, 2000

M.S., South Dakota State University, 2002

A DISSERTATION

Submitted in partial fulfillment of the

requirements for the degree

DOCTOR OF PHILOSOPHY

Department of Electrical and Computer Engineering

College of Engineering

KANSAS STATE UNIVERSITY

Manhattan, Kansas

2006

Approved by:

Major Professor

Dr. Balasubramaniam Natarajan

ABSTRACT

Wireless broadband communications is a rapidly growing industry. New enabling technologies such as multi-carrier code division multiple access (MC-CDMA) are shaping the future of wireless systems. However, research efforts in improving MC-CDMA receiver performance have received limited attention and there is a need for innovative receiver designs for next generation MC-CDMA. In this thesis, we propose novel multi-user detection (MUD) schemes to enhance the performance of both synchronous and asynchronous MC-CDMA. First, we adapt the ant colony optimization (ACO) approach to solve the optimal MUD problem in MC-CDMA systems. Our simulations indicate that the ACO based MUD converges to the optimal BER performance in relatively few iterations providing more that 95% savings in computational complexity.

Second, we propose a new MUD structure specifically for asynchronous MC-CDMA. Previously proposed MUDs for asynchronous MC-CDMA perform the detection for one user (desired user) at a time, mandating multiple runs of the algorithm to detect all users' symbols. In this thesis, for the first time we present a MUD structure that detects all users' symbols simultaneously in one run by extending the receiver's integration window to capture the energy scattered in two consecutive symbol durations. We derive the optimal, decorrelator and minimum mean square error (MMSE) MUD for the extended window case. Our simulations demonstrate that the proposed MUD structures not only perform similar to a MUD that detects one user at a time, but its computational complexity is significantly lower. Finally, we extend the MUD ideas to multicarrier implementation of single carrier systems. Specifically, we employ the novel MUD structure as a multi-symbol detection scheme in CI-CDMA and illustrate the resulting performance gain via simulations.

DEDICATION

To my parents

Contents

List of Figures

Glossary

Operators and Transformations

argmax$\{\cdot\}$ argument maximizing the expression in brackets

argmin$\{\cdot\}$ argument minimizing the expression in brackets

exp the exponent operator

diag$(\cdot)$ diagonal matrix with elements equal to the entries of a vector argument or the columns of a matrix argument, respectively

det$(\cdot)$ determinant of a matrix mod modulo operation

tr$(\cdot)$ trace of a matrix

$E(\cdot)$ expectation

Pr$(\cdot)$ unconditional probability

Pr$(\cdot|\cdot)$ conditional probability

$\mathfrak{Re}\{\cdot\}$ real part of a complex number

$\mathfrak{Im}\{\cdot\}$ imaginary part of a complex number

$(\cdot)^H$ Hermitian transposition

$(\cdot)^T$ transposition

$(\bar{\cdot})$ complex conjugation

$(\cdot)^{-1}$ inversion operation

$\odot$ matrices element wise multiplication

$\mathbb{R}$ the real number set

$\mathbb{I}$ the integer number set

$\mathbb{C}$ the complex number set

Constants

j imaginary unit

π the number pi $\pi = 3.14159265358979\ldots$

e Euler number $e = 2.718281828\ldots$

Variables

g path counter

n subcarrier counter

k user counter

h_n channel fading on n^{th} subcarrier

$\mathfrak{F}$ Fourier transform operation

$\mathbf{h}$ channel fading vector $h = [h_1, h_2, \cdots h_N]$

α_g g^{th} path fading

δ the impulse function

f_c center frequency

K number of users

P_I interference power

G_{SS} spreading gain

N number of subcarriers

N_p Number of paths

b_k the k^{th} user symbol

$\mathbf{b}$ user symbols' vector

$\mathbf{r}$ matched filter output vector

$c_{k,n}$ the n^{th} element of the k^{th} user spreading code $\mathbf{c}_k$

Δf channel spacing

t time

T_b symbol duration

T_s OFDM symbol duration

ρ_f frequency correlation coefficient

ρ_t time correlation coefficient

$\mathbf{n}$ noise victor

$\widetilde{\mathbf{C}}$ channel adjusted spreading matrix

R is a $K \times K$ cross-correlation matrix of the user's spreading sequences

A power control matrix

ACKNOWLEDGMENTS

I wish to convey warmest thanks to my parents; Lutfi Hijazi and Houria Zedan, who have given me endless support, and provided me with the opportunity to reach this far with my studies.

I wish to thank my Advisor Dr. Bala Natarajan whose enthusiasm, encouragement, and guidance made this work possible.

I also thank Dr. Carl Nassar of the Department of Electrical Engineering at Colorado State University for his guidance and input, especially at the beginning of this project.

Much thanks also goes to Dr. Sanjoy Das, for our invaluable discussions on ant colony optimization.

I am grateful to all of my committee members for their guidance and support.

I would also like to thank my colleagues in the WiCom group for their support as friends and office-mates.

I also would like to thank the faculty and staff of the Electrical and Computer Engineering Department at Kansas State University for their kind help.

Chapter 1

Introduction

Wireless communications has been one of the fastest growing fields in the past several years. This growth has been primarily driven by the huge demand for mobile phones and wireless local area networks (WLAN). It is forecasted that in future generation wireless networks (4G and beyond), a convergence of mobile phone technology, computing, internet access, and potentially many other multimedia applications will occur. Hence, an increase in the available spectrum and better spectral efficiency is mandatory to support the demand for new applications and services [1]. Multicarrier code division multiple access (MC-CDMA), the focus of this thesis, is a potential candidate for the physical layer of 4G mobile systems. In this thesis, we present techniques for improving the spectral efficiency of MC-CDMA systems via the design of advanced receiver structures.

This chapter is organized as follows. In Section 1.1, we provide an introduction to wireless communication systems. Section 1.2 contains a brief survey and background of an advanced reception technique called multi-user detection. Section 1.3 outlines the motivation for this research. Finally, section 1.4 highlights the key contributions of this thesis.

1.1 Wireless Communication Systems

In the past decade, a dramatic increase in demand on wireless communication services has been observed. For example, from year 1994 to year 2004, the number of cellular users has increased by a factor of ten. This trend is expected to continue for the next decade. Moreover, it is forecasted that in the next few years users' thirst for non-voice applications will drive the demand for faster and more reliable wireless communication services. Specifically, the increasing demand on voice and multimedia communications mandates future generation wireless systems to support transmission rates up to several Mbps and to accommodate a large number of users. In order to meet this goal, innovations in technology are imperative. We discuss some of the promising enabling technologies that are in use currently and could play a major role in the future.

1.1.1 Code Division Multiple Access

To accommodate the increase in demands on wireless services, future communication systems have to incorporate new technologies that support high capacity. In [2], [3], it has been shown that code division multiple access (CDMA) systems support higher information capacity over time division multiple access (TDMA) [4] and frequency division multiple access (FDMA) [5] systems. Moreover, it has been shown that CDMA based communication is more resilient to narrow band interference. For these reasons, CDMA has been incorporated in many wireless standards (e.g. universal mobile telecommunications system (UMTS) [6]-[7], CDMA2000 [8] and IS-95 [9]) over the past decade, and is considered to be the enabling technology for future 3GPP2 standards [10].

In CDMA, every communicator will be allocated the entire spectrum all of the time [11]. Unlike FDMA or TDMA, CDMA uses codes to identify users. This situation can be compared with many people in one room talking at the same time in different languages. If one dedicated language is known, it is possible to listen to the speaker with only minor distraction from other

speakers. If more people would speak in the same language, it would be more complicated or even impossible to listen to one individual. Therefore, in CDMA all users' information are present over the entire bandwidth all the time. To do so, each user is assigned a unique spreading code. When spreading is performed in time domain via direct multiplication of the transmitted symbols with a spreading sequences, the resultant communication system is referred to as direct sequence CDMA (DS-CDMA).

1.1.2 Orthogonal Frequency Division Multiplexing

In the past few years, several protocols have been developed such as IEEE802.11a, IEEE802.11g [**?**], IEEE 802.16a/d/e [**?**]-[**?**], DAB [12], and DVB [13] that are based on orthogonal frequency division multiplexing (OFDM) [14]- [17]. OFDM is a multi-carrier transmission technique that has been recently recognized as an excellent method for high speed wireless data communication. OFDM's history dates back to the 1960s, but it has recently surfaced and become popular because integrated circuits that can perform the high speed digital operations necessary have become available. OFDM effectively squeezes multiple modulated carriers tightly together, reducing the required bandwidth but keeping the modulated signals orthogonal so they do not interfere with each other. The increasing interest in OFDM based communications has been driven by OFDM's resilience to inter-symbol interference in multipath channels. Conventional single carrier systems like TDMA and DS-CDMA require a large bandwidth, making them more susceptible to frequency-selective fading. In other words, dealing with high data rates forces single carrier systems to operate with short pulse/chip duration which leads to severe inter-pulse/chip interference.

1.1.3 Enabling 4G: Multicarrier-CDMA

The commercial rollout of 4G systems is likely to begin around 2008 - 2012 [18], to replace current networks. It is widely believed that 4G will aim to extend the capabilities of 3G networks to allow a greater range of applications and improved universal access. Ultimately 4G

networks should encompass all current wireless applications such as broadband wireless services, high definition television (HDTV) and electronics interconnectivity. However, to realize this application, cost of service must be reduced significantly from its current threshold. For this reason, one of the main focuses of 4G researchers is to significantly improve spectral efficiency.

Recently, a novel transmission technique combining DS-CDMA and OFDM has been proposed. This technique is known as Multicarrier-CDMA (MC-CDMA) [19]. Specifically, like the more popular DS-CDMA, MC-CDMA users' data coexists in the same frequency-band simultaneously. While DS-CDMA spreads users' data in time by modulating each user symbol with a high-rate spreading sequences, MC-CDMA spreads its users' symbols by transmitting each user's data on multiple subcarriers simultaneously, spanning a large bandwidth. To facilitate the separability of transmitted symbols in MC-CDMA, each user's symbol is encoded with a unique spreading code that enables the receiver to distinguish different users' symbols. The main advantage of using MC-CDMA over DS-CDMA, is that while a DS-CDMA receiver (e.g., RAKE receiver [20]) processes the received signal in the time domain, an MC-CDMA receiver operates in the frequency domain. while the time domain and frequency domain processing provides similar performance in AWGN channel [17], in [19] the authors show that processing in the frequency domain is preferable over processing in the time domain for multipath channels. Specifically, in a multipath channel, to exploit path diversity, a RAKE receiver (i.e., a receiver uses several baseband correlators to individually process several signal multipath components) is required. As the number of paths increases, the RAKE receiver needs more taps to harness the energy scattered in time. On the other hand, processing in the frequency domain enables the receiver to effectively recover the scattered energy without any increase in receiver complexity. For this reason, [21] proposes a multicarrier implementation for all single carrier systems. These features make MC-CDMA a prime candidate for next generation wireless systems.

1.2 Multiuser Detection

Detecting the transmitted symbols in a CDMA system depends on the channel over which the communication system is operating. For example, for a system transmitting over an additive white Gaussian noise (AWGN) channel, a simple matched filter bank represents the optimal reception technique (in terms of performance) if orthogonal spreading sequences are considered [22], [23]. However, in a multipath channel, the channel destroys orthogonality among symbols. As a result, the estimate of any transmitted symbol (assuming linear estimation) suffers interference from other users' data symbols. In other words, the k^{th} user's matched filter output is composed of both the k^{th} user's information and the interference from all other users, which is known as multi-user interference (MUI) [24]. Single-user receivers process the MUI as an additional noise term, and consequently, the presence of MUI degrades the BER performance of these receivers. Moreover, the MUI problem gets even more severe when asynchronous communications are considered. This is due to the fact that the MUI terms in asynchronous systems has contribution from three successive symbol periods rather than only one period in the synchronous case. Therefore, there is a need for more sophisticated receivers to overcome these limitations.

In 1984, Verdu [22] introduced multi-user detection (MUD) for CDMA systems as a solution to the limitations introduced by MUI. Unlike single-user receivers [25], MUD-based receivers exploit the MUI as additional information about the transmitted symbols [26]- [33] . Specifically, MUD detects all users' information symbols from the matched filters outputs simultaneously, reducing the effect of the interference caused by users' symbols on each another. Therefore, MUD significantly outperforms any single-user reception technique.

The maximum likelihood (ML) MUD offers the best BER performance among all reception techniques for CDMA systems, hence it is called the optimal MUD receiver [22]. The ML-MUD maximizes the joint probability by evaluating a maximum-likelihood function over the set of all possible users' symbol sequences, forming an NP-hard optimization problem. The optimal MUD has a computational complexity that is prohibitive for any practical implementation; this

is due to the fact that a MUD's complexity grows exponentially with the number of users. To overcome this constraint, several suboptimal techniques have been considered [22]-[34] [23]- [40]. During the search for simpler receiver strategies, suboptimum receivers applying merely linear interference suppression filters [41]-[42], [43] were devised first. Although, linear multi-user detectors outperform single user detectors, their performance is significantly inferior to the ML-MUD performance. Throughout the years, numerous more sophisticated receiver schemes have been proposed. For example, sphere decoding [23], lattice detection [44], and several iterative multiuser algorithms (for references see [14]). In these methods, the receivers performance either does not match the ML-MUD performance or do not converge to it with a feasible complexity. Recently, researchers have considered employing artificial intelligence techniques to create suboptimal MUDs [45], [34].

1.3 Motivation

While MUDs for DS-CDMA systems have been extensively researched, the amount of literature and research in the area of MUD for MC-CDMA is significantly lower. Since MC-CDMA is the front runner for 4G systems, there is a need to better investigate the MUD problem in MC-CDMA systems and to find new approaches to reduce the MUD's complexity without compromising its performance. Furthermore, the MUD problem for *asynchronous* MC-CDMA has not received any substantial treatment in the literature. Therefore, it is necessary to propose and analyze new ideas to simplify and improve the MUD performance for asynchronous MC-CDMA systems.

As discussed earlier, one of the key issues that deters the use of optimal MUD in both DS-CDMA and MC-CDMA is complexity. There is a need for novel low complexity implementation with close to optimal performance. One such approach is to use sphere decoding to reduce the search space and consequently reduce system' complexity [23]. However, in sphere decoding, the number of operations is polynomially related to the number of users while it is related

exponentially to radius. The radius is typically chosen to be proportional to the noise variance [23]. Therefore, complexity of sphere decoding grows exponentially as noise increases (SNR decreases). Recently, evolutionary algorithms has been proposed to solve the MUD problem in DS-CDMA [46]- [48]. However, the GA based MUD suffers from strong dependance on the initial decisions, high computation complexity along with a slow convergence to a near-optimum solution.

Nature inspired optimization techniques (e.g., genetic algorithms (GA) [49], evolutionary programming [50], particle swarm optimization [51], and ant colony optimization [52]) have been shown to be an effective approach for solving complex problems. Ant colony optimization (ACO) is a relatively new member of the swarm intelligence optimization family that has been proposed by Dorego. ACO is based on the foraging behavior of ants [52]. In [53], it has been shown that ACO has the ability to outperform other nature-inspired optimization methods in solving NP-complete optimization problems, such as the traveling salesman problem. In this dissertation, for the first time, we highlight the ability of ACO in solving the MUD problem. We design and analyze a low complexity near-optimal MUD utilizing ACO for DS and MC-CDMA systems [34], [48], [46], [47], [54].

The complexity issue involved in MUD design in general forces its implementation to be restricted to the base station. As a result, one has to consider the asynchronous uplink in MUD design. In asynchronous setting, users' lack of alignment complicates the MC-CDMA receiver's design by increasing the amount of interference experienced by each user. Consequently, this misalignment significantly degrades receiver's BER performance. Previously proposed MUDs ([55]-[56]) for asynchronous MC-CDMA perform the detection for one user (desired user) at a time. Consequently, multiple runs of the algorithm are necessary to detect all users' symbols. There is a need for a one-shot MUD that detects all users simultaneously. In this dissertation, we present a MUD structure that detects all users' symbols simultaneously in one run by extending the receiver's integration window to capture the energy scattered in two consecutive OFDM block durations [54].

1.3.1 Key Contributions

The key contributions of this dissertation are summarized in this section.

In Chapter 4, we adopt the ACO algorithm to solve the optimal MUD problem. We present a novel low complexity algorithm that employs ACO to implement an optimal MUD for synchronous DS-CDMA and MC-CDMA up-links. This analysis yields the following important findings:

- To the best of authors' knowledge, this is the first attempt to apply swarm intelligence to MUD design.
- Our novel ACO based MUD for DS-CDMA systems converges to the optimal BER performance in relatively few iterations providing 95% saving in computational complexity.
- The reduction in complexity is retained even while considering users with unequal received powers. It is also interesting to note that the ACO based MUD significantly outperforms GA-assisted MUDs and is far less complex to implement.
- In MC-CDMA systems, our ACO-based MUD matches the BER performance of the optimal MUD with more than 98% savings in terms of computational complexity with respect to the exhaustive search approach.
- We demonstrate that we can decrease the number of iterations in the ACO by a factor of four and only suffer a 1 dB performance loss relative to the optimal MUD.
- The ACO based receiver is a step towards realizing the dream of implementing an optimal low-complexity MUD.
- Unlike the sphere decoding MUD approach, ACO based MUD complexity is not a function received SNR.

We next investigate the MUD problem in asynchronous MC-CDMA systems in Chapter 5. Here, we present a novel MUD structure that detects all users' symbols simultaneously by

extending the receiver's integration window to capture the energy scattered in two consecutive symbol durations. We then derive the optimal, decorrelator and minimum mean square error(MMSE) MUD for the extended window setting. The key findings from this research include:

- The presented novel MUD for asynchronous MC-CDMA detects all users' symbols simultaneously in one run.
- The proposed MUD for asynchronous structure is based on extending the observation time of the receiver to $2T_s$.
- The extension of the integration window enables the receiver to fully recover the i^{th} symbols' energy for all users (i.e., unlike prior work, the proposed MUD for asynchronous MC-CDMA is not limited to a desired user scenario and detects all users' symbols simultaneously).
- Our simulations demonstrate that the proposed structure is capable of reducing the computational complexity at the receiver while providing a comparable BER performance to that of a MUD employing a single T_s observation window.

While it is evident that extending the observation window (Chapter 5) reduces complexity, it degrades the performance of the linear multiuser detectors. Hence, in Chapter 6, we propose new methods to improve the performance of linear MUDs for the extended observation window setting. Here, our key contributions are:

- We present modified linear receivers for the extended observation window setting. Specifically, we analyze and adjust the decorrelator detector of Section 6.1 to better exploit the additional information made available by extending the observation window.
- The proposed adjustment have been shown capable of improving the Decorrelator MUD BER performance significantly (e.g., $5dB$ improvement at BER of 10^{-2}).

- We present a simplified MMSE-MUD that reduce the complexity of the MMSE MUD presented in 6.3 by 57% saving of the computation complexity of the MMSE-MUD of Section 5.3.3 without any degradation in its performance.

Finally, in Chapter 7, we propose a new multi-carrier platform to optimize the efficiency of wireless operators' licensed bands *and* to enable flexible sharing of licensed and unlicensed bands (in different spectral regions). The key contributions of this chapter are:

- This research supports a recent FCC proposal which goes beyond suggesting improved spectral efficiency, and instead suggests innovative spectrum management regulations.
- This work presents a multi-carrier platform capable of
  - achieving high spectral efficiency by application of "narrow" orthogonal carriers;
  - enables flexible spectral sharing across different licensed and unlicensed bands via operator borrowing/lending.
- We suggest a carrier interferomitry (CI) based multi-carrier platform to meet the new spectral policy requirements.
- Using CI-based DS-CDMA (CI-CDMA) as an example we demonstrate the ability of the proposed multi-carrier platform to:
  - provide high spectral efficiency (i.e., large bit/s/Hz) in each spectral band;
  - enable efficient sharing of wireless spectrum across different channels in the same band and/or across different bands;
  - maintain low interference among adjacent systems.
- We also present a comparative analysis (in terms of BER performance) of different spectral sharing strategies for CI-based wireless systems.

- For the first time, we apply the MUD idea to multicarrier implementation of single carrier systems incorporating the novel MUD schemes in Chapter 3 as a multi-symbol detection in CI-CDMA systems.

This dissertation is organized as follows; Initially we introduce multicarrier communication and MUD in Chapters 2 and 3. Then we present ACO and adapt it to solve the MUD problem in synchronous DS and MC-CDMA systems in Chapter 4. In Chapter 5, we extend our discussion to asynchronous MC-CDMA systems. Further discussion and analysis for the asynchronous MC-CDMA systems is presented in Chapter 6. Finally, we extend our analysis to multicarrier implementation of single carrier systems in Chapter 7.

Chapter 2

Introduction to OFDM and MC-CDMA

In this chapter, we start by presenting an overview of the commonly used multiple access techniques. Then, we describe the system model in an orthogonal frequency division multiplexing (OFDM) system and detail the motivation behind using this technology. Next, we introduce the spread spectrum counterpart of OFDM, namely, multi-carrier code division multiple access (MC-CDMA). We conclude the chapter with a detailed analysis of an MC-CDMA system.

2.1 Multiple Access Techniques

The technical differences and restrictions that apply to communication systems result from the fact that several transmitters and receivers want to simultaneously exchange different types of information in the same geographical region. Rules have to be found for different users to make sure that the desired information can be separated from the undesired information in the receiver (i.e., minimize the interference between the different users' data). Multiple access refers to any method which allows multiple users to share a common channel. In wireless communications, multiple access schemes allow multiple users to share the limited radio spectrum.

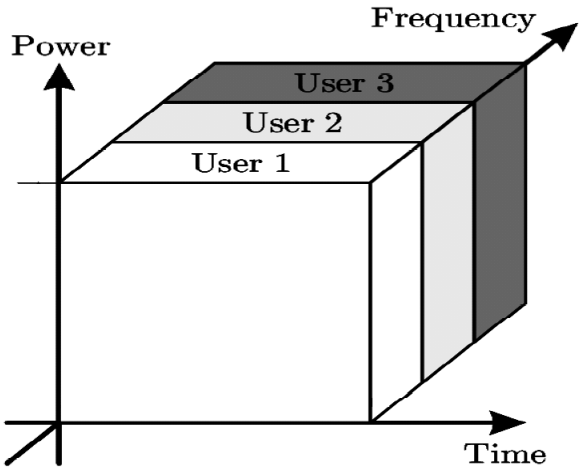

Figure 2.1: FDMA concept

2.1.1 Frequency Division Multiple Access (FDMA)

Figure 2.1 illustrates the idea of FDMA. In FDMA, signals from various users are separated in frequency and guard bands are maintained between adjacent signal spectra to minimize crosstalk between channels. FDMA was a widely used multiple access technique in analog communications; it is, for example, used in analog cellular telephones, where the different users are separated by using different carrier frequencies f_c in different frequency bands [5].

2.1.2 Time Division Multiple Access (TDMA)

TDMA systems divide the radio spectrum into time slots and in each slot only one user is allowed to either transmit or receive. This is shown in Figure 2.2. The concept of TDMA is analogous to the way in which a radio station schedules its broadcast period by assigning time slots for different programs. Each user in TDMA occupies a cyclically repeating time slot that reoccurs every frame, where K time slots comprise a frame. Consequently, to transmit the information of K users in a limited time-frame, the duration of each user symbol has to be decreased by a factor of $1/K$ when compared to users' sampling period. It is important to note that in TDMA, users buffer the information and send it out as a burst during their allotted time slot. Therefore, user transmission is not continuous. Hence, TDMA implementation is

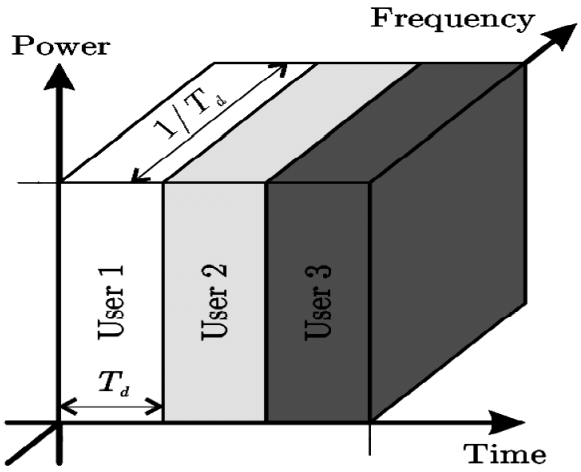

Figure 2.2: TDMA concept

possible only with digital communication [5].

2.1.3 Code Division Multiple Access (CDMA)

CDMA falls under the category of spread spectrum (SS) technology where signals have a transmission bandwidth much higher than the minimum required RF bandwidth [2]. Unlike FDMA or TDMA, in CDMA we separate the users by different spreading codes. In CDMA all users' information are present over the entire bandwidth (all the time as shown in Figure 2.3). To do so, each user is assigned a unique spreading code. These codes have to have low cross correlation (cross correlation is a measure estimating the degree to which two codes are correlated) so that different users can use the same frequency band, with their individual spreading code, without significantly interfering with each other.

The multiple access techniques described above all have one thing in common. To capture the desired information, the receiver has to have knowledge about how to find this information in the received signal. For example, in FDMA it is necessary to know the transmission band of the user of interest. In TDMA, it is necessary to know the start of the TDMA-frame and the position of the desired slot in the frame, to detect the transmitted symbol information. Similarly, in CDMA, it is necessary to know the code used to spread the desired information.

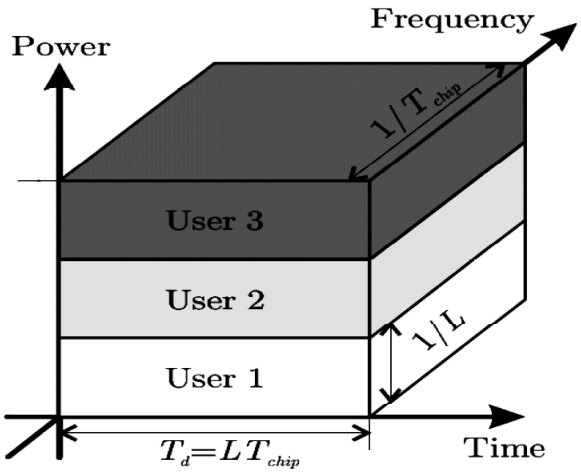

Figure 2.3: CDMA concept

One of the main criteria for choosing a certain type of multiple access technique is how reliable the transmitted information can be detected in the receiver. The reliability of recovering the transmitted data depends on how immune the transmitted signal is to effects that are imposed by the physical transmission channel. This fact grants SS modulation a critical advantage especially in fading channels. When a deep fade attenuates a portion of transmitted signal bandwidth, only a part of the transmitted energy will be affected. Additionally, a narrowband interferer with power P_I is spread by the receiver sequence and has only a resultant effective power of P_I/G_{SS} where G_{SS} is called the spread spectrum spreading gain. Consequently, a narrowband interferer is attenuated by 10 $\log(G_{SS})$dB. Furthermore, information theoretic analysis demonstrates that CDMA based systems offers higher capacity compared to FDMA and TDMA based systems [3]. For these reasons, CDMA based systems have gained a great deal of attention for the past decade [2].

2.2 Orthogonal Frequency Division Multiplexing

In wireless communication, the most harmful effect is the fading that results due to multipath propagation. Multipath fading is caused by signals reflected from trees, hills, building, people, cars, etc. These reflected signals arrive at the receiver at different times. The combi-

nation of these echoes results in fading and inter symbol interference. Depending of the signal wavelength and the geometry of the channel, this combination could be either constructive or destructive. Consequently, some frequency components of the transmitted signal are enhanced, while others are attenuated. This phenomenon is usually referred to in literature [5],[57] as the frequency selective nature of wireless channels. The frequency selective fading significantly degrades single-carrier system (e.g., direct sequence code division multiple access (DS-CDMA) and TDMA as it results in inter symbol interference in TDMA and inter-chip-interference in DS-CDMA) receivers' performance. Moreover, as the demand for fast wireless data communication increases, using single-carrier systems mandates very fast electronic circuits. For example, if we to use a DS-CDMA system to communicate data on a rate of $20Mbps$ with a spreading factor of 128, a real-time processing speed of $2.56Gbps$ is required. Such high processing (clocking) speed is currently impractical for any realizable implementation due to power consumption.

Orthogonal Frequency Division Multiplexing (OFDM) is a wideband modulation scheme that is designed to slow down clocking speed for the transmitter/receiver and cope with the multipath reception problems. For this reason, OFDM is the modulation scheme of choice for several communication standards (e.g., IEEE 802.11a/g, IEEE 802.15.3.a, IEEE 802.16a/d/e DVB and DAB).

OFDM divides a wideband frequency selective fading channel into many narrow-band subcarriers. If the number of subcarriers is large enough (or each subcarrier is narrow enough), each subcarrier could be considered experiencing flat fading (i.e., same fade over the subcarrier bandwidth). Specifically, as shown in Figure 2.4, an OFDM system utilizes many narrowband overlapping digital signals in parallel. This division of the overall bandwidth to a number of parallel transmission channels reduces the data rate on each individual subcarrier. This consequently reduces transmitter/receiver electronics' clock speed and facilitates high-data-rate communication. Moreover, the delay time of reflected echoes of transmitted waves can be suppressed to within one symbol duration simplifying the equalization scheme necessary to combat multipath effects.

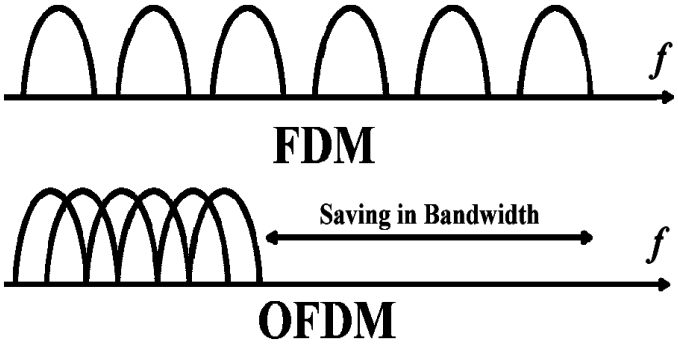

Figure 2.4: Comparison of FDM and OFDM spectrums, where B is the saving in bandwidth

In the next section, we retrace the major steps involved in the development of OFDM from the 1970's until today.

2.2.1 OFDM History

In January of 1970, A U.S. patent was issued addressing the use of parallel data streams and frequency division multiplexing (FDM) with overlapping subchannels to avoid complicated equalization and combat multipath distortion. This patent used the term multi-carrier modulation (MCM). The main distinction between OFDM and MCM is that each carrier in OFDM is orthogonal to all other carriers [58].

Figure 2.4 highlights the difference in bandwidth utilization between general FDM and OFDM. From the plot in Figures 2.4 and 2.5, it can be seen that the spectrum of OFDM signals is a superposition of sinc(.) functions with a frequency spacing equal to the transmission speed of each subcarrier. Consequently, at the center frequency of each subcarrier, there is no crosstalk from other subcarriers enabling the receiver to recover the transmitted data with no inter-carrier-interference (ICI). When MCM was first proposed, the generation of an array of sinusoids and coherent demodulators were required, which made building such a system unreasonably expensive and complex for large numbers of subcarriers. Furthermore, precise phasing of the demodulating carriers and sampling times was needed to keep crosstalk between subchannels acceptable at the receiver. In late 1971, Weinstein and Ebert proposed to use the

discrete Fourier transform (DFT) in MCM as part of the modulation and demodulation process to facilitate easy implementation of the systems [17]. This proposal eliminated the need for banks of subcarrier oscillators and filters and facilitated a completely digital implementation utilizing a fast Fourier transform (FFT) platform. Moreover, using the DFT-based modulation/demodulation technique, frequency division multiplexing is accomplished in the baseband eliminating the need for bandpass filtering.

It is not until the recent advances in VLSI technology that OFDM has become widely adopted in the communication industry. The presence of high-speed chips that can perform a large size FFT at an affordable price enables practical usage of the OFDM technology. In the 1980s, OFDM was studied for high-speed modems, digital mobile communications and high-density recording. Since the early 1990s OFDM was chosen to be the back bone for several high-data-rate communication standards such as high-speed digital subscriber lines (HDSL), asymmetric digital subscriber lines (ADSL), very high-speed digital subscriber lines (VHDSL), IEEE 802.11a/g, ETSI HIPERLAN/2, IEEE 802.15.3.a, IEEE 802.16a/d/e, Digital Video Broadcasting (DVB), Digital Audio Broadcasting (DAB) and the emerging IEEE 802.20 and IEEE 802.22 protocols.

2.2.2 OFDM Transmitter

Figure 2.6(a) illustrates the basic OFDM transmitter. From this figure, it can be seen that the high data rate stream of symbols is passed through serial to parallel converter resulting in a block of N low rate parallel data streams. This serial to parallel conversion increases the symbols' duration by a factor of N which provides robustness to the channel's delay spread. Each one of the low rate streams is then loaded onto a different subcarrier, and consequently, the baseband transmitted signal for a single OFDM block corresponds to

$$s(t) = \sum_{n=0}^{N-1} b_n exp(j2\pi n\Delta f t)p(t) \tag{2.1}$$

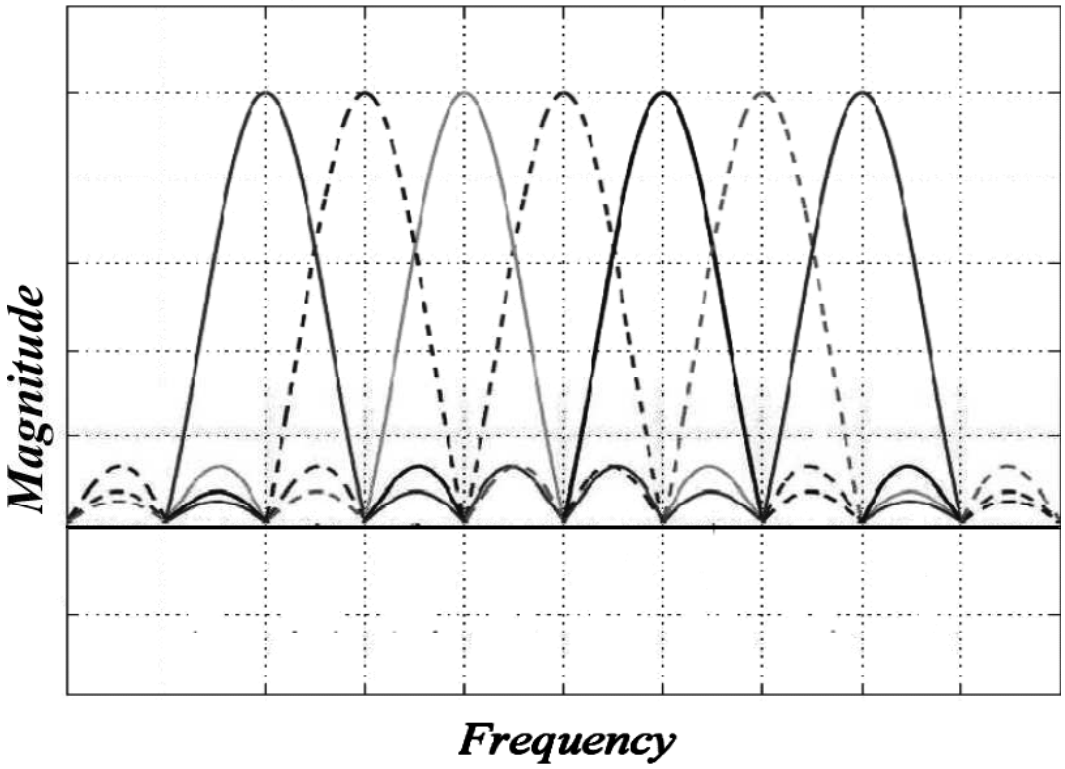

Figure 2.5: Spectra of OFDM signal

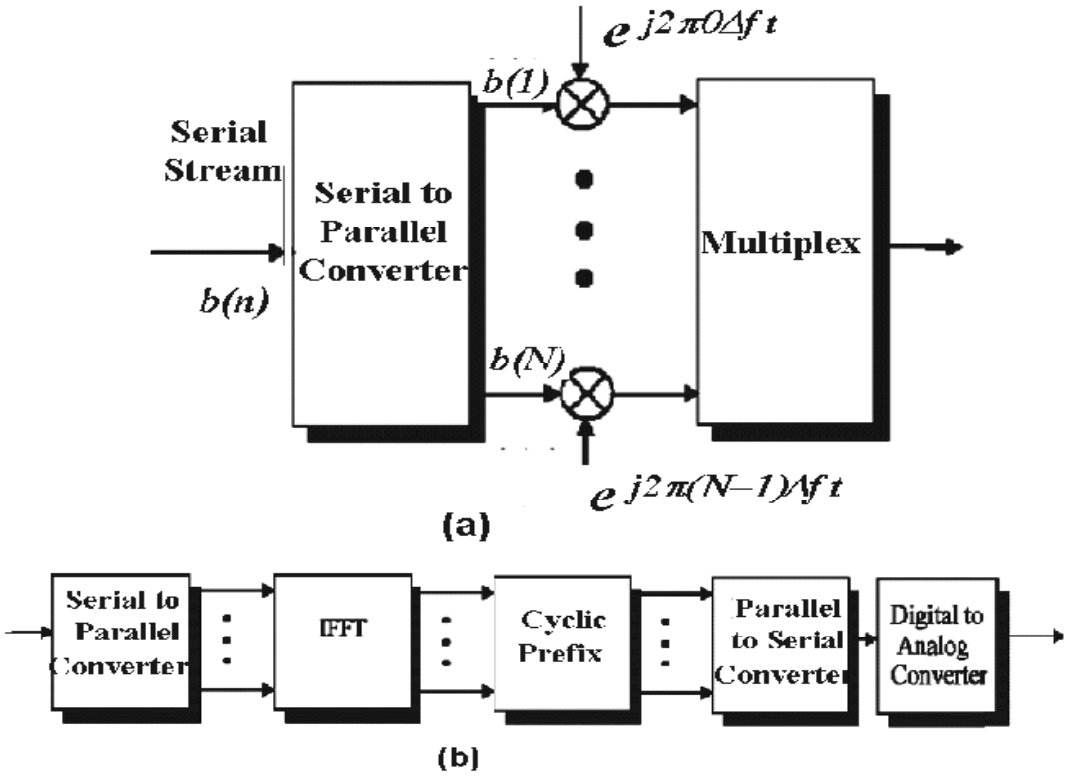

Figure 2.6: OFDM transmitter, (a) mixers' based design (b) IIFT based design

where b_n is the n^{th} data symbol of the OFDM block; N is the number of data symbols per OFDM block and is also equal to the number of subcarriers in the OFDM system. Typically, the signal in equation (2.1), with N data symbols, is referred to as an OFDM symbol. $p(t)$ is a pulse shaping function that time limits the signal to one OFDM-symbol duration, and Δf is the spacing between subcarriers. For the subcarriers to be orthogonal,

$$\Delta f = \frac{1}{T_s} = \frac{1}{N \cdot T_b}. \tag{2.2}$$

where T_b and T_s are the symbols' duration before and after the serial to parallel conversion, respectively.

The main difficulty in implementing the parallel data system as shown in Figure 2.6(a) is the complexity of the needed equipment. The complexity can be greatly reduced using the inverse discrete Fourier transform to implement the modulation process [14].

It can be easily shown that sampling equation (2.1) a rate of $1/T_b$ yields

$$\begin{aligned} s(kT_b) &= \sum_{n=0}^{N-1} b_n exp(\frac{j2\pi n(kT_b)}{NT_b}) p(kT_b) \\ &= \sum_{n=0}^{N-1} b_n exp(\frac{j2\pi nk}{N}) p(kT_b). \end{aligned} \tag{2.3}$$

Comparing this results with the the inverse discrete Fourier transform (IDFT) equation

$$x(k) = \sum_{n=0}^{N-1} X(n) exp(\frac{j2\pi nk}{N}) \tag{2.4}$$

shows that the sampled baseband transmitted OFDM signal is equivalent to the inverse discrete Fourier transform (IDFT) of the data symbols. The IDFT can in-turn be implemented using a inverse fast Fourier transform (IFFT) and algorithms. Figure 2.6(b) shows a simplified implementation of an OFDM transmitter using an IFFT engine.

To minimize the effects of inter-symbol-interference caused by the multipath nature of the channel, a guard time is introduced into the time domain sequence in the transmitter [17]. More details about the guard time are presented next

2.2.2.1 Cyclic Prefix in OFDM systems

As discussed earlier, one of the main reasons to use OFDM modulation is its resistance to multipath delay spread. Dividing the input data stream into N parallel streams extends the symbol duration by a factor of N. The extended symbol duration limits inter OFDM-symbol interference (ISI) caused by the multipath channel. To completely annihilate the ISI, a guard time is inserted in each OFDM symbol. The duration of the guard time (T_g) is chosen in accordance with the multipath characteristics of the channel.

This guard time could be made a silent period (i.e., zero energy to be wasted) but this silence would result in inter carrier interference (ICI); the multipath of the channel introduces delayed echoes of transmitted signal, if there is no integer number of cycles during the FFT interval, the orthogonality among different carriers is lost at the receiver. To avoid the creation of this ICI, a cyclic extension of the OFDM symbol is inserted in guard time. In this way, we

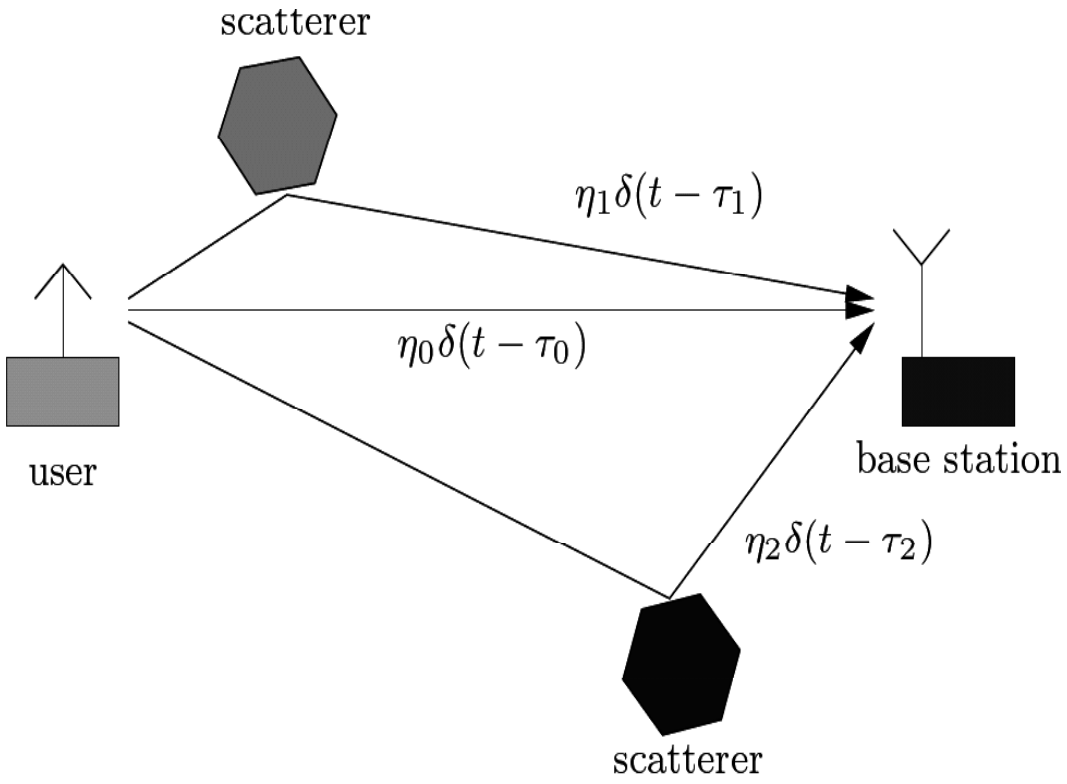

Figure 2.7: Wireless multipath propagation.

can be sure that the delayed echoes always have an integer number of cycles during the FFT interval. This kind of guard interval has been shown to have the same effects of zero padding in combating ISI without causing ICI [17]. The price to be paid is a signal to noise ratio loss in the form of energy wasted during the guard interval. For this reason, OFDM system designers always keep the guard time duration as short as possible.

2.2.3 Wireless Channel

Electromagnetic waves propagating from the transmitter's antenna arrive at the receiver's antenna via different paths. Figure 2.7 gives a simplified schematic representation of such a wireless multipath wave propagation scenario. Mathematically, the time variant channel impulse response of a multipath channel corresponds to [59]

$$h(t,\tau) = \sum_{g=0}^{N_p-1} \alpha_g(t,\tau) exp(j(2\pi f_c \tau_g(t) + \phi(t,\tau)))\delta(\tau - \tau_g(t)) \tag{2.5}$$

where N_p is the number of multipath components, $\alpha_g(t,\tau)$ is the amplitude component and $\tau_g(t)$ is the excess delay component caused by the g^{th} multipath component at time t and δ is the delta function. The term $j(2\pi f_c \tau_g(t) + \phi(t,\tau))$ represents a phase offset introduced on the g^{th} multipath component at time t. If the wireless channel is assumed to be slowly varying, its impulse response becomes time-invariant for several OFDM symbol durations. And the resulting channel impulse response model corresponds to [5]

$$h(\tau) = \sum_{g=0}^{N_p-1} \alpha_g(\tau) exp(j\phi_g)\delta(\tau - \tau_g) \tag{2.6}$$

where $\alpha_g(\tau)$ and ϕ_g is net attenuation and phase shift for each path. Equation (2.6) can be rewritten in Cartesian coordinates as

$$h(\tau) = \sum_{g=0}^{N_p-1} (x_g + jy_g)\delta(\tau - \tau_g) \tag{2.7}$$

where $\alpha_g = \sqrt{x_g^2 + y_g^2}$ and $\phi_g = \tan^{-1}\frac{y_g}{x_g}$. Assuming that the number of paths, N_p is large enough, the central limit theorem [60] implies that both x_g and y_g can be modeled as Gaussian random variables. As a result, the envelope of x_g and y_g, α_g, is distributed as a Rayleigh random variable and the phase, ϕ_g is distributed uniformly between 0 and 2π.

To model the multipath channel, we derive the autocorrelation function of the channel impulse response which is defined for wide-sense stationary channels as [48]

$$\begin{aligned} r_h(\Delta t, \tau_1, \tau_2) &= E\{h(t,\tau_1)h^*(t-\Delta t,\tau_2)\} &(2.8)\\ &= r_h(\Delta t,\tau_1)\delta(\tau_1 - \tau_2) &(2.9)\end{aligned}$$

where $E\{\}$ is the expectation operator; and $*$ is the conjugate operator. For $\Delta t = 0$, the corresponding autocorrelation function, $r_h(\tau)$, is defined as the multipath intensity profile of the channel. Since $r_h(\tau)$ yields the average power of the spectrum for delay values of τ, we define the rms delay spread, τ_{rms}, which is the largest value of τ where the multipath intensity profile exhibits a significant response [48].

Delay spreads in the time domain can be mapped to frequency correlation in the frequency

domain [5]via the spaced-time spaced-frequency correlation function. The spaced-time spaced-frequency correlation function is given by [48]

$$\begin{aligned} r_H(\Delta t, \Delta f) &= E\{h(t,f)h^*(t-\Delta t, f-\Delta f)\} \\ &= \underset{\tau \to \Delta f}{\mathcal{FT}} r_h(\Delta t, \tau) \end{aligned} \tag{2.10}$$

where $\underset{\tau \to \Delta f}{\mathcal{FT}}$ is the Fourier transform operation transforming delay, τ, to frequency Δf and $r_H(\Delta t, \Delta f)$ is the spaced-time spaced-frequency correlation function. The spaced-time spaced-frequency correlation function shows that correlation due to multiple paths translates to correlation in frequency. We define the coherence bandwidth, $(\Delta f)_c$, as the bandwidth where $r_H(0, \Delta f) = 0.5$. Based on this quantity, we also define the rank of the frequency diversity in the system as the ratio of total transmission bandwidth to coherence bandwidth. It can be shown that channel's coherence bandwidth is inversely related to rms delay spread.

The derivation of the spaced-time spaced-frequency correlation function from the channel autocorrelation function means that multipath propagation in time translates into frequency selectivity in the frequency domain. This fact can be understood as multipath echoes combines constructively or destructively. This constructive or destructive combination of the echoes' is a function of the transmitted signal wavelength. Hence, electromagnetic waves with frequencies that are close together suffer variations in their signal strength that are correlated. This correlation of fading versus frequency is measured by the coherence bandwidth. Hence, transmitted signal distortion (variation of signal's fading over its bandwidth) is minimized if the bandwidth is less than the coherence bandwidth of the channel, and this signal is called narrowband signal. On the other hand, a signal that occupies a wider bandwidth (i.e., greater than coherence bandwidth) will be subject to more distortion. However, it is important to keep in mind that if a signal bandwidth is significantly bigger than the channel's coherence bandwidth the variation in fading averages across signals bandwidth. This averaging is a result of the fact that different parts of the band suffer different levels of distortion (some frequencies are attenuated while others are amplified).

The variation of the multipath channel with time can be captured using the spaced-time

spaced-frequency correlation function given in equation (2.10). Specifically, the correlation in time is related to doppler spectrum $S_H(f_d)$ which is given by [57]

$$S_H(f_d, \Delta f = 0) = \underset{\Delta t \to f_d}{\mathcal{FT}} r_H(\Delta t, \Delta f = 0). \tag{2.11}$$

where f_d is the Doppler frequency. Similar to the spaced-time spaced-frequency correlation function, we utilize Doppler power spectrum to find a quantity known as the Doppler spread, B_D. The inverse of Doppler spread is used to calculate the coherence time, $(\Delta t)_c$ which is the amount of time for which we assume that the channel is significantly static. In our work, we assume a slow fading channel, i.e., the coherence time is large and the channel remains relatively constant for at least one OFDM symbol period.

Usually in OFDM systems, we choose carrier spacing $\Delta f = 1/T_s$ to be much smaller than channel's coherence bandwidth. This choice guarantees each subcarrier flat fading. We denote the channel's fading coefficients as $\mathbf{h} = [h_1, h_2, \cdots, h_N]^T$ (where $[\cdot]^T$ refers to the transpose operation, and h_n is the complex valued fading coefficient associated with the m^{th} subcarrier). The magnitudes of $\mathbf{h}$ are assumed to follow Rayleigh distribution. As discussed above, The elements of $\mathbf{h}$ vector exhibit correlation over time and across subcarriers.

2.2.4 OFDM Receiver

Assuming the OFDM transmitted signal in equation (2.1) is transmitted through the slowly varying multipath channel, the received signal in one OFDM block corresponds to

$$r(t) = \sum_{n=0}^{N-1} h_n b_n exp(j2\pi n \Delta f t) p(t) + n(t) \tag{2.12}$$

Figure 2.8(a) illustrates a conceptual OFDM receiver. At the receiver end, the received signal is first converted to baseband and then projected onto N orthogonal carriers. The signal on each subcarrier is integrated over the OFDM symbol period and each data symbol is then detected. This receiver structure is analogous to placing a matched filter receiver on every subcarrier.

Similar to the IFFT implementation of the OFDM transmitter, the OFDM receiver is implemented using discrete Fourier transform. Figure 2.8 shows OFDM receiver implementation.

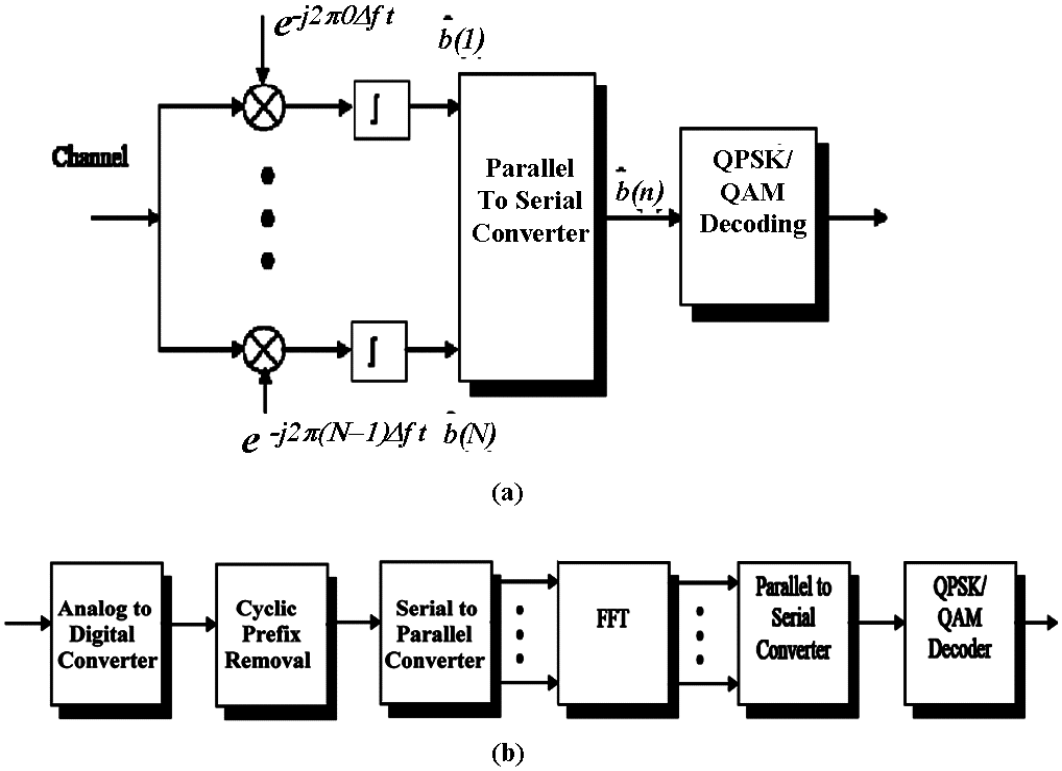

Figure 2.8: OFDM receiver

The discrete Fourier transform converts the received signal from the time domain into the frequency domain and projects each component onto its subcarrier. The FFT block outputs can be modeled as

$$\mathbf{r} = \mathbf{H}\mathbf{b} + \mathbf{n} \tag{2.13}$$

where, $\mathbf{r}$ is a vector of dimension $N \times 1$; $\mathbf{n}$ is a $N \times 1$ vector of additive white gaussian noise samples; and $\mathbf{H}$ is diagonal matrix were the diagonal quantities are the amplitudes of the $\mathbf{h}$ vector components. Here, we are assuming perfect phase synchronization (i.e., the channel phases are traced and removed perfectly). A single-tap equalizer can be used for each FFT output to remove the effects of the channel fade. Finally, a detection device selects the most probable choice of the transmitted data symbols ($\hat{b}_n$, $n = 1 \cdots N$). A parallel-to-serial conversion then restores the received data back into a serial stream ready to be processed.

As presented in Section 2.2.2, at the transmitter, a cyclic prefix was added to the transmission to mitigate the ISI effects. The receiver has to correctly remove the cyclic prefix samples prior to the DFT block.

2.2.5 OFDM Pros and Cons

The benefits of OFDM are:

- Compared to FDM, the overlapping spectra of subcarriers in OFDM yields better spectral utilization.
- OFDM systems are more robust to frequency selective fading channels.
- Because of dividing an entire channel bandwidth into many narrow subbands, the frequency response over each individual subband is relatively flat, and consequently, equalization is potentially simpler than in a serial data system. A simple equalization algorithm can minimize mean-square distortion on each subchannel, and the implementation of differential encoding may make it possible to avoid equalization altogether [61].

- By using a guard interval the sensitivity of the system to delay spread can be reduced [17].
- OFDM provides additional flexibility in transmission adaptation to varying channel conditions, by allowing modulation level and power adjustment for each symbol in a subcarrier [62].
- OFDM based system can easily accommodate multiple users by allocating different subcarriers to different users (OFDMA).

The main disadvantages of an OFDM system are:

- High sensitivity to carrier frequency offset; the offset in carrier frequency results in reducing desired symbol amplitude and introduces ICI. When comparing OFDM to a conventional single carrier system, it is in orders of magnitude more sensitive to frequency offset and Wiener phase noise [63]. This problem is expressed more in mobile applications, since a mobile channel has a time-varying nature. This offset causes the received frequency domain subcarriers to be shifted. The subcarriers are still mutually orthogonal, but the received data symbols, which were mapped to the OFDM spectrum, are in the wrong position in the demodulated spectrum, resulting in increased BER.
- Sensitivity to time-domain synchronization errors and sensitivity to phase noise: If the receiver's FFT window is shifted with respect to that of the transmitter, then at the receiver side, the timing misalignment introduces phase error between adjacent subcarriers. The influence of phase error on OFDM system depends on the modulation scheme;

    1. Coherent Modulation: In case of imperfect time synchronization, phase correction mechanisms are very crucial for coherent modulation.
    2. Pilot symbol assisted Modulation: Pilots are interspersed with the data symbols in the frequency domain and the receiver can estimate the evolving phase error from the received pilots' phases.

3. Deferential Modulation: Differential encoding can be implemented both between corresponding subcarriers of consecutive OFDM blocks or between adjacent subcarriers of the same OFDM block to alleviate the effect of phase error.

- Large peak to average power ratio (PAPR): The outputs of the IFFT block in the OFDM transmitter are nothing but a linear transformation of the input symbol stream. Regardless of the modulation scheme used to express the transmitted symbols, the maximum simple energy is very close to the average one. After performing the IFFT operation, the signal generally consists of a large sum of independently modulated subcarriers, then we might see large signal excursions resulting in a significant increase in the peak value while preserving the average level of the signal. For this reason, a large PAPR is observed. Consequently, every block following the IFFT chip has to have a wide dynamic range to avoid distorting the IFFT outputs. If any block's dynamic range is smaller than that necessary to preserve the IFFT output's integrity, a nonlinear distortion is observed. Therefore, an OFDM signal is very vulnerable to non-linear distortion caused by any nonlinear element in the system such as high power amplifiers. The effect of a nonlinearity on an OFDM signal can be seen from two different point of views. First, the large signal excursions occasionally reach the non-linear region of any non-linear element in the system (saturation point) and hence the non-linearity output is a distorted replica of the input. Second, any nonlinear element in the system introduces severe harmonic distortion and intermodulation distortion due to the multi-carrier nature of an OFDM signal. Harmonics that fall in-band, are associated with signal error probability degradation and the harmonics that fall out-of-band are associated with signal spectral spreading.

The above sections gave a brief introduction to OFDM and the importance of multicarrier techniques. Also, we outlined the advantages and challenges of OFDM systems. In the coming sections we will study the CDMA version of OFDM, namely MC-CDMA and discuss its advantages.

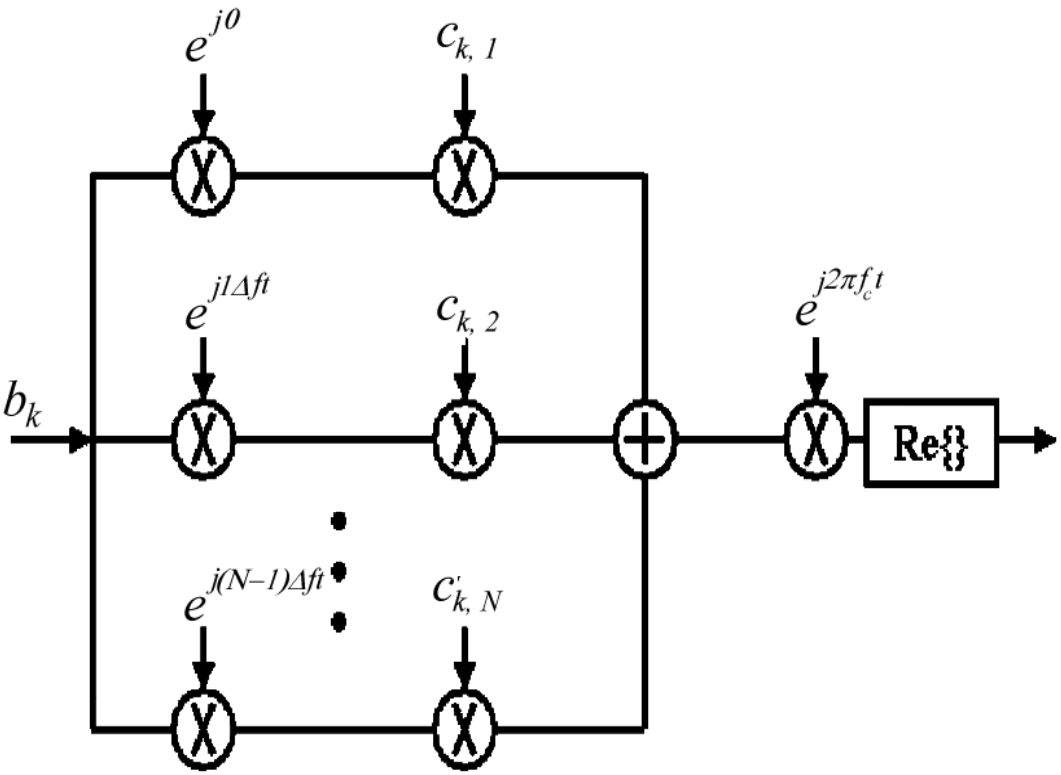

Figure 2.9: One user MC-CDMA transmitter

2.3 Multi-carrier Code Division Multiple Access (MC-CDMA)

In OFDM, the entire bandwidth is subdivided into several narrow-band channels operating at lower data rates enabling high data rate communication over extremely hostile wireless channels at a relatively low complexity. This transmission scheme combined with the SS technology, results in what is known as a MC-CDMA system.

In MC-CDMA, each data symbol is spread over multiple sub-carriers with a user-specific code. Each data-modulated chip of the spreading code is transmitted on different sub-carriers. Consequently, all users share the same frequency band, i.e., the same subcarriers, at the same time, as shown in Figure 2.10. Details of an MC-CDMA system is provided next.

2.3.1 MC-CDMA system model

2.3.1.1 MC-CDMA Transmitter

Figure 2.9, illustrates the MC-CDMA transmitter for user k. Here, the data symbols of user k during the i^{th} MC-CDMA-symbol b_k^i is transmitted on all N orthogonal subcarriers and multiplied by $c_{n,k}$, which is the spreading code element for the k^{th} user on the n^{th} subcarrier. The N signal components are then summed and converted to passband prior to transmission. The transmitted signal corresponding to the k^{th} user during the i^{th} MC-CDMA block is

$$s_k^i(t) = \Re e[\sum_{n=0}^{N-1} b_k^i c_{n,k} exp(j2\pi n\Delta f t) exp(j2\pi f_c t) p(t)] \tag{2.14}$$

where Δf is the spacing between carriers ($\Delta f = 1/T_s$ such that, T_s is the MC-CDMA-symbol duration); f_c is the carrier frequency, and $p(t)$ is a pulse shaping function that time limits the signal to one MC-CDMA-symbol duration.

2.3.1.2 Channel

Typical to OFDM-based systems, we choose $\Delta f = 1/T_s$ to be much smaller than channel's coherence bandwidth. We denote the channel's fading coefficients for the k^{th} user during the i^{th} symbol interval as $\mathbf{h}_k^i = [h_{k,n}^i, h_{k,2}^i, \cdots, h_{k,M}^i]^T$ (where $[\cdot]^T$ refers to the transpose operation, and $h_{k,m}^i$ is the complex valued fading coefficient associated with the n^{th} subcarrier). The magnitudes of $\mathbf{h}_k^i (k = 1, \ldots K)$ are assumed to follow Rayleigh distribution. For a given k, the elements of $\mathbf{h}_k^i$ vector exhibit correlation over time and across subcarriers, where the correlation coefficients in time and frequency are ρ_f and ρ_t , respectively. For an exponentially decaying multipath power delay profile with an rms delay spread τ_{rms}, the correlation between the p^{th} and q^{th} carrier fades $E[h_{k,p}^i h_{k,q}^i]$ is a function of the distance between their center frequencies (i.e., $|f_p - f_q| = |p - q|\Delta f = g\Delta f$, g is a positive integer. And $E[h_{k,p}^i h_{k,q}^i] = \rho_f(g)$ is given by [5]

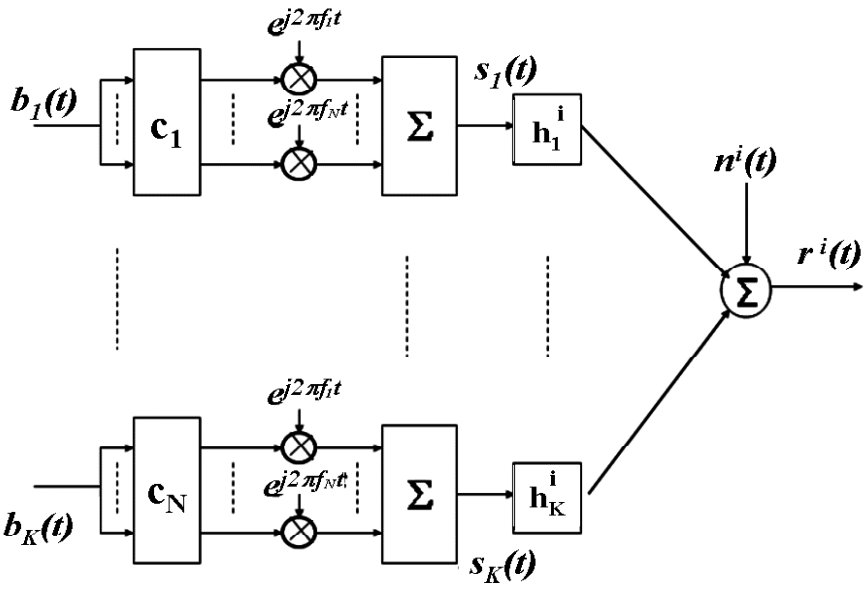

Figure 2.10: An uplink MC-CDMA system

$$\begin{aligned} \rho_f(g) &= \frac{1}{1 + j\pi\tau_{rms}|f_p - f_q|} \\ &= \frac{1}{1 + j\pi\tau_{rms}g/Ts} \end{aligned} \tag{2.15}$$

The time correlation between two OFDM/MC-CDMA blocks separated in time by $\Delta t = wT_s$, (where w is a positive integer) in a channel with maximum Doppler frequency f_{max} is given as [17]

$$\rho_t(\Delta t) = J_0(2\pi f_{max}\Delta t)$$

where $J_0(x)$ is the zeroth order Bessel function of the first kind. On the other hand, the $\mathbf{h}_k^i \ \forall \ k = 1, \ldots K)$ are assumed to be independent across different users (i.e., $E[\mathbf{h}_j^i \mathbf{h}_k^i] = 0 \ \forall \ j \neq k$).

2.3.1.3 MC-CDMA Receiver

The receiver reverses the operation of the transmitter as shown in Figure 2.11. The first step is to perform the FFT operation to transform the received signal to the frequency domain (i.e.,

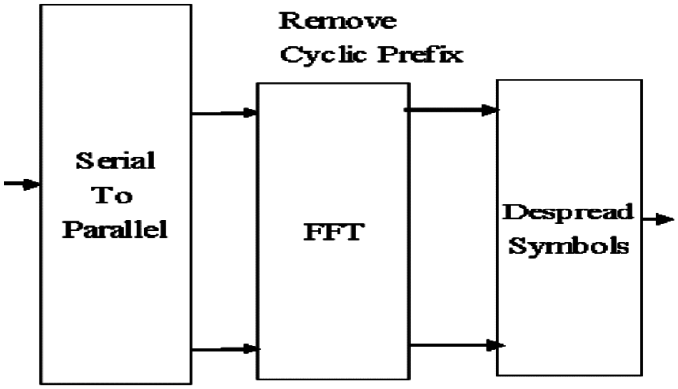

Figure 2.11: MC-CDMA receiver

extract the signal loaded on the various subcarriers). Hence, during the i^{th} OFDM symbol period, the k^{th} user received signal at the output of the FFT (in Figure 2.11) block can be represented as

$$\mathbf{r}_k^i = \mathbf{h}_k^i \odot \mathbf{c}_k b_k^i + \mathbf{n}_k^i \tag{2.16}$$

where, $\mathbf{r}_k^i$ is a vector of dimension $N \times 1$; the operator $(\odot)$ represents an element wise multiplication of two vectors, $\mathbf{c}_k$ is the k^{th} user spreading code, and $\mathbf{n}_k^i$ is a $N \times 1$ vector of additive white gaussian noise samples. Assuming perfect phase synchronization (i.e., the channel phases are traced and removed perfectly at the receiver), the received vector can be redefined as

$$\mathbf{r}_k^i = \tilde{\mathbf{c}}_k^i b_k^i + \mathbf{n}_k^i. \tag{2.17}$$

Here, $\tilde{\mathbf{c}}_k^i = [|h_{k,1}^i| c_{k,1}, \cdots, |h_{k,N}^i| c_{k,N}]^T$.

Figure 2.10 illustrates an up-link MC-CDMA based systems with K users. In such a system, the received signal corresponds to

$$r^i(t) = \sum_{n=0}^{N-1} \sum_{k=1}^{K} c_{k,n} b_k^i h_{k,n}^i e^{j2\pi n \Delta f t} e^{j2\pi f_c t} p(t) + n^i(t). \tag{2.18}$$

Consequently, the output of the FFT block at the base station can be represented as

$$\mathbf{r}^i = \sum_{k=1}^{K} \mathbf{r}_k^i = \tilde{\mathbf{C}}^i \mathbf{b}^i + \mathbf{n}^i \tag{2.19}$$

where $\mathbf{b}^i$ is the vector of users' data defined as $[b_1^i, b_2^i, \ldots, b_K^i]^T$; $\mathbf{n}^i$ is a vector of independent AWGN samples on each carrier, and $\tilde{\mathbf{C}}^i = [\tilde{\mathbf{c}}_1^i \cdots \tilde{\mathbf{c}}_K^i]$. Finally, the receiver will attempt to detect the transmitted data symbols based on $\mathbf{r}^i = [r_1^i, r_2^i, \cdots, r_N^i]$.

To detect the k^{th} user data symbol, the N subcarrier components $\mathbf{r}^i$ are despread using the conjugate of the k^{th} user spreading code $\overline{\mathbf{c}}_k = [\overline{c}_{k,1} \cdots \overline{c}_{k,N}]$ (where $\bar{\cdot}$ denotes the conjugate operation). First, we multiply each subcarrier component r_n^i with the corresponding element in the $\overline{\mathbf{c}}_k$ vector and denote the output of this product as $\overline{\mathbf{c}}_k \bigodot \mathbf{r}^i = [r_{k,1}^i, r_{k,2}^i, \cdots, r_{k,N}^i]$. To make a decision on the k^{th} user symbol, a weighted combining of $r_{k,n}^i$ is employed. Hence, the decision statistic for the k^{th} symbol is

$$R_k^i = \sum_{n=0}^{N-1} w_{k,n}^i r_{k,n}^i \tag{2.20}$$

Several methods, known as combining techniques, exist to extract the data from the decision statistics. Examples of these techniques are equal gain combining (EGC), minimum mean square error combining (MMSEC), and maximum ratio combining. This work focuses on the first two combining techniques, EGC and MMSEC because they are the simplest and most effective combining techniques, respectively.

2.3.1.4 Equal Gain Combining

In EGC, all subcarrier components are equally weighed and summed (i.e., $w_n^i = 1, n = 1 \cdots N$). EGC is optimal in AWGN channels, but not in fading channels. One benefit of EGC is that this technique does not require any channel state information.

2.3.1.5 Minimum Mean Square Error Combiner

MMSEC has been shown to provide the best performance among all combining schemes in a frequency-selective fading channel [64]. MMSEC is most effective because it minimizes error from the noise as well as multiple access interference (MAI). In deriving the MMSEC weights,

we use the fact that the error in R_k^i is orthogonal to the input, i.e., $E[(b_k^i - R_k^i) \cdot r_{k,n}^i] = 0, n = 0 \cdots N-1, p = 1 \cdots K$, where $E[\cdot]$ is the expectation operation. To satisfy this requirement,

the MMSEC weights can be found using the Wiener filter criterion [64]. Hence, MMSEC weight $w^i_{p,n}$ is

$$w^i_{p,n} = (C^i_{p,n})^{-1} A^i_{p,n} \tag{2.21}$$

where $C^i_{p,n} = E[r^i_{k,n} \cdot \overline{r}^i_{k,n} | h^i_{k,n}] = |c^i_{p,n}|^2 [\sum_{k=1}^{K} |h^i_{k,n}|^2 |c^i_{k,n}|^2 + \frac{N_0}{2}]$ and $A^i_{p,n} = E[b^i_k \cdot r^i_{k,n} | h^i_{k,n}] = |c^i_{p,n}|^2 h^i_{p,n}$. If BPSK modulation is used, the resulting weights in an MMSEC scheme correspond to

$$w^i_{p,n} = \frac{h^i_{p,n}}{\sum_{k=1}^{K} |h^i_{k,n}|^2 |c^i_{k,n}|^2 + \frac{N_0}{2}} \qquad n = 0....N-1 \tag{2.22}$$

From equation (2.22), it is clear that the minimum mean square error combiner requires accurate knowledge of both the channel attenuation coefficients for all subcarriers and the power of the additive white gaussian noise. In this work, we assume perfect knowledge of the **h** vectors.

Figure 2.12 presents the EGC and the MMSEC performances in an uplink MC-CDMA system. Here we assume a system with 16 subcarrier and 16 user communicating over a channel with 4 fold-diversity. In the figure we see two curves; the top curve represent the EGC performance. The bottom line stands for the MMSEC performance. From these figures, it is evident that the MMSEC outperforms the EGC significantly. However, both of these single-user-detection technique suffer an error floor in the uplink channel. To understand the source of this error floor, it is important to note that in any combining technique, the decision statistic used in detecting the p^{th} user has the form

$$R^i_p = \alpha^i_{p,p} b^i_p + \sum_{k=1, k\neq p}^{k=K} \alpha^i_{p,k} b^i_k + n^i_p \tag{2.23}$$

where $\alpha^i_{p,k}$ represents the k^{th} user energy in the p^{th} user decision statistic. R^i_p in equation (2.23) is composed of three term. The first one is $\alpha^i_{p,p} b^i_p$ which is the desired user information. The second term is the $\sum_{k=1,k\neq p}^{k=K} \alpha^i_{p,k} b^i_k$; this term is the interference caused by the other users in the system, and is referred to as the MAI component. The last term is the channel noise. It is obvious that the MAI component can be minimized if we utilize our knowledge about the other users information. Hence, jointly detecting all users information is a logical conclusion. Joint detection for all user information is referred to as multi-user detection (MUD) and it is

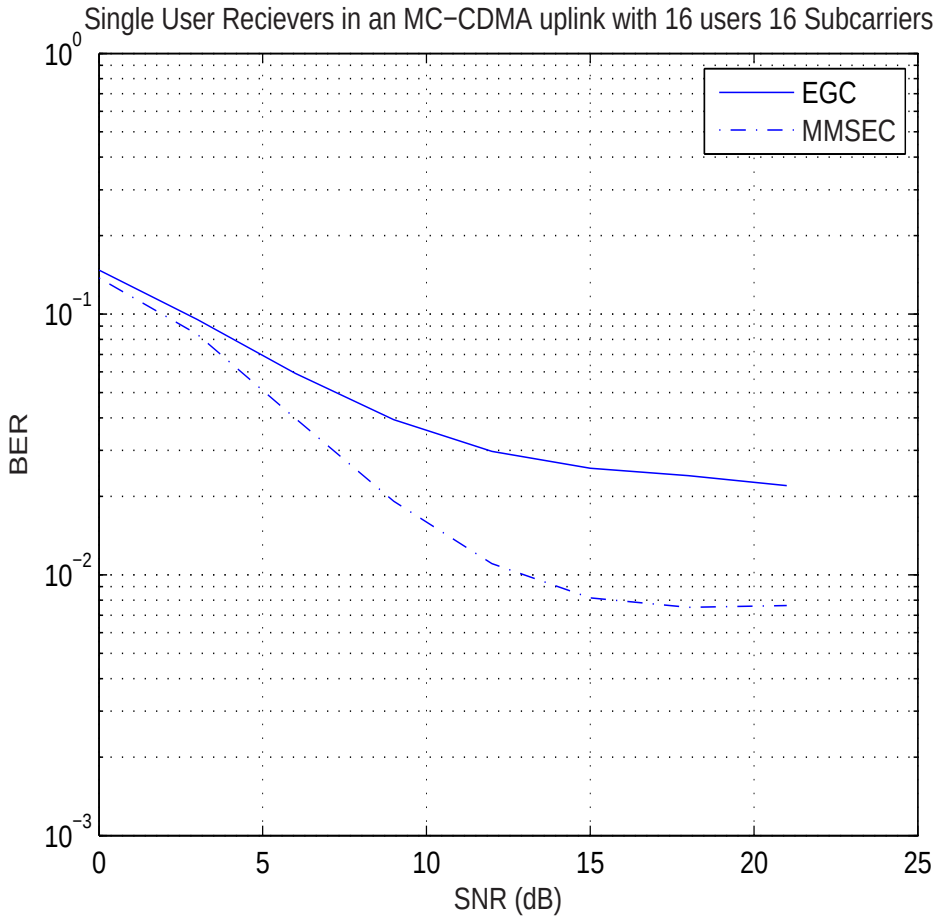

Figure 2.12: Single-user detection performance

the subject of next chapter.

Chapter 3

Multiuser Detection

In this chapter, we present the methods of ameliorating the effects of MAI. As discussed in the previous chapter, MAI severely degrades CDMA system performance. Especially in the uplink communication scenario, single-user detection methods (combining techniques) suffer from high error-floor. This error-floor is a direct consequence of the combining techniques inability to mitigate the MAI. Even in the absence of Gaussian noise (in uplink communication), combiners are incapable of separating different users symbols perfectly. For this reason, in the early 1980's, Verdu proposed joint detection of all users a DS-CDMA system. Since then, joint detection in CDMA systems has been the focus of extensive research and referred to as multiuser detection (MUD).

This chapter is organized as follows; in Section 3.1 we present the basic concepts of MUD. In Section 3.2 we introduce MUD to MC-CDMA Systems. Finally we present recent developments in optimal MUD design in Section 3.3.

3.1 Basic Concepts of MUD

Figure 3.1 illustrates a DS-CDMA system with K synchronous users. The baseband DS-CDMA transmitted signal corresponds to each user's data symbol spread by a unique code waveform. At the receiver end, the total received signal is composed of the sum of all users' signals. In

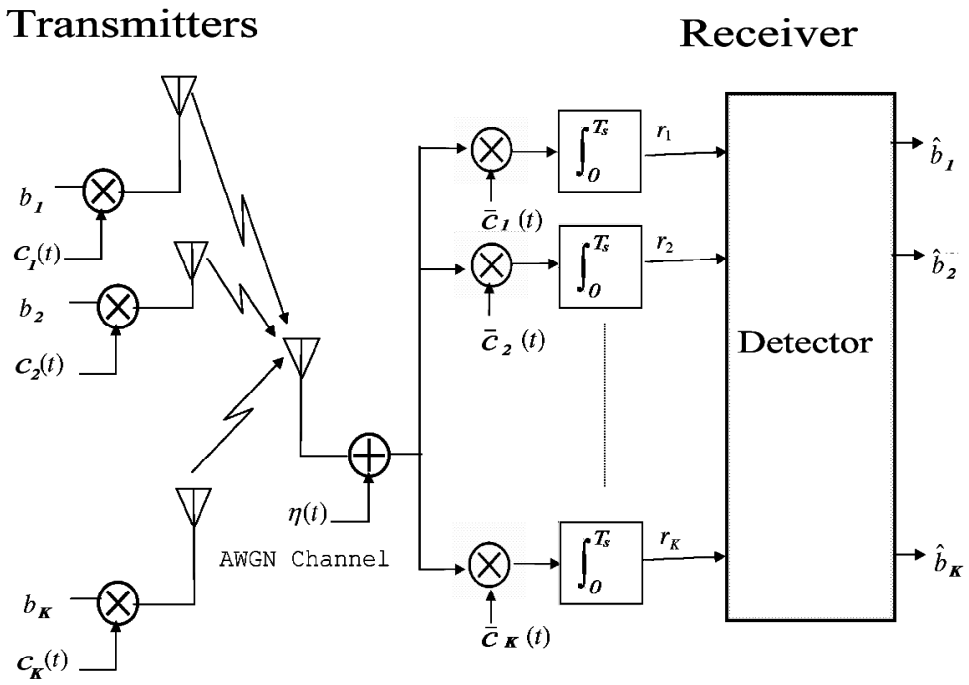

Figure 3.1: Block diagram of a synchronous up-link DS-CDMA system

a conventional DS-CDMA single-user receiver, each user's symbol is independently detected using a matched filter matched to the unique spreading code used by that user.

If the spreading sequences are correlated, the output of the matched filter for a given user will contain interference from all other users. In single-user receiver, this interference is treated as an additive noise component. By using a sufficiently large spreading factor, the desired user can be detected after despreading as the other users' signal strengths are reduced by the spreading factor. This is illustrated in Figure 3.2.

In a synchronous DS-CDMA system with K users, the matched filter outputs at the receiver end (as shown in Figure 3.1) can be represented as

$$\mathbf{r} = \mathbf{RAb} + \mathbf{n} \tag{3.1}$$

In equation (3.1) $\mathbf{b}$ is a vector of the K users' symbols (i.e., $\mathbf{b} = [b_1, b_2, \cdots b_K]^T$); $\mathbf{A}$ is a diagonal $K \times K$ matrix of user amplitudes (i.e., $\mathbf{A}$ is a power control matrix); $\mathbf{R}$ is a $K \times K$ cross-correlation matrix of the user's spreading sequences, i.e., $R_{ij} = E[c_i(t)c_j(t)]$ where $c_k(t)$ is the k^{th} user spreading sequence; And $\mathbf{n}$ is a correlated noise victor such that $E[\mathbf{nn}^T] = \frac{N_0}{2}\mathbf{R}$.

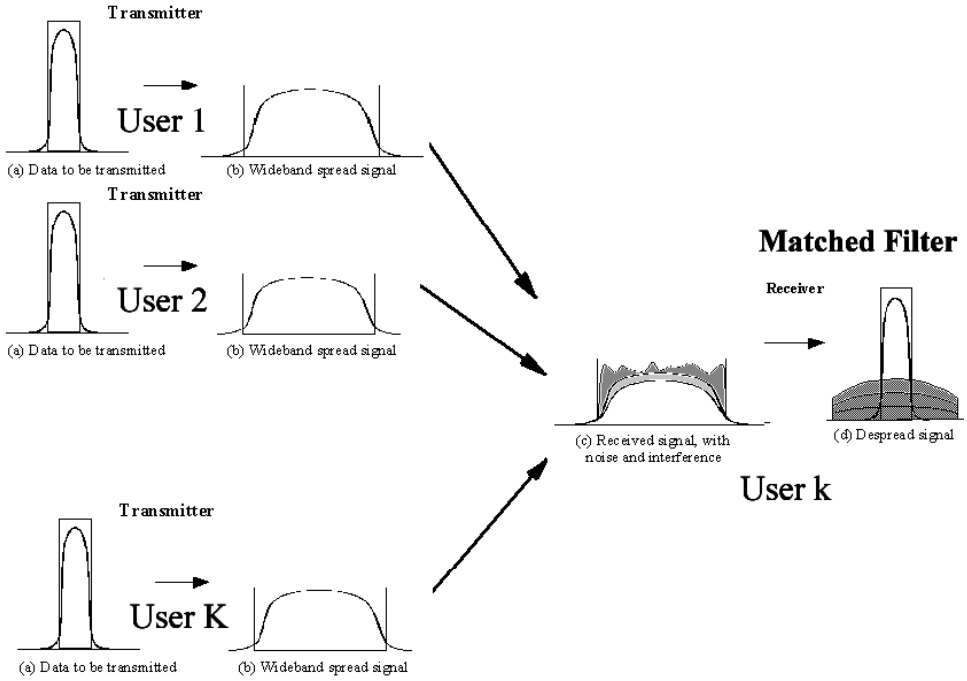

Figure 3.2: Despreading concept

In single-user receiver, the decisions on $\mathbf{b}$ are made directly from $\mathbf{r}$, element-wise. Hence, it considers the MAI as a noise component in addition to the channel noise. As a result, MAI degrades the performance of these single-user receivers and limits the system capacity. However, MUDs consider the MAI as additional information and detect all users' information symbols simultaneously. It has been shown that by reducing the effect of interference caused by the users' symbols MUD can increase system's capacity.

3.1.1 Optimum Multiluser Detection

The optimum multiuser detector [22] is the detector that minimizes the probability of error. Here, the optimality is based on maximum likelihood (ML) criterion. To do so, the optimal MUD has to find the set of $\hat{\mathbf{b}}_{opt}$, that most likely results in the received vector $\mathbf{r}$. Mathmatically, this can be written as

$$\hat{\mathbf{b}}_{opt} = \underset{\hat{\mathbf{b}}\epsilon\mathcal{X}_K}{\text{argmax}}\{Pr(\mathbf{b} = \hat{\mathbf{b}}|\mathbf{r})\} \tag{3.2}$$

where $\mathcal{X}_K$ is the set of all possible transmitted vectors; and $\hat{\mathbf{b}}_{opt}$ is the maximum-a-posteriori

(MAP) estimate for the transmitted vector $\mathbf{b}$ given the received vector $\mathbf{r}$. It is worth pointing out, under the condition that all possible vectors $\mathbf{b}\epsilon\mathcal{X}_K$ are equally probable, maximum-a-posteriori estimation is equivalent to maximum-likelihood estimation (MLE) [65]. It can be shown that solving for $\hat{\mathbf{b}}_{opt}$ in equation (3.2) is analogous to maximizing [22]

$$\Omega_K(\hat{\mathbf{b}}_{opt}) = 2\hat{\mathbf{b}}_{opt}^T\mathbf{A}\mathbf{r} - \hat{\mathbf{b}}_{opt}^T\mathbf{A}\mathbf{R}\mathbf{A}\hat{\mathbf{b}}_{opt}. \tag{3.3}$$

Maximizing Ω_K in equation (4.2) is increasingly complex as K increases and have a complexity of $\mathcal{O}(2^K)$ (assuming a BPSK modulation). It has shown in [66] that discovering a less complex deterministic method for finding the optimum $\mathbf{b}$ is unlikely, as it would also solve a number of theoretic NP-hard combinatorial problems.

While the optimal detector provides a significant improvement in system's bit-error-rate performance (and consequently an increase in overall systems capacity) over the conventional matched filter detector, the computational complexity needed to solve the optimal detection problem is cumbersome. This problem has motivated the search for low-complexity suboptimum multiuser receivers. These receivers are divided into two main categories: linear detectors and nonlinear or interference cancelers.

3.1.2 Linear MUDs

Linear multiuser detection is an important subclass of the suboptimal techniques that are used to attain as much as possible of the optimal MUD benefits with a feasible implementation utilizing the well understood linear filters. Hence, linear multiuser detector is simply a filter designed to attenuate MAI according to certain criterion.

There are two important types of linear multiuser detectors, and they are known as the decorrelating detector, and the minimum mean square error (MMSE) multiuser detector [22]. They are highly analogous to the zero-forcing and MMSE equalizers used to combat inter-symbol interference in a single-user channel [67].

The decorrelating detector attempts to completely eliminate the MAI for all users. The

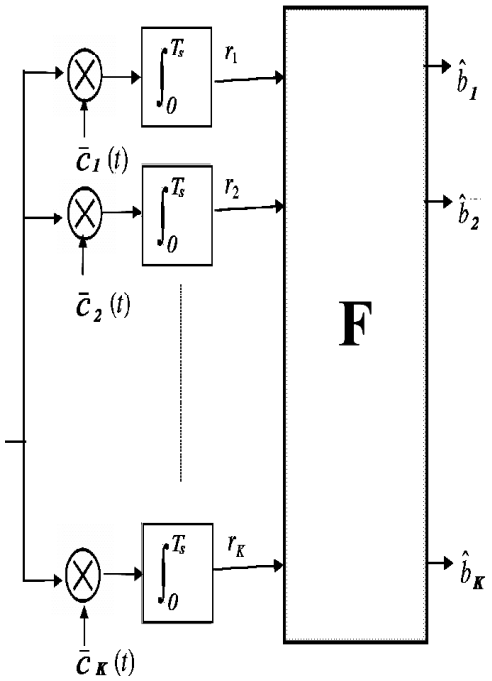

Figure 3.3: Linear MUD diagram

MMSE Multiuser detector instead tries to minimize the square of the residual noise plus interference. Hence, the decorrelating detector is simply a special case of the MMSE multiuser detector, where the noise is zero. The decorrelating detector often results in unacceptable noise enhancement. Furthermore, it is undefined for the situation where there are more users simultaneously using the channel than spreading chips per information bit, since it is impossible to drive the interference to zero in this situation.

A generic diagram of linear multiuser detector is depicted in Figure 3.3. From the diagram, it can be seen that the characteristic property of linear multiuser detectors is that the received signal is fed into a filter in order to derive an estimate for the K users' data symbol $\mathbf{b}$. Mathematically, the filter outputs is obtained by

$$\hat{\mathbf{b}}_{linear} = \mathbf{Fr} \tag{3.4}$$

3.1.2.1 Decorrelating MUD

The decorrelating detector applies the inverse of the correlation matrix

$$\mathbf{F}_{decor} = \mathbf{R}^{-1}$$

to the matched filter outputs $\mathbf{r}$ (equation (3.4)) in order to decouple the data. Hence, the soft estimate of this detector is

$$\hat{\mathbf{b}}_{decor} = \mathbf{R}^{-1}\mathbf{r} = \mathbf{A}\mathbf{b} + \mathbf{R}^{-1}\mathbf{n} \tag{3.5}$$

which is just the decoupled data plus a noise term. Thus, we see that the decorrelating detector completely eliminates the MAI. This detector is very similar to the zero-forcing equalizer [67] which is used to completely eliminate ISI. The decorrelating detector was initially proposed in [68]-[69] and extensively analyzed by Lupas and Verdu. They have shown that the decorrelating multiuser detector has many important properties such as [70]-[71]:

- Provides substantial performance/capacity gains over the conventional detector under most conditions [45].
- Has computational complexity significantly lower than that of the maximum likelihood sequence detector.
- Has a probability of error independent of the signal energies.
- Provides the best resilience to the near-far problem [70]
- Can decorrelate one bit at a time. For bit k, we only need apply the k^{th} row of $\mathbf{R}^{-1}$ to the matched filter bank outputs.

The main disadvantage of this detector is that it causes noise enhancement (similar to the zero-forcing equalizer). The power associated with the noise term $\mathbf{R}^{-1}\mathbf{n}$ at the output of the decorrelating detector in equation (3.5) is always greater than or equal to the power associated with the noise term at the outputs of the matched filters in equation (3.1) for each bit [72]. Despite this drawback, the decorrelating detector generally provides significant improvements

over the conventional detector. Another disadvantage of the decorrelating multiuser detector is that the computations needed to invert the matrix $\mathbf{R}$ are difficult to perform in real time. There have been numerous suboptimal approaches to implementing the decorrelating detector [43]-[73].

3.1.2.2 MMSE MUD

The minimum mean-squared error multiuser detector [43] is a linear detector which takes into account the background noise and utilizes knowledge of the received signal powers. This detector implements the linear mapping which minimizes $E[|\mathbf{b} - \hat{\mathbf{b}}_{linear}|^2]$, the mean-squared error between the actual data and the soft output of the linear filter. Hence, the matrix $\mathbf{F}$ that leads to the MMSE between the transmitted data symbol vector and the linear filter output $\hat{\mathbf{b}}_{MMSE} = \mathbf{F}_{MMSE}\mathbf{r}$ is the solution to the optimization problem

$$\mathbf{F}_{MMSE} = \underset{F}{\text{argmin}}\{\mathbf{b} - \mathbf{Fr}\} \tag{3.6}$$

The Wiener filter is well know to be the optimal stationary linear detector to recover a distorted (noisy) signal if the signal and the noise (distortion) are second-order stationary processes. To understand the functionality of the Wiener filter, let us assume that D is a noisy observation vector that can be modeled as

$$\mathbf{d} = \Lambda\mathbf{s} + \epsilon \tag{3.7}$$

where $\mathbf{s}$ is the desired signal vector, Λ is a linear distortion, and ϵ is an additive noise. In this case, the best linear estimate of $\mathbf{s}$ is

$$\hat{\mathbf{s}} = \mathbf{Wd} \tag{3.8}$$

where

$$\mathbf{W} = \mathbf{C}\Lambda^H(\Lambda\mathbf{C}\Lambda^H + \mathbf{N})^{-1} \tag{3.9}$$

In (5.8), the $(\cdot)^H$ represents the hermitian operation; $\mathbf{C}$ is the covariance matrix of the desired signal (i.e.,$E[\mathbf{ss}^H]$); and $\mathbf{N}$ is the noise covariance matrix (i.e.,$E[\epsilon\epsilon^H]$).

This result yields the well known solution for equation (3.6) [64]

$$\begin{aligned} \mathbf{F}_{MMSE} &= E[\mathbf{b}\mathbf{r}^H]E[\mathbf{r}\mathbf{r}^H]^{-1} \\ &= [\mathbf{R} + (N_0/2)\mathbf{A}^{-2}]^{-1} \end{aligned} \tag{3.10}$$

As can be seen in equation (3.10), the MMSE multiuser detector is nothing but a partial or modified inverse of the correlation matrix. The amount of modification is directly proportional to the background noise; the higher the noise level, the less complete an inversion of $\mathbf{R}$ can be done without noise enhancement causing performance degradation. Thus, the MMSE detector balances the desire to decouple the users with the desire to not enhance the background noise.

Because MMSE MUD takes the background noise into account, the MMSE detector generally provides better probability of error performance than the decorrelating detector. As the background noise goes to zero, the MMSE detector converges in performance to the decorrelating detector. An important disadvantage of this detector is that, unlike the decorrelating detector, it requires estimation of the received amplitudes (i.e., the $\mathbf{A}$ matrix). And consequently, its performance depends on the powers of the interfering users.

3.1.3 Non-linear MUD

While a linear multiuser detector is easier to analyze, and can be implemented using adaptive algorithms, the linearity constraint can restrict performance. In this section, a number of non-linear techniques are briefly introduced.

Decision-Feedback (DF) multiuser detectors [74] are developed in analogous to the decision-feedback equalizers used for inter-symbol interference suppression [75]. Here, the feed-forward filter is the Cholesky factorization of the correlation matrix $\mathbf{R}$, which yields a lower triangular matrix. The problems with this technique are similar to that of the linear multiuser detectors: accurate channel estimates are required, and a matrix inversion must be performed . If the channel estimates are accurate, the DF detector outperforms the linear detectors. However, the integration of error-correction with this design is not straightforward. Due to its complexity

and questionable robustness, it is doubtful that DF MUD can be applied to a realistic wireless channel.

Turbo MUD is a fairly recent type of nonlinear multiuser detection based on the best known technique for decoding concatenated error correcting codes [35]- [40]. Decoding in turbo MUD is accomplished via an iterative process in which soft-decisions are passed back and forth between two soft-input soft-output channel decoders, with interleaving. The early versions of turbo MUD [35]- [39] showed impressive capacity approaching the optimum detector, but at the cost of exponential complexity. Later work has reduced the complexity significantly [40], while also combating other cell interference. The problems with turbo MUD are that it still requires a complex implementation with significant latency, and there are a number of unproven issues with regards to its robustness in a multipath fading channel. Nevertheless, this could be an interesting technique in the years to come.

Interference cancellation is decision-driven suboptimal MUD in which the multiple access interference is first estimated and then subtracted from the desired signal. Interference cancellation methods can be classified into two broad categories: successive and parallel interference cancellation [76]. In successive interference cancellation (SIC), interference due to other users is canceled sequentially [77]- [80]. This process involves a large decoding delay to accomplish interference cancellation for all the users. Pipelined SIC (PSIC) scheme has been proposed [81] to compensate the problem of decoding delay and is shown to have a better performance than SIC with same decoding delay. Further improvement in the performance is achieved by adaptive PSIC [82]. In case of parallel interference cancellation (PIC), the MAI experienced by the desired user is canceled in one shot [83]. PIC requires more hardware than SIC but is more attractive due to its higher speed. The performance of these interference cancellation techniques depends on the precise estimation of MAI. To improve the reliability of interference estimation, a different method called partial PIC (pPIC) is discussed in [84]- [86] and is shown to have a better performance than conventional PIC. In case of pPIC, the interference is canceled partially depending on the reliability of the estimated data. In [87], it is shown that

the performance can be further improved by employing the interference cancellation schemes iteratively.

In all non-linear MUD techniques, feedback is used to reduce MAI. Hence, it is evident that there is some overlap between previously presented non-linear MUDs and interference cancellation techniques as they all use previously made decisions to reduce the multiple-access interference. In the next section, we will provide analogous discussion for MUD in MC-CDMA systems.

3.2 MUD in MC-CDMA Systems

In this section, we present the basics of MUD for synchronous MC-CDMA systems (in this work we use the term synchronous in reference to time-synchronization). As in equation (1.19), the received signal in a synchronous MC-CDMA system corresponds to

$$\mathbf{r}^i = \tilde{\mathbf{C}}^i \mathbf{b}^i + \mathbf{n}^i. \tag{3.11}$$

The process of jointly detecting the transmitted users symbols out of the received signal vector $\mathbf{r}$ in equation (3.11) is analogous to the discussion in the previous section. The MUD process in MC-CDMA systems can be categorized in to three main categories: (1) optimal MUD, (2) linear MUD, and (3) non-linear MUD.

3.2.1 Optimal MC-CDMA MUD

The optimal MUD simultaneously detects all users' data to jointly minimize the effects of MAI. The optimal MUD is the maximum likelihood receiver that yields the optimal estimate of the transmitted data, $\hat{\mathbf{b}}^i$.

$$\hat{\mathbf{b}}^i_{opt} = \underset{\hat{\mathbf{b}}}{\text{argmax}}\{P(\mathbf{b}=\hat{\mathbf{b}}|\mathbf{r}^i)\} \tag{3.12}$$

$$= \underset{\hat{\mathbf{b}}}{\text{argmax}}\{P(\mathbf{r}^i=\tilde{\mathbf{C}}^i\hat{\mathbf{b}}^i+\mathbf{n}^i|\mathbf{b})\} \tag{3.13}$$

$$= \underset{\hat{\mathbf{b}}}{\text{argmax}}\{P(\mathbf{n}^i=\mathbf{r}^i-\tilde{\mathbf{C}}^i\hat{\mathbf{b}}|\mathbf{b})\} \tag{3.14}$$

The joint pdf of the noise corresponds to

$$p(\mathbf{n}^i) = \frac{1}{(2\pi\sigma^2)^{N/2}} e^{-\frac{1}{2\sigma^2}(\mathbf{n}^i)^H|\mathbf{I}|^{-1}(\mathbf{n}^i)} \tag{3.15}$$

where σ^2 is the variance of the noise and N is the number of carriers. Combining equations (3.14) and (3.15)

$$\begin{aligned}
\hat{\mathbf{b}}^i_{opt} &= \underset{\hat{\mathbf{b}}}{\text{argmin}}\{(\mathbf{n}^i)^H|\mathbf{I}|^{-1}(\mathbf{n}^i)\} \\
&= \underset{\hat{\mathbf{b}}}{\text{argmin}}\{(\mathbf{n}^i)^H(\mathbf{n}^i)\} \\
&= \underset{\hat{\mathbf{b}}}{\text{argmin}}\{(\mathbf{r}^i-\tilde{\mathbf{C}}^i\hat{\mathbf{b}})^H(\mathbf{r}^i-\tilde{\mathbf{C}}^i\hat{\mathbf{b}})\} \\
&= \underset{\hat{\mathbf{b}}}{\text{argmin}}\{(\mathbf{r}^i)^H\mathbf{r}^i-\hat{\mathbf{b}}^H(\tilde{\mathbf{C}}^i)^H\mathbf{r}^i-(\mathbf{r}^i)^H\tilde{\mathbf{C}}^i\hat{\mathbf{b}}^i+(\hat{\mathbf{b}}^i)^H(\tilde{\mathbf{C}}^i)^H\tilde{\mathbf{C}}^i\hat{\mathbf{b}}^i\}
\end{aligned} \tag{3.16}$$

Ignoring all terms that are independent of $\hat{\mathbf{b}}^i$, the optimal MUD for MC-CDMA systems corresponds to

$$\begin{aligned}
\hat{\mathbf{b}}^i_{opt} = \underset{\hat{\mathbf{b}}}{\text{argmax}}\{&Q(\hat{\mathbf{b}})=2\Re\text{e}\{(\hat{\mathbf{b}})^H(\tilde{\mathbf{C}}^i)^H\mathbf{r}^i\} \\
&-(\hat{\mathbf{b}})^H(\tilde{\mathbf{C}}^i)^H\tilde{\mathbf{C}}^i\hat{\mathbf{b}}\}
\end{aligned} \tag{3.17}$$

Inspecting equation (3.17), we observe that the optimal MUD consists of a difference of two terms. Only the first term depends on the received signal vector. However, it has been premultiplied by $(\tilde{\mathbf{C}}^i)^H$ and the product is nothing but the output of the maximum ratio combining receiver (MRC). Hence, MRC outputs represent sufficient statistics to perform maximum likelihood detection. Furthermore, it can be seen that MRC output provides the optimal estimation of the transmitted data symbol if a single user is considered. Because MRC receivers are simple to implement and provide optimal performance for one user, they are often implemented in

systems with multiple users. Since the MRC receiver does not jointly minimize the affects of MAI from other users, it is suboptimal and considered a single user receiver.

Similar to optimal DS-CDMA MUD [22], the solution for the optimal MC-CDMA MUD requires an exhaustive search over a set of M^K possible solution vectors where M is the number of points in the signal constellation (e.g., $M = 2$ for BPSK) and K is the number of users. The complexity of this receiver increases exponentially with the number of users. Therefore, it is impractical to implement.

By noting the similarities between the optimal DS-CDMA MUD and the optimal MC-CDMA MUD, it can be easily shown that the optimal MC-CDMA MUD problem belongs to a large class of combinatorial problems known as NP-complete optimization problems. NP-complete problems are optimization problems (e.g., the traveling salesman and integer programming problems) that cannot be solved in polynomial time and the best solution technique is to implement an exhaustive search over all possible solutions.

3.2.2 Linear MUD for MC-CDMA systems

The big gap in performance and complexity between the single user and the ML-MUD motivated the development of other MUDs that exhibit good performance/complexity tradeoffs. In this section, we present the main sub-optimal linear MUDs: (1) decorrelator detector; and (2) minimum mean square error (MMSE) MUD.

3.2.2.1 Decorrelator

In [88], the authors present a causal and stable design of the decorrelator MUD in MC-CDMA setting. In the linear MUD, the receiver multiplies received $\mathbf{r}^i$ vector with $(\tilde{\mathbf{C}}^i)^{-1}$. Then, the resultant victor $\mathbf{b} + (\tilde{\mathbf{C}}^i)^{-1}\mathbf{n}^i$ of this product is fed to a hard decision block to detect transmitted symbols. This linear detector exhibits the same degree of near-far resistance as the ML-MUD. The decorrelator detector eliminates the correlation between different users by restoring their orthogonality. However, while restoring orthogonality, the decorrelator might

amplify the noise. Hence, at low SNR, where AWGN is the dominant source of error, noise magnification degrades decorrelator MUD BER performance significantly when compared to the ML-MUD performance. The noise amplification problem can be constrained utilizing the Wiener filter criterion [89] to designing an MMSE MUD.

3.2.2.2 MMSE MUD

Like the decorrelator MUD, MMSE MUD is a linear detector where the transmitted signal is estimated via linear transformation of the receiver observations. However, the MMSE MUD differs from the decorrelator detector as it exploits the receiver's knowledge about the SNR.

By direct substitution of the result in (5.8), the MMSE MUD for $\mathbf{b}^i$ based on the observation vector $\mathbf{r}^i$ (as defined in equation(3.11)) is

$$\hat{\mathbf{b}}_{MMSE} = \text{sign}\{\mathbf{M}^i\mathbf{r}^\mathbf{i}\} \tag{3.18}$$

where

$$\mathbf{M}^i = (\tilde{\mathbf{C}}^i)^H(\tilde{\mathbf{C}}^i(\tilde{\mathbf{C}}^i)^H + \sigma^2\mathbf{I})^{-1} \tag{3.19}$$

where σ^2 is the noise variance, and $\mathbf{I}$ is the identity matrix.

3.2.3 Non-Linear MUD

In non-linear MUDs, the interference term is annihilated by introducing iterative feedback to the detection process. In each iteration, an updated estimate of the transmitted bits is created utilizing the other user information. In calculating these estimates, the MAI is estimated and removed. This removal is done either serially or in parallel forming which is know as Serial interference cancellers (SIC) or parallel interference cancellers (PIC). [90] investigates the performance of the asynchronous MC-CDMA systems with nonlinear multiuser detectors namely SIC and PIC. And the authors propose two variants of PIC known as (1) Threshold PIC (TPIC) and (2) Block-PIC.

3.3 Recent Development in Optimal MUD Design

Verdu in [66] showed that the maximum likelihood-MUD based on equation(3.2) belongs to a large class of combinatorial problems known as NP-complete optimization problems. NP-complete problems are optimization problems (e.g., the traveling salesman and integer programming problems) that cannot be solved in polynomial time and the best solution technique is to do an exhaustive search over all possible solutions. Therefore, in order to solve an NP-complete problem for any non-trivial problem size, one of the following approaches is used: (1) Approximation: An algorithm which quickly finds a suboptimal solution which is within a certain range of the optimal one [22], [23]; (2) Probabilistic: An algorithm which probably yields good average runtime behavior for a given distribution of the problem instances; and (3) Heuristic: An algorithm which works "reasonably well" on many cases, but for which there is no proof that it is always fast (e.g., evolutionary techniques).

Evolutionary techniques such as the genetic algorithm (GA) have been proposed for optimal MUD design for DS-CDMA [45]. Genetic algorithms (GAs) are known for their ability to solve complex optimization problems [49]. A genetic algorithm is a search technique used to solve optimization problems. GAs are classified under the evolutionary algorithms umbrella (optimization techniques inspired by biologic evolutionary principals such as inheritance, mutation, natural selection, and crossover). In computer simulations, GAs are typically implemented over a population of candidate solutions to an optimization problem. And the GA program job is to evolve this population toward better solutions in an iterative manner. Usually, the evolution starts from a completely random population and happens over a series of successive generations. In each generation, the fitness of the whole population is evaluated, multiple individuals are stochastically selected from the current population (based on their fitness), modified (mutated or recombined) to form a new population, which becomes current in the next iteration of the algorithm.

Based on the ML rule, GAs are developed in order to jointly estimate the various users' transmitted bit sequences on the basis of the statistics provided by a bank of matched filters

at the receiver. [45] demonstrate that such a GA-based multiuser detector can be applied to symbol detection over a fading channel, if the channel parameters are known. Using computer simulations, the authors showed that the proposed receiver can achieve a near-optimum bit-error-rate (BER) performance upon assuming perfect channel estimation at a significantly lower computational complexity than that required by the ML optimum multiuser detector. However, the GA-based approaches suffer from: (1) slow convergence; (2) high computational complexity, and (3) strong dependance on initial "guesses" [45]. Recently, particle swarm intelligence has inspired optimization algorithms that have been proposed for NP-complete optimization problems. Ant Colony Optimization is one such technique that is discussed in the following section.

Chapter 4

Ant Colony Optimization and the MUD problem

In the previous chapter we presented several multiuser detectors for DS-CDMA and MC-CDMA systems. It has been shown that solving the optimal MUD problem is cumbersome and impractical. For this reason there is a need for new methods to simplify the search process for the optimal solution in the MUD problem. Recently, researchers proposed the use of artificial intelligence techniques to solve the optimal MUD problem presented in the previous chapter. Specifically, in [46] and [47] the authors proposed utilizing neural networks and genetic algorithms to search for the optimal solution for the MUD problem. In [53], Dorego proposed an optimization technique based on the foraging behavior of ants known as ant colony optimization (ACO). ACO is an attractive technique that is very effective in solving optimization problems that have discrete and finite search space. Since the optimal MUD design problem involves a search process across a finite number of possible solutions, ACO is an ideal candidate to solve this problem. In this chapter we adapt ACO to solve the optimal MUD problem in synchronous DS-CDMA and MC-CDMA systems.

This chapter is organized as follows. Initially, we present the basics of ACO in Section 4.1, then we develop the ACO based MUD for synchronous DS-CDMA systems in Section. Finally,

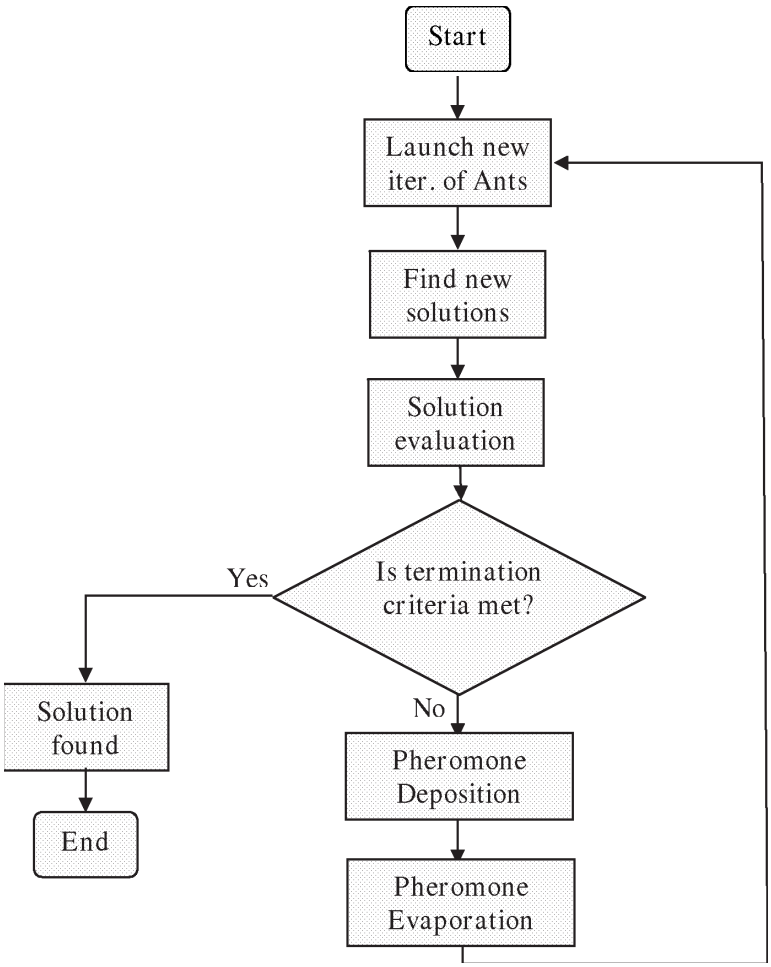

Figure 4.1: A flowchart depicting the structure of ACO algorithm

in Section 4.1 we introduce the ACO based MUD for synchronous MC-CDMA systems.

4.1 Ant Colony Optimization (ACO)

In recent years, particle swarm intelligence has inspired optimization algorithms that have been proposed for NP-complete optimization problems. In [53], Dorigo showed that ACO is well suited in solving NP-complete problems (e.g., the traveling salesman problem). Specifically, he demonstrated that the ACO is a superior approach to solving certain discrete optimization problems relative to GAs.

ACO is based on the behavior of a colony of ants searching for food. In the ACO ap-

proach, several artificial ants perform a sequence of operations iteratively as shown in Figure 4.1. Within each iteration, several ants search in parallel for good solutions in the solution space. In each iteration of the algorithm, one or more ants are allowed to execute a move, leaving behind a pheromone trail for others to follow. An ant traces out a single path, probabilistically selecting only one element at a time, until an entire solution vector is obtained. In the following iterations, the traversal of ants is guided by the pheromone trails, i.e., the stronger the pheromone concentration along any path, the more likely an ant is to include that path in defining a solution. In each iteration, the quality of produced solution is estimated via a cost function. This estimate of a solution quality is essential in determining whether or not to deposit pheromone on the traversed path. In addition to the pheromone values, the ants are also guided by a problem-specific greedy heuristic (desirability function) to aid in its search for good solutions.

It is easy to see that, as the search progresses, deposited pheromone dominates ants' selectivity, reducing the randomness of the algorithm. Therefore, ACO is an exploitive algorithm that seeks solutions using information gathered previously, and performs its search in the vicinity of good solutions. However, since the ant's movements are stochastic, ACO is also an exploratory algorithm that samples a wide range of solutions in the solution space. This exploratory-exploitive approach is characteristic of many heuristic based optimization approaches, including GAs [49], tabu search [91] and particle swarm [92].

4.2 ACO based MUD for synchronous DS-CDMA systems

The first stage in designing our ACO-based MUD involves the selection of ACO parameters that fit the optimization problem as presented in the previous chapter. In section 3.1.1, it has been shown that optimal MUD problem in DS-CDMA corresponds to

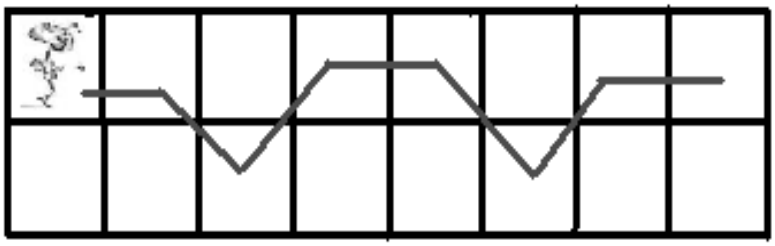

Figure 4.2: Ants' moving pattern

$$\mathbf{b}_{opt} = \underset{\mathbf{b}\epsilon\mathcal{X}_K}{\text{argmax}}\{\Omega_K(\mathbf{b})\} \tag{4.1}$$

where

$$\Omega_K(\mathbf{b}) = 2\mathbf{b}^T\mathbf{A}\mathbf{r} - \mathbf{b}^T\mathbf{A}\mathbf{R}\mathbf{A}\mathbf{b}.$$

Hence, the solution for the MUD problem in DS-CDMA systems corresponds to $\mathbf{b}_{opt}$ which is a length-K vector. Each element of the solution vector takes one out of M possible values, where M is the constellation size (in this work, we assume BPSK modulation, i.e., $M = 2$); M^K solutions are possible (2^K for BPSK). In our ACO algorithm, every ant builds a solution vector in each iteration. This building process is accomplished via K jumps inside a $2 \times K$ table as shown in Figure 4.2. The first row in this table represents an initial solution. The second row is nothing but the complement of the first row. Thus, any solution (out of the 2^K possible solutions) can be formed by selecting K elements from this table, one element from each column. Hence, in each jump, the ant selects (based on a desirability function and pheromone concentration) either the initial solution element or its complement. After every iteration, pheromone deposition and evaporation takes place.

When higher order modulation is considered (i.e., QPSK), the solution vector may be formed in the same manner. However, in this case, the ants will move inside a bigger table ($4 \times K$ table assuming QPSK modulation) and the best solution (out of 4^K possible solutions) is once again determined by selecting K elements from this table.

In single-user receivers, a suboptimal solution vector ($\mathbf{b}$) is created by performing hard

decisions based on MF outputs. In our ACO algorithm, we have used this vector as an initial solution. Hence, all ants begin their search at a specific position along the ($\mathbf{b}$) vector. The ants cyclically move down the $\mathbf{b}$ vector, selecting the best element at each stage. The value of the element chosen by an ant is derived from the corresponding element values in either $\mathbf{b}$ or $\overline{\mathbf{b}}$ ($\overline{\mathbf{b}} = [\overline{b}_1, \overline{b}_2, \cdots \overline{b}_K]^T$ where $\overline{b}_l = +1$ if $b_l = -1$ and vice-versa $\forall\ l$). The desirability function is used to help the ant decide if a particular element value of the solution vector should come from $\overline{\mathbf{b}}$ instead of $\mathbf{b}$. Since the magnitude of the conventional single user MF outputs provide a rough estimate of the quality of users' hard decisions, it is used in evaluating the desirability function of the ants. The desirability function for an ant starting at j^{th} element in the $\mathbf{b}$ vector is defined as:

$$D(j) = \frac{1}{2 + |r_j|} \tag{4.2}$$

equation(7.4) reflects the fact that when $r_j = 0$, b_j and $\overline{b}_j$ are equally likely to be chosen. As the ant moves along the elements of the solution vector, the desirability function at the $(j+i)^{th}$ stage can be redefined as follows:

$$D(j+i) = \frac{1}{2 + |r_{j+i}| + \sum_{l \in P} |r_l|}. \tag{4.3}$$

where P is a set of positions where the ant had previously selected $\overline{\mathbf{b}}$ element values. The desirability function defined in Eqns.(7.4) and (4.6) ensure that an ant does not significantly deviate from the initial solution. For example, if an ant chooses the element value from $\overline{\mathbf{b}}$ at the j^{th} position, its desirability to select another element value from $\overline{\mathbf{b}}$ decreases. Therefore, ants' starting positions in a single iteration should be as far as possible from one another along the solution vector. It is important to note that, while restricting ants' movements to the vicinity of the initial solution is not a necessary condition, it is useful when the reliability of initial data estimates is high (e.g., high SNR or more sophisticated receiver structure).

The second challenge in designing ACO based MUD algorithm, is to develop a meaningful pheromone deposition mechanism. In our algorithm, pheromones are deposited in a $2 \times K$

table where the first row corresponds to the elements of $\mathbf{b}$, and the second row corresponds to the elements of $\overline{\mathbf{b}}$. At the beginning of the search process, the pheromone table has equal amounts (unity) of pheromone in all of its entries. As the search progresses , pheromones are deposited and evaporated based on the path traversed by the ants. The deposition rate (DR) and evaporation rate (ER) are parameters of the ACO. In our algorithm, the DR and ER are inversely related to the number of iterations, V. At any stage during the search, the higher the pheromone value in an entry (in the pheromone table), the greater is the probability of selecting the corresponding element value from $\mathbf{b}$ or $\overline{\mathbf{b}}$. Since $\Omega_K(\mathbf{b})$ determines the quality of a solution, it is used to control the amount of pheromone deposition. Furthermore, we use the elitism philosophy in our pheromone deposition mechanism, i.e., only the ants that find good paths are allowed to deposit pheromones.

Our complete ACO based MUD algorithm is summarized below:

- Create a $2 \times K$ pheromone table $PT \in \mathbb{R}^{2\times K}$; $PT(m,n) = 1 \ \forall \ m,n$ [pheromone values are initialized]
- for $iter = 1 : V$, {
  1. Decide the starting positions for ζ ants $(st_1, st_2, \cdots st_\zeta)$.

     for $move = 0 : K-1$, {
     (a) The i^{th} ant selects $\overline{\mathbf{b}}$ element values with probability $p_i(move) = PT(2, (st_i + move) \text{mod } K) \cdot D((st_i + move) \text{mod } K) \ \forall \ i = 1, 2, \cdots \zeta$. [This probability is evaluated for for all ants]
     (b) Store the selected elements in $\mathbf{b}_i \ \forall \ i = 1 \cdots \zeta$.
     (c) The 2-dimensional indices of chosen locations in PT constitute the trail for each ant. Store the trail for the i^{th} ant in $Tr_i \in \mathbb{I}^{2\times K} \forall \ i = 1 \cdots \zeta$.
       - The 1^{st} row & 2^{nd} row of Tr_i represents row and column indexes of selected PT locations, respectively;

     }

2. if $\Omega_K(\mathbf{b}_i) \geq \Omega_K(\mathbf{b})$ [Check for 'elite' ants]

   – Deposit pheromones: $PT(Tr_i(1,k), Tr_i(2,k)) = PT(Tr_i(1,k), Tr_i(2,k)) + \triangle PT$, where $\triangle PT = DR \cdot \frac{\Omega_K(\mathbf{b}_i)}{K}$

3. Evaporate pheromones: $PT(m,n) = PT(m,n) \cdot (1 - ER) \; \forall \; m,n$

}

- In the pheromone table, the trail with the highest pheromone concentration and its corresponding values from $\mathbf{b}$ and $\overline{\mathbf{b}}$ provide the final solution $\widehat{\mathbf{b}}_{opt}$.

When comparing ACO based MUD and sphere decoding based reception [23], we observe an interesting similarity. In both cases, the search process is limited to the vicinity of the received vector. However, in ACO the search process is not restricted by a radius constraint. Furthermore, the ants are provided with tools (heuristics-desirability and pheromone concentration) to explore the search area intelligently. In essence, the ACO based MUD can be perceived as a smart variant of sphere decoding without the drawbacks (determining the appropriate sphere radios) of sphere decoding. Moreover, unlike ACO-based MUD, it is not possible to extend sphere decoding to time varying fading channel without increasing the computational complexity. This increase in complexity is due to the fact that the search space has to be constantly modified to account for channel variations.

4.2.1 Computational Complexity

In order to compare complexity of the ACO based MUD with GA based MUD, we define the product $Q = \zeta \cdot V$ as the measure of the computational complexity of our algorithm (e.g., an ACO with 8 ants and 25 iterations results in a $Q = 200$). This measure is consistent with Hanzo's measure of computation complexity for GA based MUDs in [45]. However, it is important to note that for the same Q value, the ACO based MUD has a far less complicated structure than that of GA-assisted MUDs. The lower complexity can be attributed to the ease of performing the operations involved in the ACO relative to the operations in a GA. In GAs,

crossover, *mutation* and *selection* are the main operations that need to be performed in each iteration. These operations are far more cumbersome than the pheromone evaporation and deposition operations in an ACO.

A more general measure of complexity of MUD is the number of arithmetic operations. This measure is useful to compare the complexity of ACO-MUD with an exhaustive search technique as well as the sphere decoding. For all these MUDs, the fitness function (equation (4)) evaluation requires K^2 operations. Hence, the computational complexity of the exhaustive search based MUD can be written as $\mathcal{O}(K^2 2^K)$.

In the case of sphere decoding, the number of operations is polynomially related to K while it is related exponentially to radius. The radios is typically chosen to be proportional to N_0 (single-sided noise power spectral density)[23]. Therefore, complexity of sphere decoding grows exponentially as noise increases (SNR decreases). For our ACO based MUD, we require $\mathcal{O}(K^2)$ operations for desirability function calculation for each ant in one iteration. This is in addition to the $\mathcal{O}(K^2)$ operations involved in the evaluation of $\Omega_K(\mathbf{b})$. Hence, for one ant, the computation complexity is $\mathcal{O}(K^2)$. Considering ζ ants being involved in V iterations, the total complexity of the ACO can be written as $\mathcal{O}(K^2 \zeta V)$ or $\mathcal{O}(K^2 Q)$.

4.2.2 Simulation Parameters and Results

We evaluate the ACO based MUD performance for a synchronous DS-CDMA system with: (1) processing gain = 15; (2) $K = 15$ (unless otherwise specified); (3) the correlation coefficient between any two spreading codes is equal to 0.1, and (4) transmission over AWGN channel. These values were selected in order to compare our proposed receiver with optimal MUD performance provided in [22]. The following ACO parameters were employed: number of ants, $\zeta = 8$; $DR = 7/V$, and $ER = 10/V$.

Figure 4.6 presents four BER versus SNR curves where the 16 users suffer equal attenuation (i.e., A is an identity matrix). The top most curve represents the MF BER performance ($V = 0$). The other three curves (from top to bottom), are the ACO based MUD performance curves for

increasing number of iterations, (25, 50 and 100). The bottom most curve corresponds to the ACO MUD performance after 100 iterations and it matches the optimal maximum likelihood-MUD performance [22]. From Figure 4.6, it is clear that BER performance improves with increasing number of ACO iterations. Specifically, doubling the number of iteration/complexity level (from 50 to 100 iterations) results in 1 dB gain in performance. Figure 4.6 also illustrates the effectiveness of ACO based MUDs with relatively few iterations. For example, with $V = 25$ iterations, the ACO MUD performance is about 1.5 dB off the optimal MUD performance at a BER of 10^{-3}. Figure 4.4 presents the BER performance of the ACO-MUD receiver as a function of the total number of iterations. Once again, we see that the algorithm converges to optimal MUD performance after a small number iterations (40 iterations). Figures 4.6 and 4.4 demonstrate that it is possible to achieve the optimal BER performance with 95% ($\frac{2^{16}-800}{2^{16}}$) lower computational complexity (corresponding to 100 iterations) relative to an exhaustive search.

Similar to Figure 4.6, Figure 4.3 presents two overlapping BER versus SNR curves. Here, we assume that processing gain = 16; $K = 16$. And, half the users suffer an additional 3 dB of attenuation. This difference in attenuation factors simulate a scenario where half the users are farther away from the base station (this is usually referred to as the near-far problem in CDMA literature). As can be seen in Figure 4.6, the ACO based MUD is identical to the optimal MUD performance after 100 iterations. Specifically, once again the ACO-based MUD matches the BER performance of the optimal MUD with more than 95% savings in terms of computational complexity over the exhaustive search approach.

Figure 4.5 presents three BER performance curves for a synchronous 20-user DS-CDMA system utilizing random codes with a spreading gain of 31. We once again assume an AWGN channel. The bottom most curve represents the optimal MUD performance achieved using an exhaustive search. The other two curves present ACO based MUD and GA assisted MUD (presented in [45]) performances with complexity measure Q = 2000 and Q = 4800, respectively. From the plots, it is evident that ACO based MUD is able to match the GA assisted MUD

performance with less than half the computation complexity. Specifically, an ACO based MUD demonstrates close to optimal BER performance with 58% lower computation complexity relative to GA assisted MUD. This result further demonstrates the gain achievable using ACO based MUDs.

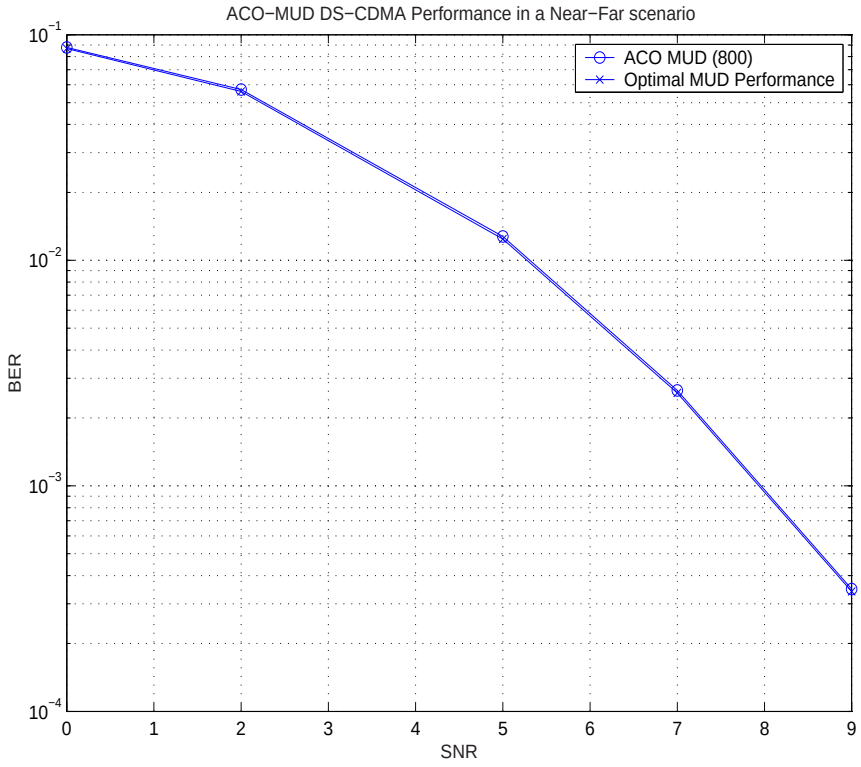

Figure 4.3: ACO-MUD performance versus SNR in a near-far scenario with $Q = 800$, $\zeta = 16$ and $K = 16$

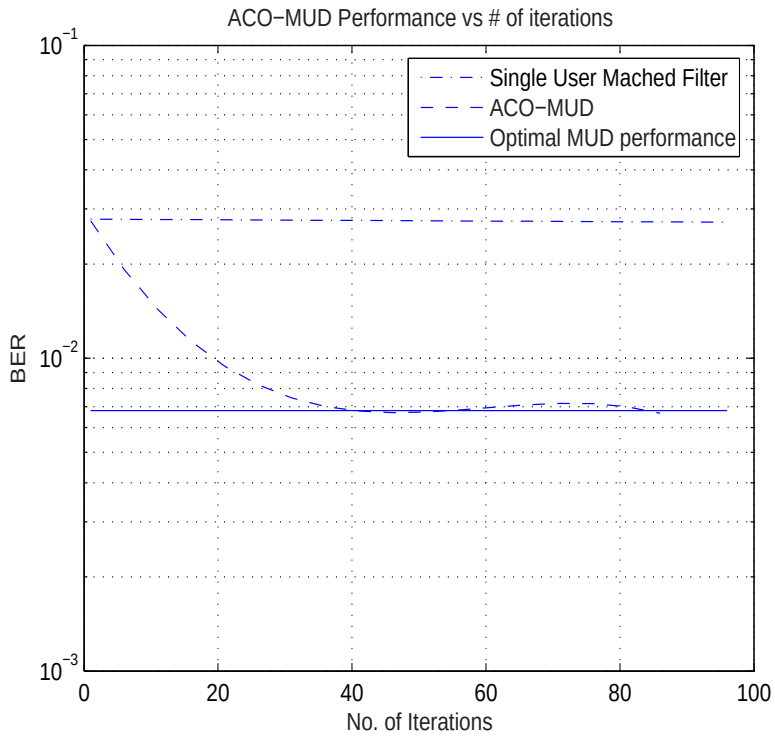

Figure 4.4: Performance versus number of iterations at $SNR = 5dB$, $\zeta = 15$, and $K = 15$

4.3 ACO based MUD for synchronous MC-CDMA systems

Let us revisit the optimal MUD problem for MC-CDMA systems as presented in Section 3.2. It has been shown that the solution for the MUD problem corresponds to

$$\begin{aligned} \mathbf{b}_{opt} &= \underset{\mathbf{b}}{\text{argmax}}\{Q(\mathbf{b}) = 2\Re\text{e}\{(\mathbf{b})^H(\tilde{\mathbf{C}})^H\mathbf{r}\} \\ &\quad -(\mathbf{b})^H(\tilde{\mathbf{C}})^H\tilde{\mathbf{C}}\mathbf{b}\} \end{aligned} \tag{4.4}$$

In equation (4.4), we dropped the i superscript because we are considering a synchronous MC-CDMA system in this chapter. To solve the MUD problem in equation (4.4), we have to start by selecting the ACO parameters that fit the optimization problem in hand. The solution for the MUD problem in an MC-CDMA MUD system corresponds to a vector of length K ($\mathbf{b}_{opt}$). Like in DS-CDMA, each element of $\mathbf{b}_{opt}$ takes one out of M possible values, where M

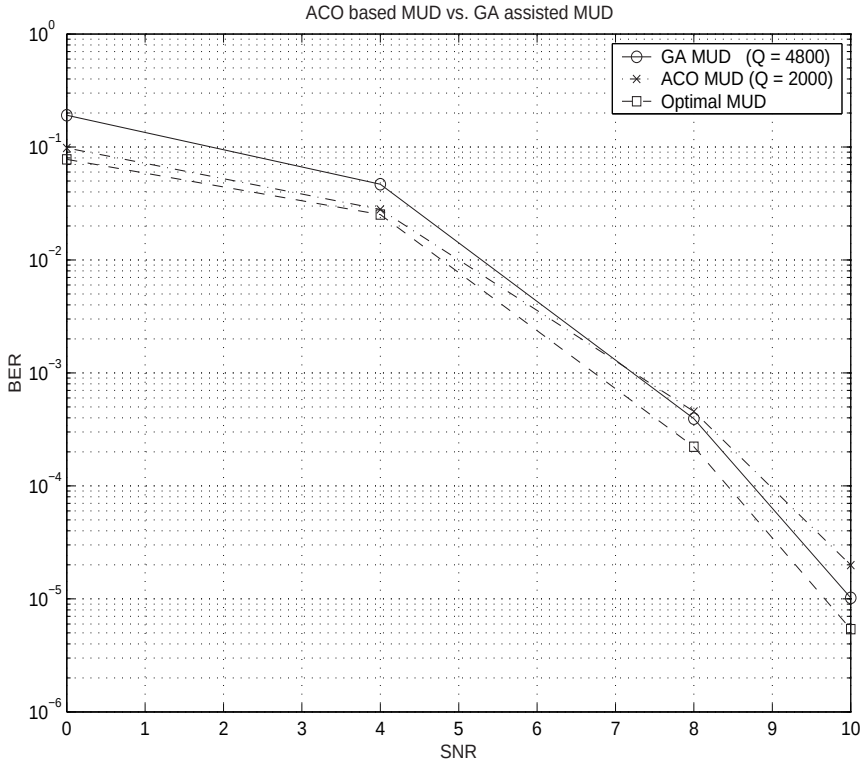

Figure 4.5: Performance of ACO based MUD versus GA assisted MUD; $\zeta = 31$ and $K = 20$

is the constellation size. In this work, we assume BPSK modulation. Therefore, M^K possible solutions exist (2^K for BPSK). In our ACO algorithm, every ant builds a solution vector in each iteration. This building process is accomplished via K jumps inside a $2 \times K$ table. The first row in this table represents an initial solution. The second row is merely the complement of the first row. Thus, any solution (out of the 2^K possible solutions) can be formed by selecting K elements from this table, one element from each column. Hence, in each jump, the ant selects (based on a desirability function and pheromone concentration) either the initial solution element or its complement. When employing higher order modulation schemes, the dimensions of solution table becomes $M \times K$ with the first row containing the initial solution and each column containing one of the remaining $M-1$ possible data symbols. Similar to the presented case which employs BPSK, the solution is formed by selecting a set of K elements, one from each column.

In single-user receivers, a suboptimal solution vector ($\mathbf{b}$) is created by performing hard decisions based on single user receiver outputs. In this work, we employ the output of the MRC based single user receiver as the initial solution vector (i.e.,$\mathbf{b} = \underset{\mathbf{b}\in\{\pm 1\}}{\operatorname{argmax}}\{\widetilde{\mathbf{C}}\mathbf{r}\}$) . In the ACO algorithm, all ants begin their search at a specific position along the ($\mathbf{b}$) vector. The ants cyclically move down the $\mathbf{b}$ vector, selecting the best element at each stage. The value of the element chosen by an ant is derived from the corresponding element values in either $\mathbf{b}$ or $\overline{\mathbf{b}}$ ($\overline{\mathbf{b}} = [\overline{b}_1 \overline{b}_2 \cdots \overline{b}_K]^T$ where $\overline{b}_l = +1$ if $b_l = -1$ and vice-versa $\forall\ l$). The desirability function is used to help the ant decide if a particular element value of the solution vector should come from $\overline{\mathbf{b}}$ instead of $\mathbf{b}$. Since the magnitude of the conventional single user receiver outputs provide a rough estimate of the quality of users' hard decisions, it is used in evaluating the desirability function of the ants. The desirability function for an ant starting at j^{th} element in the $\mathbf{b}$ vector is defined as:

$$D(j) = \frac{1}{2 + |R_j|} \tag{4.5}$$

where $R_j = \widetilde{\mathbf{C}}_j \mathbf{r}$ is the soft decision value of the j^{th} received data symbol. Equation (7.4) reflects the fact that when $R_j = 0$, b_j and $\overline{b}_j$ are equally likely to be chosen. As the ant moves

along the elements of the solution vector, the desirability function at the $(j+i)^{th}$ stage can be redefined as follows:

$$D(j+i) = \frac{1}{2 + |R_{j+i}| + \sum_{l \in P} |R_l|}. \tag{4.6}$$

where P is a set of positions where the ant had previously selected $\overline{\mathbf{b}}$ element values. The desirability function defined in Eqns.(7.4) and (4.6) ensure that an ant does not significantly deviate from the initial solution. For example, if an ant chooses the element value from $\overline{\mathbf{b}}$ at the j^{th} position, its desirability to select another element value from $\overline{\mathbf{b}}$ decreases. Therefore, ants' starting positions in a single iteration should be as far as possible from one another along the solution vector. It is also important to note that while restricting ants' movements to the vicinity of the initial solution is not a necessary operation, but it is useful when the reliability of initial data estimates is high.

The second challenge in designing an ACO based MUD algorithm, is to develop a meaningful pheromone deposition mechanism. In our algorithm, pheromones are deposited in a $2 \times K$ table where the first row corresponds to the elements of $\mathbf{b}$, and the second row corresponds to the elements of $\overline{\mathbf{b}}$. At the beginning of the search process, the pheromone table has equal amounts (unity) of pheromones in all of its entries. As the search progresses , pheromones are deposited and evaporated based on the path traversed by the ants. The deposition rate (DR) and evaporation rate (ER) are parameters of the ACO. In our algorithm, the DR and ER are inversely related to the number of iterations, V. At any stage during the search, the higher the pheromone value in an entry (in the pheromone table), the probability of selecting the corresponding element value from $\mathbf{b}$ or $\overline{\mathbf{b}}$ is greater. Since $Q(\mathbf{b})$ determines the quality of a solution, it is used to control the amount of pheromone deposition. Furthermore, we use the elitism philosophy in our pheromone deposition mechanism, i.e., only the ants that find good paths ("elite ant") are allowed to deposit pheromones. Furthermore, if ants find excessively poor solutions ("weak ant"), pheromones are removed from those paths.

Our complete ACO based MUD algorithm is summarized below:

- Create a $2 \times K$ pheromone table, $\tau \in \mathbb{R}^{2 \times K}$; $\tau(m,n) = 1 \ \forall \ m,n$ [pheromone values are

initialized]

- Set $\mathbf{b}_{elite} = \mathbf{b}$ where $\mathbf{b}_{elite}$ is the best solution found.
- for $iteration = 1 : V$, {

  1. Decide the starting positions for A ants

     $(st_1, st_2, \cdots st_A)$.

     for $move = 1 : K$, {

     (a) The i^{th} ant selects $\overline{\mathbf{b}}$ element values with probability

     $$\begin{aligned} p_{(i)}(move) &= \tau(2, (st_i + move)\text{mod}K) \\ &\quad \cdot D((st_i + move)\text{mod}K) \\ &\quad \forall i = 1, 2, \cdots A \end{aligned}$$

     This probability is evaluated for for all ants.

     (b) Store the selected elements in $\mathbf{b}_i \ \forall \ i = 1 \cdots N$ (note that $\mathbf{b}_i$ is the i^{th} ant's proposed solution vector).

     (c) The 2-dimensional indices of chosen locations in τ constitute the trail for each ant. Store the trail for the i^{th} ant in $Tr_i \in \mathbb{I}^{2 \cdots K} \forall \ i = 1 \cdots N$.

     – The 1^{st} row & 2^{nd} row of Tr_i represents row and column indexes of selected τ locations, respectively.

     }

  2. if $Q(\mathbf{b}_i) \geq S_E \cdot Q(\mathbf{b}_{elite})$ [Check for "elite" ants (note: S_E is a scale parameter denoting the threshold value for elite ants)]

     – Deposit pheromones:

     $$\begin{aligned} \tau(Tr_i(1,k), Tr_i(2,k)) &= \\ \tau(Tr_i(1,k), Tr_i(2,k)) + \triangle\tau &\ , \end{aligned}$$

     where $\triangle\tau = DR \cdot \frac{Q(\mathbf{b}_i)}{K}$

3. if $Q(\mathbf{b}_i) \leq S_W \cdot Q(\mathbf{b}_{elite})$ [Check for "weak" ants (note: S_W is a scale parameter denoting the threshold value for weak ants)]

   – Evaporate pheromones:

$$\tau Tr_i(1,k), Tr_i(2,k)) \quad =$$

$$\tau(Tr_i(1,k), Tr_i(2,k)) - \triangle\tau$$

4. Evaporate pheromones:

$$\tau(m,n) = \tau(m,n) \cdot (1 - ER) \forall m, n$$

5. if $Q(\mathbf{b}_i) > Q(\mathbf{b}_{elite})$ [Check if new solution is the elitist solution]

$$\mathbf{b}_{elite} = \mathbf{b}_i$$

}

- The final solution vector
  $\widehat{\mathbf{b}}_{ACO} = \text{argmax}\{Q(\mathbf{b}_{elite}), Q(\mathbf{b}_{ph})\}$ where $\mathbf{b}_{ph}$ is the trail with the highest pheromone concentration.

In order to compare the complexity of the ACO based MUD with the optimal MUD, we define the product $\Upsilon = A \cdot V$ as the order of the computational complexity of our algorithm (e.g., an ACO with 8 ants and 100 iterations result in a $\Upsilon = 800$).

4.3.1 Performance Results

We evaluate the ACO based MUD performance for a synchronous uplink MC-CDMA system uplink with: (1) $N = 16$ carriers; (2) $K = 16$ users; (3) Hadamard Walsh spreading codes; (4) BPSK modulation, and (5) four-fold frequency diversity. The following ACO parameters were employed: number of ants, $A = 8$; $V = 25$ ($\Upsilon = 200$) and $V = 100$ ($\Upsilon = 800$). Since the order of the complexity of this optimal MUD (employing BPSK modulation) is $2^{16} = 65636$, the savings in complexity for $V = 25$ and $V = 100$ are 99.7% and 98.7%, respectively.

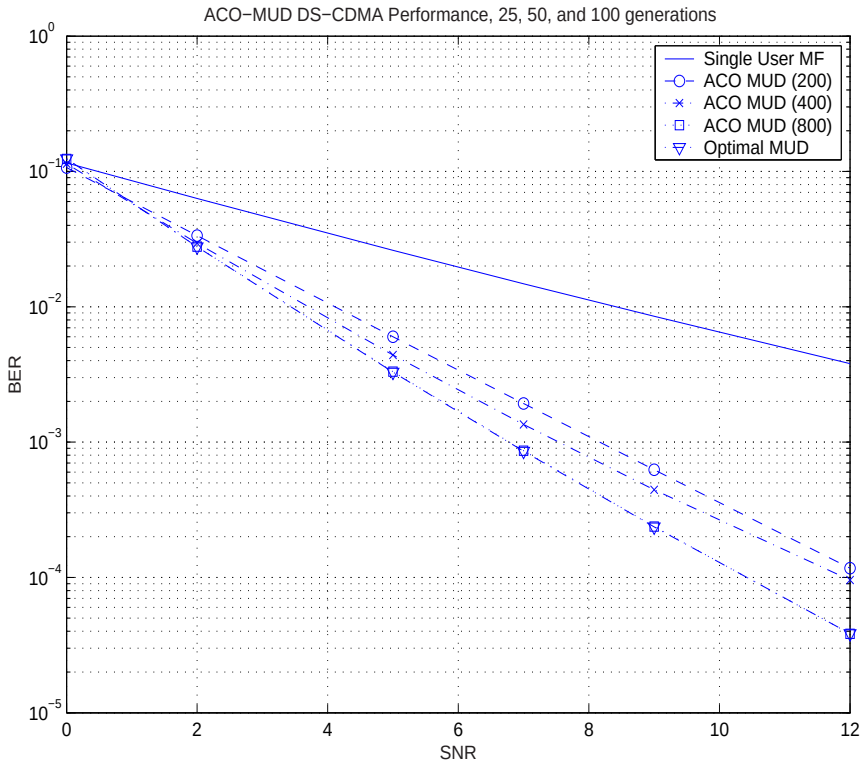

Figure 4.6: BER Performance versus SNR for MF and ACO-MUD, $\zeta = 15, K = 15$

Figure 4.7 presents four signal to noise ratio (SNR) vs. BER curves. The top most curve represents the maximum ratio combining (MRC) receiver BER performance. The remaining three curves show the performance of the optimal MUD and the performance of the ACO based MUD with $V = 25$ and $V = 100$. From Figure 4.7, it is evident that the MRC-based single user receiver has the worst performance. Furthermore, the ACO based MUDs approach the performance of the optimal MUD. Specifically, the ACO based MUD with $V = 100$ matches the performance of the optimal MUD. Moreover, it is possible to decrease the ACO complexity to $V = 25$ (by a factor of four versus the $V = 100$ case) and only suffer a 1 dB loss in performance at a BER of $4 \cdot 10^{-3}$. While the ACO approach significantly outperforms an exhaustive search technique, it is important to remember that the ACO based MUD requires additional memory to store pheromone table.

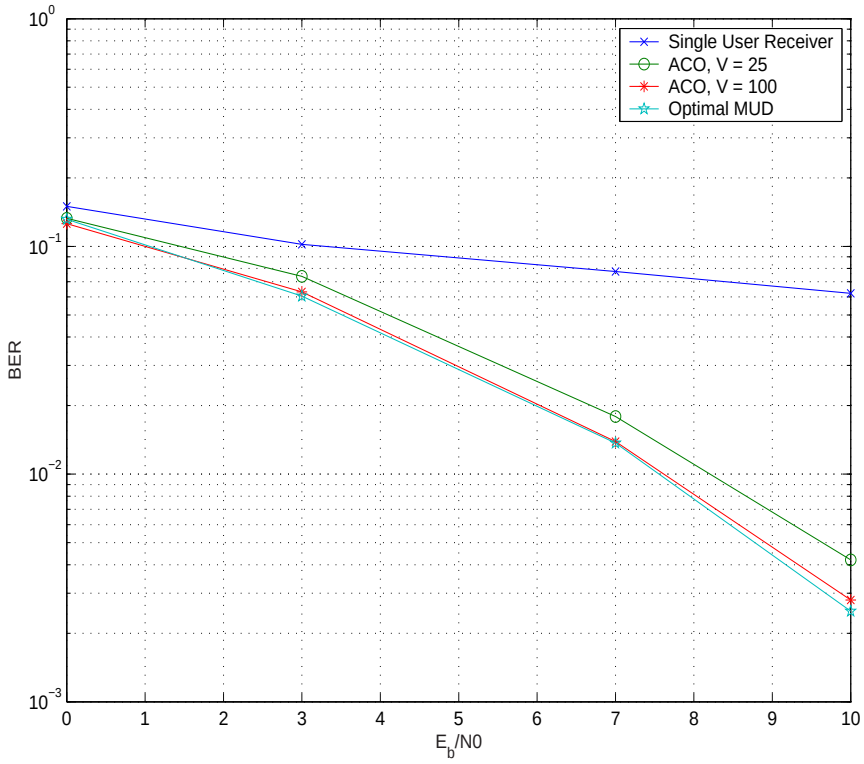

Figure 4.7: Performance of Single User Receiver, Optimal MUD, and ACO-based MUD

4.4 Conclusions

This work presents a novel low complexity algorithm that employs ACO to implement an optimal MUD for synchronous DS-CDMA systems and MC-CDMA synchronous up-link. To the best of authors' knowledge, this is the first attempt to apply swarm intelligence to MUD design. An optimal MUD based on exhaustive search suffers an exponential increase in complexity versus number of users. This increase in complexity makes the implementation of an optimal MUD receiver impractical. Here, we have developed an ACO based MUD for DS-CDMA systems that converges to the optimal BER performance in relatively few iterations providing 95% saving in computational complexity. Furthermore, this reduction in complexity is retained even while considering users with unequal received powers. It is also interesting to note that the ACO based MUD significantly outperforms GA-assisted MUDs and is far less complex to implement. In MC-CDMA systems, our ACO-based MUD matches the BER performance of the optimal MUD with more than 98% savings in terms of computational complexity. Moreover, we demonstrate that we can decrease the number of iterations in the ACO by a factor of four and only suffer a 1 dB performance loss relative to the optimal MUD. In summary, the ACO based receiver is a step towards realizing the dream of implementing an optimal low-complexity MUD.

Chapter 5

MUD for Asynchronous MC-CDMA

In the previous chapter, we addressed the MUD problem for synchronous MC-CDMA systems. However, in asynchronous setting, users' lack of alignment complicates the MC-CDMA receiver's design by increasing the amount of interference experienced by each user. The synchronicity assumption is valid in the downlink communication. While the uplink, where the MUD implementation is more feasible, is characterized by its asynchronous nature. The timing misalignment in asynchronous systems destroys orthogonality among subcarriers as well as between spreading codes. Consequently, this misalignment significantly degrades receiver's BER performance. For this reason, in this chapter, we present a novel multi-user-detector for asynchronous MC-CDMA systems. Previously proposed MUDs ([55]-[56]) for asynchronous MC-CDMA perform the detection for one user (desired user) at a time . Consequently, multiple runs of the algorithm are necessary to detect all users' symbols. Here, we present a MUD structure that detects all users' symbols simultaneously in one run by extending the receiver's integration window to capture the energy scattered in two consecutive symbol durations. We derive the optimal, decorrelator and minimum mean square error(MMSE) MUD for the extended window case. Our simulations demonstrate that the proposed MUD structure not only performs similar to a MUD that detects one user at a time, but its computational complexity is significantly lower.

This chapter is organized as follows; in Section 5.1 we introduce ant colony optimization.

Sections 5.2 and 5.3 presents ACO based MUD for synchronous DS-CDMA and MC-CDMA systems respectively. Finally, we summarize and conclude Section 5.4.

5.1 Introduction

Multi-user detection (MUD) techniques were proposed by Verdu [22] in order to effectively combat multi-user interference (MUI) in direct sequence code division multiple access (DS-CDMA) systems. Unlike single-user matched filter receivers that deal with MUI as additional noise terms, multiuser detectors jointly demodulate all users' symbols and have been proved to be the optimal reception technique for DS-CDMA systems in fading channels [22]. Optimal and sub-optimal MUDs [22] -[34] have also been investigated for MC-CDMA systems [14] - [19] . While single-user receiver performance in asynchronous MC-CDMA has been analyzed in [93] and [94], much of the prior work in MUDs is focused on downlink (forward link) communication where the users are synchronized. Given that MUDs are typically more complex to implement than single user receivers, their deployment at the base station is more practical than at the mobile. Therefore, it is critical to investigate the implementation of MUDs in the uplink (asynchronous transmission scenario). In Figure 5.1, it can be seen that in an asynchronous setting, joint demodulation of all users' symbols within one symbol interval T_s is much harder than it is in a synchronous system. For example, in a fully loaded system ($K = N$) the MUD must detect $2N - 1$ symbols utilizing N observations. Moreover, out of these $2N - 1$ symbols the receiver cannot provide a reliable estimate for more than one symbol/user at a time. This user is usually referred to as the desired user. In [94]-[48], the authors suggest several reception techniques for asynchronous MC-CDMA systems to achieve a satisfactory BER performance. However, in both [94] and [48] the authors focus on recovering a desired user's information. This limitation is a result of the fact that by synchronizing to a single desired user's signal only one symbol energy can be fully captured within one T_s observation time. Consequently, if all users' symbols are to be detected, several runs of the algorithm have to be performed.

In [42], Bar-ness proposed a partial sampling minimum mean square error (PS-MMSE) receivers for asynchronous (MC-CDMA) system under frequency-selective Rayleigh fading channel. Bar-ness suggested extending the observation time to $2T_s$. This extension of the observation time enables the receiver to capture the entire desired symbol energy without the knowledge of the starting point of the desired signal. However, similar to [94]-[48], the receiver proposed in [42] detects only one user's symbol (the desired user) at a time and requires multiple runs of the basic algorithm to detect all users' data. For example, in a system with K users, if the complexity of one run of the algorithm to find the i^{th} user symbol is χ, the computational

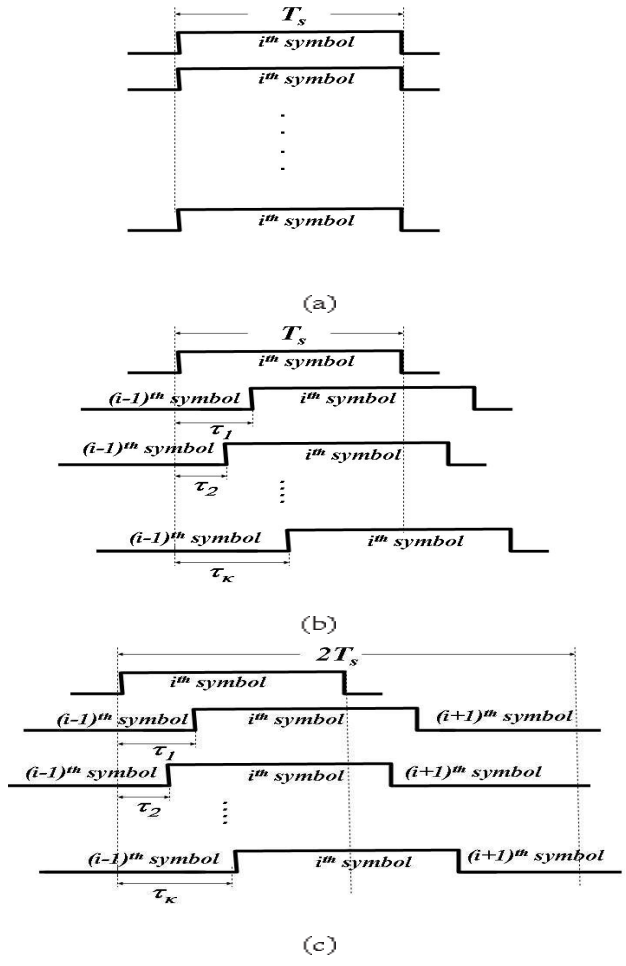

Figure 5.1: Observation window in (a) synchronous (b) asynchronous with one T_s observation window (c) proposed two T_s observation window

complexity to detect all users' symbols is $K \cdot \chi$.

In this chapter, we present a MUD structure that detects all users' symbols simultaneously in one run without specifying a desired user. The proposed structure is based on extending the observation time of the receiver to $2T_s$. In Figure 5.1(c) the difference between utilizing observation time of T_s and $2T_s$ is highlighted. It is evident that the i^{th} symbols' energy for all users is fully recovered when the observation time is extended to $2T_s$. This enables us to design a MUD for asynchronous MC-CDMA that is *not* limited to a desired user scenario and detects all users' symbols simultaneously. It is important to note that extending the observation time to $2T_s$ corresponds to considering two consecutive FFT outputs at the receiver in making decisions. To optimally detect these symbols, the receiver maximizes a cost function based on the maximum likelihood (ML) criterion. In this chapter, we first derive the optimal MUD based on the extended observation window. The optimal MUD receiver results in an NP-hard optimization problem with computational complexity that increases exponentially with the number of users and is prohibitive for practical implementation. Hence, there is a need to develop MUDs that exhibit good performance/complexity tradeoff. So, we derive and analyze linear decorrelator detector and minimum mean square error (MMSE) MUD for the extended observation window setting. Our simulation results indicate that the proposed structure significantly reduces computational complexity at the receiver without harming systems's BER performance. Specifically, for a system with 4 users and 8 sub-carriers, the amount of computations needed by the MMSE-MUD to recover the four users' symbols with the extended observation window is 4 times less than that needed for the MMSE-MUD employing one T_s window. This saving in complexity is achieved with either no or slight degradation in BER relative to a MMSE MUD employing a single T_s observation window.

5.2 Asynchronous MC-CDMA System Model

We consider an asynchronous uplink MC-CDMA system with N carriers and K users in a frequency selective channel. Typical to OFDM-based systems, we assume that carrier spacing $\Delta f = 1/T_s$ is much smaller than channel's coherence bandwidth. This assumption guarantees flat fading over each subcarrier while fading coefficients across different subcarriers of the same user maybe correlated as discussed in Section 2.3.1.2.

Figure 5.2(a) represents the asynchronous transmission model over a frequency-selective channel. Here, it can be seen that all users transmissions arrive at the base station with different delays ($[\tau_1, \tau_2, \cdots, \tau_K]$ where τ_k is the delay experienced by the k^{th} user) that are uniformly distributed in $[0, T_s]$. Consequently, the received signal is given by

$$r(t) = \sum_{i=-\infty}^{+\infty} \sum_{k=1}^{K} \sqrt{\frac{E_{bk}}{2}} b_k^{(i)} \sum_{n=1}^{N} h_{k,n} c_{k,n}^{i} e^{(j\frac{2\pi n}{T_s}(t+\tau_k))} P(t - iT_s - \tau_k) + n(t) \tag{5.1}$$

where E_{bk} is the k^{th} user symbol energy; $b_k^{(i)}$ is the i^{th} symbol of the k^{th} user (e.g., $b_k^{(i)} \in (1, -1), k = [1, .., K]$ if BPSK modulation is considered); $\mathbf{e}_k = [\varepsilon_{k,1}, \varepsilon_{k,2}, \cdots, h_{k,N}]^T$ is the k^{th} user spreading vector; T_s is the symbol duration; $P(t)$ is the symbol duration; $P(t)$ is a rectangular pulse function with additive white Gaussian noise (AWGN) with 0 mean and two sided power spectral density $N_0/2$.

Figure 5.2(b) shows the proposed receiver structure. Here, the received signal $r(t)$ is first decomposed into its N subcarrier components. Our proposed approach involves the extension of the integration time to $2T_s$. However, it is not practically feasible to increase the integration time to $2T_s$ in the front-end integrator block. This is because, in MC-CDMA and other OFDM-based systems, we employ a cyclic prefix in every transmitted symbol. Hence, we implement the $2T_s$ integration idea by concatenating two single T_s integrator outputs. This is illustrated in Figure 5.2(b), where a delay of T_s is incorporated to capture two successive front-end outputs. By extending the observation time window, we can successfully retrieve the i^{th} block energy of all users data. On the other hand, when one T_s observation window is used (Figure 5.1(a)), the receiver has to synchronize its observation window to one of the users' symbols (usually

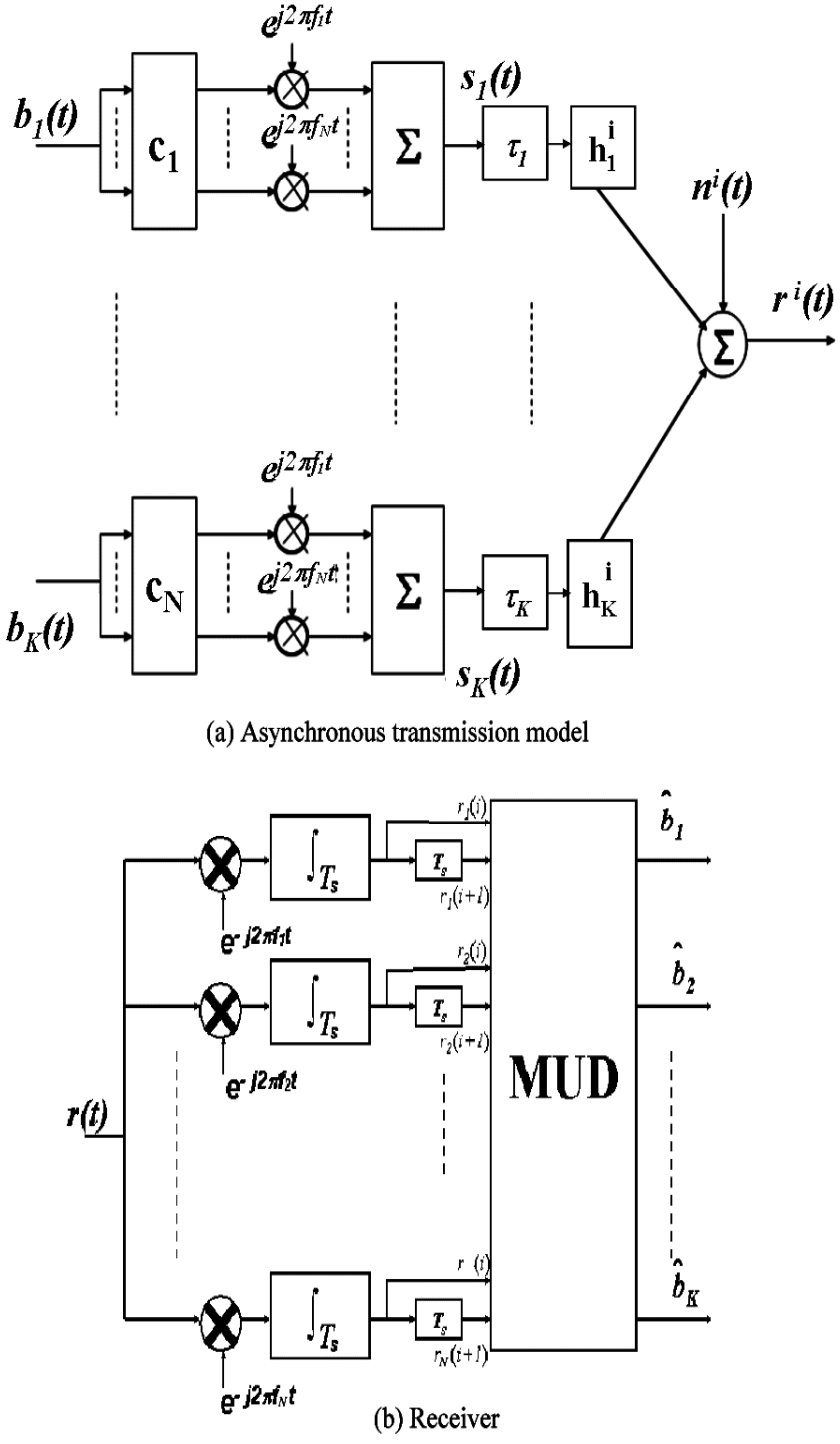

Figure 5.2: Transmitter and receiver for asynchronous MC-CDMA system

referred to as the "desired user"). While the receiver fully captures the desired user's symbol energy, other users' information (interfering users' symbols) are only captured partially. This

partial acquisition of the interfering users energy degrades receiver's ability to detect these users' symbols. In order to successfully detect all users' information symbols, repeated runs of the detection algorithm is required, with each run synchronized to one specific user. Therefore, if K users are active in a system, the MUD algorithm has to be executed K times to effectively detect all users' symbols. As will be seen next, extending the observation window enables the receiver to detect all users' symbols simultaneously without harming detected symbols reliability (no degradation in receiver's BER performance).

The i^{th} output of the front-end at subcarrier m correspond to

$$r_m(i) = \frac{1}{\sqrt{T_s}} \int_{iT_s}^{(i+1)T_s} r(t) e^{(-j\frac{2\pi m}{T_s}t)} dt = \sum_{k=1}^{K} [h_{k,m}^i b_k(i) + \overline{h}_{k,m}^{(i-1)} b_k(i-1)] + \eta_m(i),$$

where

$$\begin{aligned}
h_{k,m}^i &= \frac{1}{\sqrt{T_s}} \sum_{n=1}^{N} \sqrt{\frac{E_{bk}}{2}} h_{k,n} c_{k,n}^i e^{-j2\pi m\tau_k/T_s} \int_{\tau_k}^{T_s} e^{j2\pi(n-m)t/T_s} dt \\
&= \frac{1}{\sqrt{T_s}} \sum_{n=1}^{N} \sqrt{\frac{E_{bk}}{2}} h_{k,n} c_{k,n}^i e^{-j2\pi m\tau_k/T_s} e^{-j2\pi(n-m)(T_s-\tau_k)/2T_s} \\
&\quad \frac{\sin(2\pi(n-m)(T_s-\tau_k)/2T_s)}{2\pi(n-m)/2T_s} \\
\overline{h}_{k,n}^i &= \frac{1}{\sqrt{T_s}} \sum_{n=1}^{N} \sqrt{\frac{E_{bk}}{2}} h_{k,n} c_{k,n}^i e^{-j2\pi m\tau_k/T_s} \int_{0}^{\tau_k} e^{j2\pi(n-m)t/T_s} dt \\
&= \frac{1}{\sqrt{T_s}} \sum_{n=1}^{N} \sqrt{\frac{E_{bk}}{2}} h_{k,n} c_{k,n}^i e^{-j2\pi m\tau_k/T_s} e^{-j2\pi(n-m)\tau_k/2T_s} \\
&\quad \frac{\sin(2\pi(n-m)\tau_k/2T_s)}{2\pi(n-m)/2T_s} \\
\eta_n(i) &= \frac{1}{\sqrt{T_s}} \int_{iT_s}^{(i+1)T_s} n(t) e^{(-j\frac{2\pi m}{T_s}t)} dt
\end{aligned}$$

Combining the front end outputs during the i^{th} period results in a vector $\mathbf{r}(i) = [r_1(i), r_2(i), \cdots, r_N(i)]^T$ given by $\mathbf{r}(i) = \mathbf{E}^i\mathbf{b}(i) + \overline{\mathbf{E}}^{i-1}\mathbf{b}(i-1) + \eta(i)$. Similarly, considering the $(i+1)$ period, the $\mathbf{r}(i+1)$ vector corresponds to $\mathbf{r}(i+1) = \mathbf{E}^{i+1}\mathbf{b}(i+1) + \overline{\mathbf{E}}^i\mathbf{b}(i) + n(i+1)$

where

$$\begin{aligned}
\mathbf{E}^i = [\mathbf{e}_1^i, \mathbf{e}_2^i, \cdots, \mathbf{e}_K^i] \quad &; \quad \overline{\mathbf{E}}^i = [\overline{\mathbf{h}}_1^i, \overline{\mathbf{h}}_2^i, \cdots, \overline{\mathbf{h}}_K^i] \\
\mathbf{e}_k^i = [\varepsilon_{k,1}^i, \varepsilon_{k,2}^i, \cdots, \varepsilon_{k,N}^i]^T \quad &; \quad \overline{\mathbf{h}}_k^i = [\overline{\varepsilon}_{k,1}^i, \overline{\varepsilon}_{k,2}^i, \cdots, \overline{\varepsilon}_{k,N}^i]^T \\
\mathbf{b}(i) = [b_1(i), b_2(i), \cdots, b_K(i)]^T \quad &; \quad \eta(i) = [n_1(i), n_2(i), \cdots, n_N(i)]^T
\end{aligned} \tag{5.2}$$

In the remainder of this work, we assume perfect knowledge of the channel fades and delays at the receiver. Since, the goal of this chapter is to present the basic functionality of the new MUD structure, the simplifying assumptions will be later removed to show the effect of using noisy channel estimates.

The $\mathbf{r}(i)$ and $\mathbf{r}(i+1)$ can be stacked into one vector $\mathbf{r} = [\mathbf{r}(i)^T \ \mathbf{r}(i+1)^T]^T$, that correspond to

$$\mathbf{r} = \mathbf{A}\mathbf{b}(i-1) + \mathbf{B}\mathbf{b}(i) + \mathbf{C}\mathbf{b}(i+1) + n \tag{5.3}$$

where $\mathbf{A}$, $\mathbf{B}$ and $\mathbf{C}$ are $2N \times K$ matrices and there values are: $\mathbf{A}^T = [\mathbf{E}^{i-1^T} \ \mathbf{0}]$ where $\mathbf{0}$ is a $K \times N$ zeros matrix; $\mathbf{B}^T = [\overline{\mathbf{E}}^{i^T} \ \mathbf{E}^{i^T}]$ and $\mathbf{C}^T = [\mathbf{0} \ \overline{\mathbf{E}}^{(i+1)^T}]$. In the next section, we derive the optimal and the suboptimal MUD starting from equation (5.3).

5.3 MUD for Asynchronous MC-CDMA

5.3.1 Optimal MUD

From equation (5.3), the objective function of the optimum maximum likelihood (ML) MUD assuming $2T_s$ observation window can be easily shown to be

$$\hat{\mathbf{b}} = \underset{\hat{\mathbf{b}}(i-1), \hat{\mathbf{b}}(i), \hat{\mathbf{b}}(i+1)}{\operatorname{argmin}} \{\Omega(i)\} \tag{5.4}$$

where $\Omega(i) = \|\mathbf{r} - \mathbf{A}\mathbf{b}(i-1) - \mathbf{B}\mathbf{b}(i) - \mathbf{C}\mathbf{b}(i+1)\|^2$. Here $\|\cdot\|$ denotes the Euclidian norm of a complex quantity; and $\hat{\mathbf{b}} = [\hat{\mathbf{b}}(i-1)^T \hat{\mathbf{b}}(i)^T \hat{\mathbf{b}}(i+1)^T]^T$. Therefore, to mitigate the MUI and achieve the optimum performance, the receiver has to search all of the possible symbol sequences in order to find the sequence that minimizes the metric $\Omega(i)$. Searching for the

optimal solution of the MUD problem in (5.4) results in an NP-hard optimization problem [22]. The size of the search space increases exponentially with the number of users, K. Specifically, the search space corresponds to M^{3K} where M is the constellation size. Here we can see that complexity of the optimal MUD in asynchronous MC-CDMA is significantly higher than that of synchronous MC-CDMA. When perfect synchronization is assumed, the search space is exponentially related to K (i.e., M^K) instead of $3K$ [34]. Hence, the size of the search space for asynchronous MC-CDMA is M^3 times that of the synchronous one.

To reduce the search space in (5.4), we attempt to remove the effect of $\mathbf{b}(i-1)$ by using an estimate of $\mathbf{b}(i-1)$ ($\hat{\mathbf{b}}(i-1)$). This estimate $\hat{\mathbf{b}}(i-1)$ is based on the MUD outputs during the $(i-1)^{th}$ period. Although this is a suboptimal strategy, in high signal to noise ratio (SNR) scenario, we may argue that the $\hat{\mathbf{b}}(i-1)$ vector is very close to $\mathbf{b}(i-1)$. With this assumption, the size of the search space reduces to N^{2K}. An optimal mud that performers an exhaustive search over the N^{2K} space also suffers from prohibitive complexity (for large K). To address the complexity issue, the authors have recently proposed an ant-colony approach to implement the optimal MUD [34]. This approach exploits the foraging behavior of ants to help search for the optimal solution where a large discrete search space is involved. While we have not described the ACO approach in this chapter, readers are encouraged to read [34] for more information on this.

It is important to note that in this chapter, we assess receiver's performance based on its ability to detect $\hat{\mathbf{b}}(i)$ correctly. This is because at any time, the observation window completely captures *only* the i^{th} block symbol energy, while the $i-1$ and $i+1$ blocks' energies are recovered partially.

5.3.2 Decorrelator MUD

The big gap in performance and complexity between the single user and the ML-MUD is the motivation for other suboptimal MUDs that exhibit good performance/complexity tradeoff. Here, we present a causal and stable design of the decorrelator MUD for asynchronous MC-

CDMA with the extended observation window setting. To achieve this goal, we reformulate equation (5.3) as

$$\mathbf{r} \;=\; \mathbf{Q}\mathbf{b}+\mathbf{n} \quad \text{where} \quad \mathbf{Q}=\begin{bmatrix} \mathbf{E}^{(i-1)} & \overline{\mathbf{E}}^{i} & \mathbf{0} \\ \mathbf{0} & \mathbf{E}^{i} & \overline{\mathbf{E}}^{(i+1)} \end{bmatrix} \quad \text{and} \quad \mathbf{b}=[\mathbf{b}(i-1)^T\mathbf{b}(i)^T\mathbf{b}(i+1)^T]^T \tag{5.5}$$

Based on 5.5, the decorrelator can be defined as

$$\hat{\mathbf{b}} = \text{sign}(\mathbf{Q}^{\dagger}\mathbf{r}) \tag{5.6}$$

where $(\cdot)^{\dagger}$ represents the pseudo-inverse operation. We have to note that this decorrelator model is useful *only when* $K \leqslant \frac{2}{3}N$. Otherwise, the problem defined in (5.6) becomes under-determined and results in a high error-floor. To overcome this limitation, and to reduce problem's dimensionality, we attempt to cancel the interference caused by the symbols $(i-1)^{th}$ block. This cancelation is done by subtracting the $(i-1)^{th}$ block symbol estimates $\mathbf{E}^{(i-1)}\hat{\mathbf{b}}(i-1)$ from $\mathbf{r}$ resulting in $\grave{\mathbf{r}} = \mathbf{r} - \mathbf{A}\hat{\mathbf{b}}(i-1)$. Hence, we can rewrite the linear model as

$$\grave{\mathbf{r}} \;=\; \grave{\mathbf{Q}}\grave{\mathbf{b}}+\mathbf{n} \quad \text{where} \quad \grave{\mathbf{Q}}=\begin{bmatrix} \overline{\mathbf{E}}^{i} & \mathbf{0} \\ \mathbf{E}^{i} & \overline{\mathbf{E}}^{(i-1)} \end{bmatrix} \quad \text{and} \quad \grave{\mathbf{b}}=[\mathbf{b}(i)^T\mathbf{b}(i+1)^T]^T \tag{5.7}$$

Hence, decorrelator MUD can be defined as $\hat{\grave{\mathbf{b}}} = \text{sign}(\grave{\mathbf{Q}}^{-1}\grave{\mathbf{r}})$. This linear detector exhibits the same degree of near-far resistance as the ML-MUD but may result in noise amplification. The noise amplification problem can be combated using an MMSE MUD described below.

5.3.3 MMSE MUD

Assume that $\mathbf{D}$ is a noisy observation vector that can be modeled as $\mathbf{D} = \Lambda\mathbf{S} + \epsilon$, where $\mathbf{S}$ is the desired signal vector, Λ is a linear distortion, and ϵ represents additive noise. In this case, the best linear unbiased estimate (and is known as the MMSE estimate) of $\mathbf{S}$ is [89]

$$\hat{\mathbf{S}} = \mathbf{W}\mathbf{D} \quad \text{where} \quad \mathbf{W} = C\Lambda^H(\Lambda\mathbf{C}\Lambda^H + \mathbf{N})^{-1} \tag{5.8}$$

In (5.8), the $(\cdot)^H$ represents the hermitian operation; $\mathbf{C}$ is the covariance matrix of the desired signal (i.e.,$E[\mathbf{S}\ \mathbf{S}^H]$); and $\mathbf{N}$ is the noise covariance matrix (i.e.,$E[\epsilon\epsilon^H]$).

By direct substitution of the result in (5.8), the MMSE MUD for $\mathbf{b}$ based on the observation vector $\mathbf{r}$ (as defined in equation (5.5)) is $\hat{\mathbf{b}} = \text{sign}\{\mathbf{Mr}\}$ where $\mathbf{M} = \mathbf{Q}^H(\mathbf{QQ}^H + \sigma^2\mathbf{I})^{-1}$, where σ^2 is the noise variance, and $\mathbf{I}$ is the identity matrix. It is important to point that similar to the decorrelator defined in equation (5.6), the MMSE MUD here is useful only if the number of users K is less than 2/3 of the total number of carriers N. Whenever this condition is violated, the detector results in a high error floor.

Once again, by using the result in equation (5.8), the MMSE MUD based on the observation vector $\grave{\mathbf{r}}$ (defined in equation (5.7)) is $\hat{\grave{\mathbf{b}}} = \text{sign}\{\grave{\mathbf{M}}\grave{\mathbf{r}}\}$, where $\grave{\mathbf{M}} = \grave{\mathbf{Q}}^H(\grave{\mathbf{Q}}\grave{\mathbf{Q}}^H + \sigma^2\mathbf{I})^{-1}$.

5.4 Simulation Results

In this section, we evaluate and analyze the performance of the various MUD techniques presented in Section 5.3. In our simulations, we assume an asynchronous uplink MC-CDMA system with: (1) $N = 8$ carriers; (2) $K = 4$ or 6 users; (3) Hadamard Walsh spreading codes; (4) BPSK modulation; (5) transmission bandwidth that is four times the coherence bandwidth of the channel $B_c = 1/5\tau_{rms}$ [5] (i.e., $N/T_s = 4B_c$, which is equivalent to four-fold frequency diversity), and (6) slow fading channel where $f_{max} = 100$Hz. We also assume that the receiver is capable of estimating channel state perfectly. The reason for selecting smaller values of N and K is that the goal of this chapter is to introduce the potential of the proposed novel receiver architecture and not necessarily to mimic real system parameters.

Figures 5.3 and 5.4 provide two sets of BER versus SNR curves for asynchronous MC-CDMA uplink with 8 carriers and 4 users. The main difference between the two sets of curves is that the curves in Figure 5.4 corresponds to the case where the interference is reduced by subtracting the $(i-1)^{th}$ block symbol decisions (as discussed in Section 5.3). In both figures, the curves with squares placed over them represents the decorrelator MUD performance, and the curves with stars trace the MMSE MUD performance. To distinguish between the performances of the receivers with one T_s and two T_s observation windows, we use dashed lines for the extended

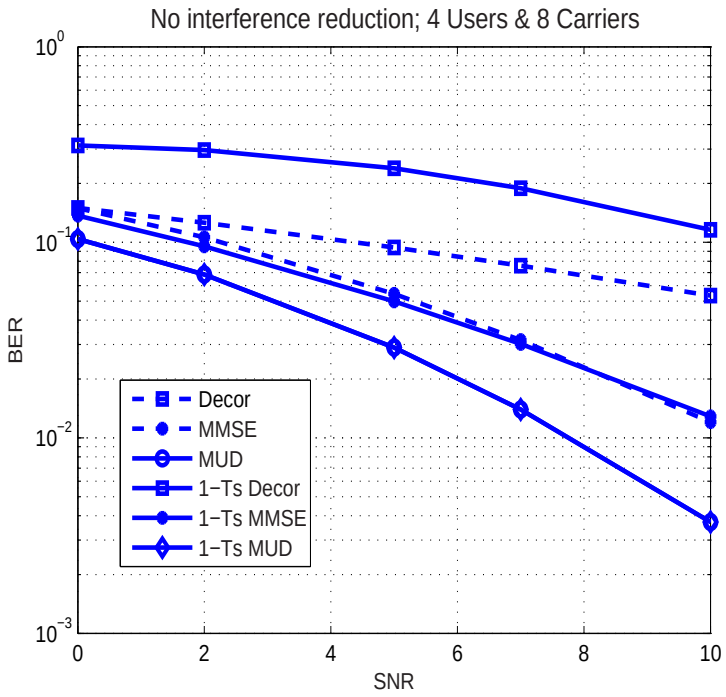

Figure 5.3: Performance of Asynchronous MC-CDMA, ($K = 4$, no interference reduction)

observation window case and solid line for the one T_s scenario. The curves with diamonds and circles superimposed on them represent the performance of the optimal ML MUD assuming one T_s and two T_s observation windows, respectively. In simulating the various MUDs with one T_s window, the first user is assumed to be the desired user, and consequently, the receiver is synchronized to this user's symbol arrival time (see Figure 5.1b). The plotted result represents the first user's (desired user) performance.

From Figures 5.3 and 5.4, it can be seen that extending the integration time does not degrade ML-MUD BER performance, and the big gap between the decorrelator and the optimal MUD performance is bridged using the MMSE MUD. Moreover, it is clear that canceling the interference caused by the $(i-1)^{th}$ block not only reduces the problem dimensionality (see Section 5.3) but also improves the receiver's BER performance. In Figures 5.3 and 5.4, the computational complexity for the decorrelator and the MMSE MUDs can be shown to be $\mathcal{O}(K^3)$ and $\mathcal{O}(K^4)$ for the extended observation window settings and in the one T_s case respectively.

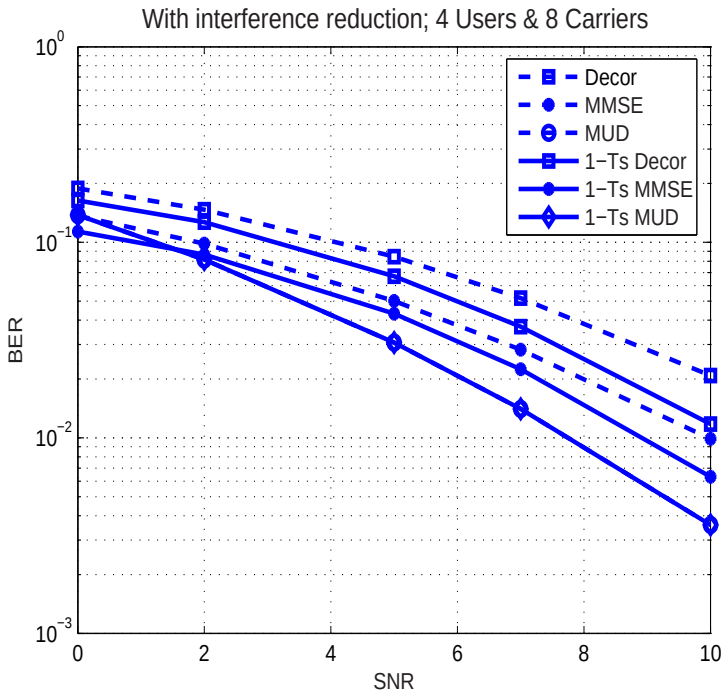

Figure 5.4: Performance of Asynchronous MC-CDMA, ($K = 4$, with interference reduction)

Consequently, the proposed MUD structure results in savings in computation at the receiver that is in the $\mathcal{O}(K)$. In the reduced interference scenario (Figure 5.4), the price to be paid for the saving in complexity is a slight degradation in receiver's BER performance (less than 1 dB the at 10^{-3} and 10^{-2} for both MMSE and Decorrelator MUDs, respectively). Without interference reduction (Figure 5.3), we observe no degradation in MMSE MUD BER performance while, the extended observation window based decorrelator outperforms the one employing one T_s integration time.

Figures 5.5 and 5.6 are provided to illustrate the effect of exceeding the $K = \frac{2}{3}N$ threshold discussed in Section 5.3. Here, the number of users K is set to 6 while $N = 8$. It can be seen that when the symbol estimates of the $(i-1)^{th}$ block are not subtracted, the receiver's performance hits an error-floor (around 10^{-4}) as expected. However, when the $(i-1)^{th}$ block symbols interference is canceled (in Figure 5.6), no error-floor is experienced as long as $K \leq N$.

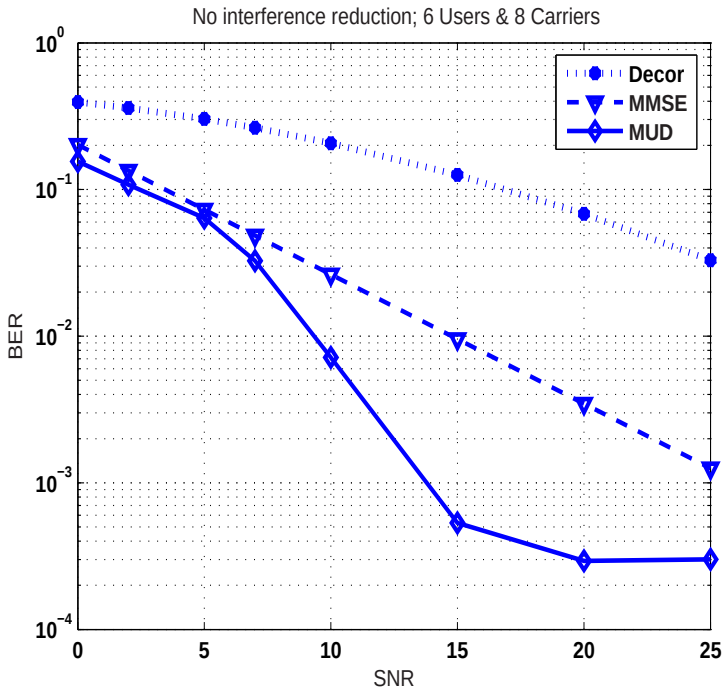

Figure 5.5: Performance of Asynchronous MC-CDMA, ($K = 6$, no interference reduction)

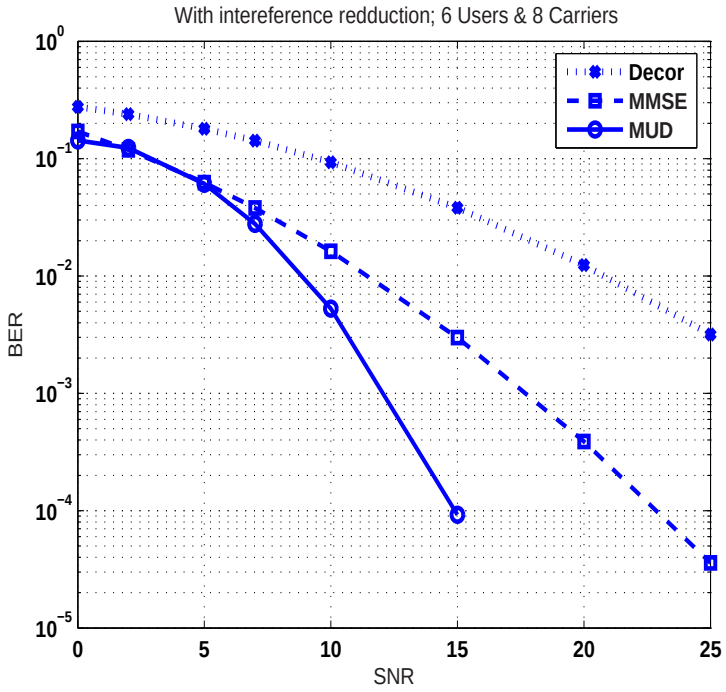

Figure 5.6: Performance of Asynchronous MC-CDMA, ($K = 6$, with interference reduction)

5.5 Conclusions

In this chapter, we present a novel MUD for asynchronous MC-CDMA that detects all users' symbols simultaneously in one run. The proposed structure is based on extending the observation time of the receiver to $2T_s$. The extension of the integration window enables the receiver to fully recover the i^{th} symbols' energy for all users (i.e., unlike prior work, the proposed MUD for asynchronous MC-CDMA is not limited to a desired user scenario and detects all users' symbols simultaneously). We derive the optimal, decorrelator and MMSE MUDs based on the extended observation window and present their performances in multipath fading channel. Our simulations demonstrate that the proposed structure is capable of reducing the computational complexity at the receiver while providing a comparable BER performance to that of a MUD employing a single T_s observation window.

Chapter 6

Modified MUD for Asynchronous MC-CDMA systems

In the previous chapter, we introduced a novel reception technique for an asynchronous MC-CDMA system. Specifically, we proposed doubling the integration window to fully capture all users' i^{th} block symbol' energy in one shot. While it is evident that extending the observation window reduces complexity, it degrades the performance of the linear multiuser detectors. Hence, there is a need for new methods to improve the performance of linear MUDs'.

In this chapter, we further analyze the linear receivers based on the extended observation window setting. In Section 6.1 we present an improved decorrelator. And in Section 6.3, we modify the MMSE receiver of Section 5.3.3 to reduce its complexity while maintaining its BER performance.

6.1 Modified Decorrelator-MUD for Asynchronous MC-CDMA

In Section 5.3.2, we presented a decorrelator detector for the extended observation window setting where the interference from the $(i-1)^{th}$ symbols is estimated and removed before

jointly detecting for the i^{th} symbols. Mathematically, this decorrelator detector has the form

$$\hat{\mathbf{b}} = \text{sign}(\grave{\mathbf{Q}}^{\dagger}\grave{\mathbf{r}}) \tag{6.1}$$

where $(\cdot)^{\dagger}$ represents the pseudo-inverse operation, and

$$\begin{aligned} \grave{\mathbf{r}} &= \begin{bmatrix} \grave{\mathbf{r}}_1 \\ \grave{\mathbf{r}}_2 \end{bmatrix} && (6.2) \\ &= \grave{\mathbf{Q}}\grave{\mathbf{b}} + \mathbf{n} && (6.3) \end{aligned}$$

where

$$\grave{\mathbf{Q}} = \begin{bmatrix} \overline{\mathbf{H}}^{i} & \mathbf{0} \\ \mathbf{H}^{i} & \overline{\mathbf{H}}^{(i+1)} \end{bmatrix}, \quad \grave{\mathbf{b}} = \begin{bmatrix} \mathbf{b}^{i} \\ \mathbf{b}^{i+1} \end{bmatrix}, \quad \text{and} \quad \mathbf{n} = \begin{bmatrix} n_1 \\ n_2 \\ \vdots \\ n_{2N} \end{bmatrix} \tag{6.4}$$

In short, the the decorrelating process is performed in two steps: inversion then projection. To analyze and understand the impact of the inversion process, we use the inverse of a conformably partitioned block matrix given by [95]

$$\begin{bmatrix} \mathbf{A}_{11} & \mathbf{A}_{12} \\ \mathbf{A}_{21} & \mathbf{A}_{22} \end{bmatrix}^{-1} = \begin{bmatrix} \mathbf{F}_{11}^{-1} & -\mathbf{A}_{11}\mathbf{A}_{12}\mathbf{F}_{22}^{-1} \\ -\mathbf{F}_{22}\mathbf{A}_{21}\mathbf{A}_{11} & \mathbf{F}_{22} \end{bmatrix} \tag{6.5}$$

where $\mathbf{F}_{11} = \mathbf{A}_{11} - \mathbf{A}_{12}\mathbf{A}_{22}^{-1}\mathbf{A}_{21}$ and $\mathbf{F}_{22} = \mathbf{A}_{22} - \mathbf{A}_{21}\mathbf{A}_{11}^{-1}\mathbf{A}_{12}$. Utilizing this result, the inverse of $\grave{\mathbf{Q}}$, in equation (6.4), can be written as

$$\begin{bmatrix} \overline{\mathbf{H}}^{i-1} & \mathbf{0} \\ -(\overline{\mathbf{H}}^{i+1})^{-1}\mathbf{H}^{i}(\overline{\mathbf{H}}^{i})^{-1} & (\overline{\mathbf{H}}^{i+1})^{-1} \end{bmatrix} \tag{6.6}$$

And consequently, the decorrelator estimate of the $\mathbf{b}^i$ vector corresponds to

$$\begin{aligned} \hat{\mathbf{b}}_1^i &= \overline{\mathbf{H}}^{i\ -1}\ \grave{\mathbf{r}}_1 && (6.7) \\ &= \mathbf{b}^i + \tilde{\mathbf{n}}_1 && (6.8) \end{aligned}$$

where $\tilde{\mathbf{n}}_1$ is a correlated noise victor such that $E[\tilde{\mathbf{n}}_1\ \tilde{\mathbf{n}}_1^H] = \mathbf{R}_D^1 = \begin{bmatrix} R_D^1(1,1) & \cdots & R_D^1(1,K) \\ \vdots & \ddots & \vdots \\ R_D^1(K,1) & \cdots & R_D^1(K,K) \end{bmatrix}$.

From equation (6.8), it is clear that in detecting the $\mathbf{b}^i$ vector, only the first integration window statistics are utilized. In other words, the decorrelator of equation (6.4) does not exploit the full energy of the i^{th} symbols available by doubling the observation window. Hence, to improve the decorrelator performance, the second period statistics should be incorporated in the decision making process for the $\mathbf{b}^i$ vector. To do so, we propose two approaches to incorporate the second period information in detecting the i^{th} block symbols: equal gain combining (EGC) and maximum ratio combining (MRC).

From equation 6.1 it is clear that $\grave{\mathbf{r}}_2$ can be expressed mathematically as

$$\grave{\mathbf{r}}_2 = \mathbf{H}^i\mathbf{b}^i + \overline{\mathbf{H}}^{i+1}\mathbf{b}^{i+1} + \mathbf{n}_2 \tag{6.9}$$

where $\mathbf{n}_2$ is an $N \times 1$ vector composed of the the $(N+1)^{th}$ to the $2N^{th}$ elements of $\mathbf{n}$

From equation (6.9), it can be seen that $\grave{\mathbf{r}}_2$ vector is composed of three components. The first component is $\mathbf{H}^i\mathbf{b}^i$ that holds the desired $\mathbf{b}^i$ symbols' energy in the second integration window. The second component of $\grave{\mathbf{r}}_2$ is $\overline{\mathbf{H}}^{i+1}\mathbf{b}^{i+1}$ which represents the interference from the $(i+1)^{th}$ block symbols. The last term in (6.9) represents the channel noise.

There are several ways to extract the $\mathbf{b}^i$ information from $\grave{\mathbf{r}}_2$. If the number of users K is less than half the number of carriers N (i.e., $K \leq N/2$), we can force the interference term in $\grave{\mathbf{r}}_2$ to zero by projecting it into the column's null space of $\overline{\mathbf{H}}^{i+1}$. Moreover, we can force our projection process to decorrelate the $\mathbf{b}^i$ elements by selecting the projection matrix $\mathbf{M}_1$ that satisfies $\mathbf{M}_1\mathbf{H}^i = \mathbf{I}_N$ while being in the column's null space of $\overline{\mathbf{H}}^{i+1}$ (i.e., $\mathbf{M}_1\overline{\mathbf{H}}^{i+1} = \mathbf{0}_N$). A simple procedure to find the the suitable projection matrix involves concatenating the two matrixes $\mathbf{H}^i$ and $\overline{\mathbf{H}}^{i+1}$ into a new matrix $\Theta = \begin{bmatrix} \mathbf{H}^i & \overline{\mathbf{H}}^{i+1} \end{bmatrix}$. The first N rows of Θ^{-1} form the projection matrix that we are looking for. To prove this result, let $\Theta^{-1} = \begin{bmatrix} \mathbf{M}_1 \\ \\ \mathbf{M}_2 \end{bmatrix}$ such that

$\mathbf{M}_1$ is the first K columns of Θ^{-1}, and $\mathbf{M}_2$ is last K columns of Θ^{-1}. Hence,

$$\begin{aligned}
\Theta^{-1}\Theta &= \mathbf{I}_{2N} \\
\begin{bmatrix} \mathbf{M}_1 \\ \mathbf{M}_2 \end{bmatrix} \begin{bmatrix} \mathbf{H}^i & \overline{\mathbf{H}}^{i+1} \end{bmatrix} &= \mathbf{I}_{2N} \\
\begin{bmatrix} \mathbf{M}_1\mathbf{H}^i & \mathbf{M}_1\overline{\mathbf{H}}^{i+1} \\ \mathbf{M}_2\mathbf{H}^i & \mathbf{M}_2\overline{\mathbf{H}}^{i+1} \end{bmatrix} &= \mathbf{I}_{2N} \qquad (6.10)
\end{aligned}$$

$$(6.11)$$

From equation (6.11), it can be seen that $\mathbf{M}_1\mathbf{H}^i = \mathbf{I}_N$ and $\mathbf{M}_1\overline{\mathbf{H}}^{i+1} = \mathbf{0}_N$. And consequently

$$\begin{aligned}
\hat{\mathbf{b}}_2^i &= \mathbf{M}_1\ \grave{\mathbf{r}}_2 \qquad (6.12) \\
&= \mathbf{b}^i + \tilde{\mathbf{n}}_2 \qquad (6.13)
\end{aligned}$$

where $\tilde{\mathbf{n}}_2$ is a correlated noise victor such that $E[\tilde{\mathbf{n}}_2\ \tilde{\mathbf{n}}_2^H] = \mathbf{R}_{ZF}^2 = \begin{bmatrix} R_{ZF}^2(1,1) & \cdots & R_{ZF}^2(1,K) \\ \vdots & \ddots & \vdots \\ R_{ZF}^2(K,1) & \cdots & R_{ZF}^2(K,K) \end{bmatrix}$.

Another way to estimate the i^{th} block symbols from the second integration period statistics is by evoking the Wiener filter criterion. This is applicable for all values of K less than or equal to N. To do so, we consider the $(i+1)^{th}$ interference term as an additional noise component. Mathematically, this corresponds to

$$\begin{aligned}
\hat{\mathbf{b}}_2^i &= \mathbf{M}^i{}_{MMSE}(2)\ \grave{\mathbf{r}}_{\mathbf{2}} \\
&= \mathbf{R}_{MMSE}^i\mathbf{b}^i + \mathbf{R}_{MMSE}^{i+1}\mathbf{b}^{i+1} + \tilde{\mathbf{n}}_{MMSE}(2) \qquad (6.14)
\end{aligned}$$

where $\mathbf{M}^i{}_{MMSE}(2) = \mathbf{H}^{iH}(\mathbf{H}^i\mathbf{H}^{iH} + \overline{\mathbf{H}}^{i+1}\overline{\mathbf{H}}^{i+1H} + \sigma^2\mathbf{I}_N)^{-1}$,

$\mathbf{R}_{MMSE}^i = \begin{bmatrix} R_{MMSE}^i(1,1) & \cdots & R_{MMSE}^i(1,K) \\ \vdots & \ddots & \vdots \\ R_{MMSE}^i(K,1) & \cdots & R_{MMSE}^i(K,K) \end{bmatrix}$, and $\tilde{\mathbf{n}}_{MMSE}(2)$ is a zero mean Gaussian noise with a correlation matrix

$\mathbf{R}_{MMSE}^2(2) = E[\tilde{\mathbf{n}}_{MMSE}(2)\ \tilde{\mathbf{n}}_{MMSE}^H(2)] = \begin{bmatrix} R_{MMSE}^2(1,1) & \cdots & R_{MMSE}^2(1,K) \\ \vdots & \ddots & \vdots \\ R_{MMSE}^2(K,1) & \cdots & R_{MMSE}^2(K,K) \end{bmatrix}$.

Now, after extracting the i^{th} block symbols energy from the two integration periods, it is mandatory to combine $\hat{\mathbf{b}}_1^i$ and $\hat{\mathbf{b}}_2^i$ to form an estimate for the i^{th} block symbols $\hat{\mathbf{b}}^i$. Incorporating the two integration windows' statistics in estimating $\hat{\mathbf{b}}^i$ can be achieved via several methods. Here we focus our attention on EGC and MRC.

6.1.1 Equal Gain Combining

In EGC we combine $\hat{\mathbf{b}^i}_1$ and $\hat{\mathbf{b}}_2^i$ directly by summing the two without weighting (i.e., $\hat{\mathbf{b}}^i = \hat{\mathbf{b}}_1^i + \hat{\mathbf{b}}_2^i$). It is clear that this method of combining is quiet simple to implement. However, it can be easily shown that this method of combining could degrades receiver's ability to detect some user's symbol. To better understand this problem, let us consider a case in which the k^{th} user experience a relatively small asynchronicity (i.e., $\tau_k \ll T_s$). In this scenario, the first integration window estimate of the k^{th} user's symbol $\hat{b}_{k,1}^i$ experiences a much higher SNR than the second window estimate $\hat{b}_{k,2}^i$. Consequently, summing the two windows' estimates without weighting them results in $\hat{b_k}^i = \hat{b}_{k,1}^i + \hat{b}_{k,2}^i$ that experiences a degraded SNR relative to $\hat{b_{k1}}^i$. For this reason, it is mandatory to properly weight the two windows' estimates before combining them. In the next section, we analyze MRC in which the two windows' estimates $\hat{b}_{k,1}^i$ and $\hat{b}_{k,2}^i$ are scaled before adding them.

6.1.2 Maximum Ratio Combining

Maximum Ratio Combining (MRC) is one of the most common linear combining techniques. In MRC, the combiner weights are chosen to maximize the output SNR. For any set of signals of the form $y_l = a_l x + \iota_l + \eta_l$ where a_l is a constant, x is the desired signal, ι_l and η_l are the interference and the noise terms respectively. The MRC weights w_l that maximizes the SNR of

$$\sum_l w_l y_l$$

are shown to be [14]

$$w_l = \frac{E[x\overline{y}_l]}{\text{var}[\iota_l + \eta_l]}.$$

Utilizing this results, the MRC weights to combine the $\hat{b}^i_{k,1}$ and $\hat{b}^i_{k,2}$ are

$$w^i_D(1) = \frac{1}{\sigma^2 R^1_D(i,i)} \tag{6.15}$$

$$w^i_{ZF}(2) = \frac{1}{\sigma^2 R^2_{ZF}(i,i)} \tag{6.16}$$

However, if $\hat{\mathbf{b}}^i_2$ of equation (6.14) is used instead (i.e., the $\mathbf{M}^i_{MMSE}(2)$ matrix is used in generating the i^{th} block symbols' estimates out of the second window statistics), w^i_2 in equation (6.16) becomes

$$w^i_{MMSE}(2) = \frac{R^i_{MMSE}(i,i)}{\sum_{\substack{j=1 \\ j\neq i}}^{K} |R^i_{MMSE}(i,j)|^2 + \sum_{j=1}^{K} |R^{i+1}_{MMSE}(i,j)|^2 + \sigma^2 R^2_{MMSE}(i,i)} \tag{6.17}$$

6.2 Simulation Results

To highlight the difference in performance between the various approaches presented in this section, we simulate an asynchronous MC-CDMA system with 4 users (i.e., $K = 4$) and 8 carriers (i.e., $N = 8$) transmitting over a fading channel. Specifically, we assume that the system bandwidth is four times the channel coherence bandwidth.

Figure 6.1 presents five curves. The top three curves represents zero forcing with EGC, typical decorrelator and Wiener filter with EGC performance respectively. It is too important to recall that the EGC is used here to combine the decorrelator outputs with the zero forcing output or the winer filter outputs of the second integration window. The bottom two curves represent the performance when MRC is used.

It is clear from Figure 6.1 that incorporating the second integration window statistics can improve the decorrelator MUD performance. Specifically, MRC has been shown to be a good choice to improve the decorrelator MUD performance in the extended observation window setting. However, we have to keep in mind that the price to be paid for this improvement in performance, is an increase in receiver's complexity.

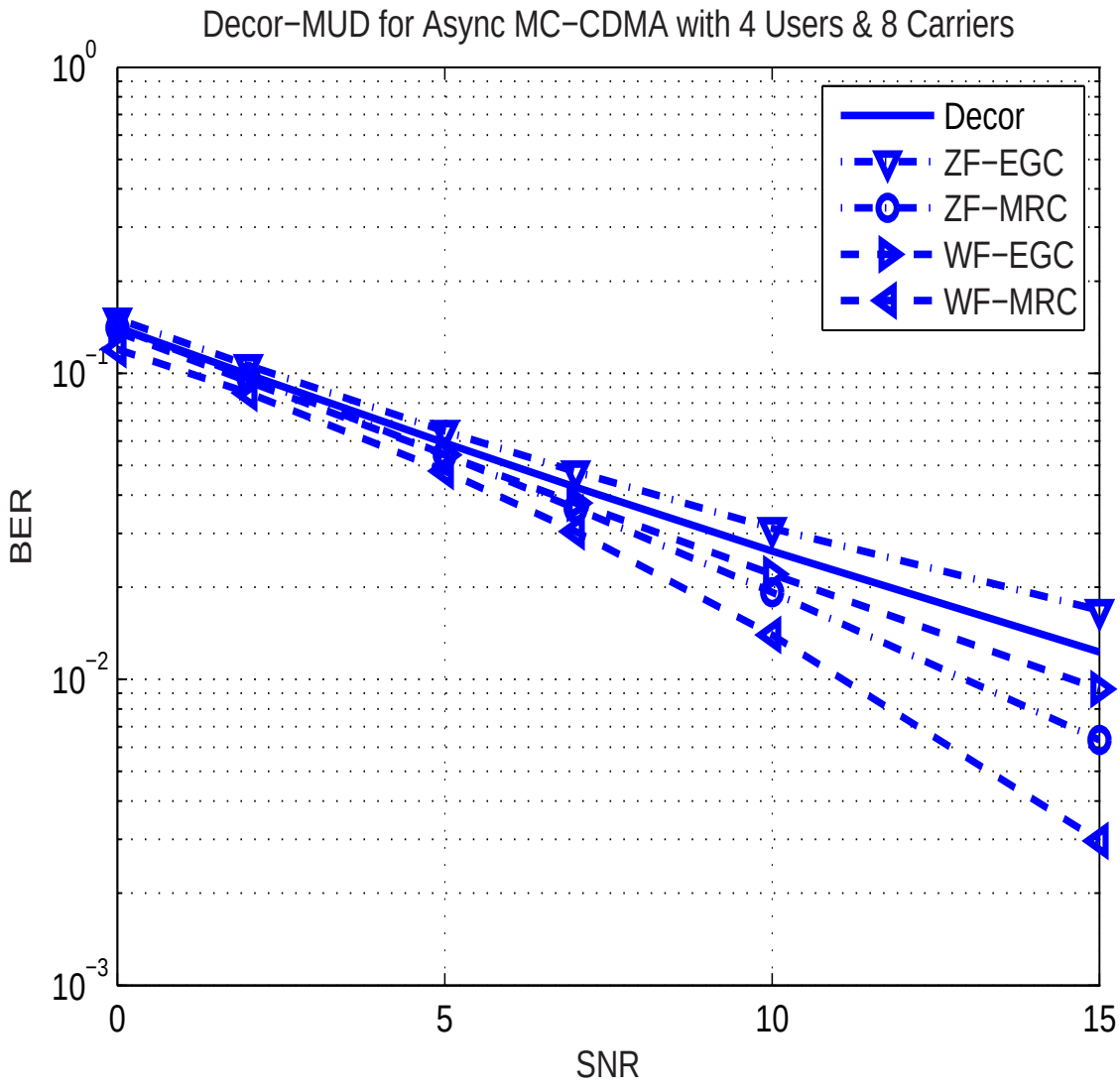

Figure 6.1: Proposed modified decorrelators' performances.

6.3 Modified MMSE-MUD for Asynchronous MC-CDMA

In the previous chapter, we presented the optimal linear detector for the extended observation window setting in Section 5.3.3. In the extended observation window setting the receiver utilizes two consecutive integration windows statistics ($\grave{\mathbf{r}}^i$ and $\grave{\mathbf{r}}^{i+1}$) which corresponds to

$$\grave{\mathbf{r}} = \begin{bmatrix} \grave{\mathbf{r}}_1 \\ \grave{\mathbf{r}}_2 \end{bmatrix} \tag{6.18}$$

$$= \grave{\mathbf{Q}}\grave{\mathbf{b}} + \mathbf{n} \tag{6.19}$$

where

$$\grave{\mathbf{Q}} = \begin{bmatrix} \overline{\mathbf{H}}^i & \mathbf{0} \\ \mathbf{H}^i & \overline{\mathbf{H}}^{(i+1)} \end{bmatrix}, \quad \text{and} \quad \grave{\mathbf{b}} = \begin{bmatrix} \mathbf{b}^i \\ \mathbf{b}^{i+1} \end{bmatrix} \tag{6.20}$$

The MMSE-MUD for the extended observation window setting corresponds to

$$\mathbf{b}^{\mathbf{i}}_{\mathbf{MMSE}} = \text{sign}(\mathbf{M}^i{}_{MMSE}\grave{\mathbf{r}}) \tag{6.21}$$

where $\mathbf{M}^i{}_{MMSE} = \grave{\mathbf{Q}}'(\grave{\mathbf{Q}}\grave{\mathbf{Q}}' + \sigma^2\mathbf{I}_{2N})^{-1}$. On the there hand, when the only one integration window (i.e, the i^th integration period) is used instead, the MMSE-MUD has the form

$$\mathbf{b}^{\mathbf{i}}_{\mathbf{MMSE}} = \text{sign}(\overline{\mathbf{H}}^{\mathbf{i}'}(\overline{\mathbf{H}}^{\mathbf{i}}\overline{\mathbf{H}}^{\mathbf{i}'} + \sigma^2.\mathbf{I}_N)^{-1}\grave{\mathbf{r}}_{\mathbf{1}}) \tag{6.22}$$

From equation (6.21), it is clear that extending the integration window increases the dimensionality of the problem (i.e., doubles the size of the matrix used in describing the linear model). From equations (6.21) and (6.22), it can be seen that solving the MMSE-MUD problem involves matrix inversion. The increase in the problem dimensionality by extending the observation window, increases the MMSE-MUD complexity (of equation (6.21) over that of equation (6.22)) by a factor of 8. In this section, we exploit the block nature of the $\grave{\mathbf{Q}}$ matrix to limit the MMSE-MUD problem complexity for the extended observation window setting.

Equation (6.11) provides a direct way to break down the inversion of a conformably partitioned block matrices. This method can be used in simplifying the MMSE-MUD problem.

By direct implementation of the result in equation (6.11),

$$\grave{\mathbf{Q}}'\left(\grave{\mathbf{Q}}\grave{\mathbf{Q}}'+\sigma^2\mathbf{I}\right)^{-1} = \begin{bmatrix} \overline{\mathbf{H}}^{i} & \mathbf{0} \\ \mathbf{H}^{i} & \overline{\mathbf{H}}^{(i+1)} \end{bmatrix}' \begin{bmatrix} \overline{\mathbf{H}}^{i}\overline{\mathbf{H}}^{i'}+\sigma^2\mathbf{I} & \mathbf{0} \\ \mathbf{H}^{i}\overline{\mathbf{H}}^{i'} & \mathbf{H}^{i}\mathbf{H}^{i'}+\overline{\mathbf{H}}^{i+1}\overline{\mathbf{H}}^{i+1'}+\sigma^2\mathbf{I} \end{bmatrix}^{-1}$$

$$= \begin{bmatrix} \mathbf{R} & \mathbf{S} \\ \mathbf{T} & \mathbf{U} \end{bmatrix} = \begin{bmatrix} \overline{\mathbf{H}^{i'}} & \mathbf{H}^{i'} \\ \mathbf{0} & \mathbf{C}' \end{bmatrix} \begin{bmatrix} \mathbf{B11} & \mathbf{B12} \\ \mathbf{B21} & \mathbf{B22} \end{bmatrix}. \tag{6.23}$$

(6.24)

where $\mathbf{B11} = \left(\overline{\mathbf{H}}^{i}\overline{\mathbf{H}}^{i'}+\sigma^2\mathbf{I}-\overline{\mathbf{H}}^{i}\mathbf{H}^{i'}\left(\mathbf{H}^{i}\mathbf{H}^{i'}+\overline{\mathbf{H}}^{i+1}\overline{\mathbf{H}}^{i+1'}+\sigma^2\mathbf{I}\right)^{-1}\mathbf{H}^{i}\overline{\mathbf{H}}^{i'}\right)^{-1}$,

$\mathbf{B12} = -\left(\overline{\mathbf{H}}^{i}\overline{\mathbf{H}}^{i'}+\sigma^2\mathbf{I}-\overline{\mathbf{H}}^{i}\mathbf{H}^{i'}\left(\mathbf{H}^{i}\mathbf{H}^{i'}+\overline{\mathbf{H}}^{i+1}\overline{\mathbf{H}}^{i+1'}+\sigma^2\mathbf{I}\right)^{-1}\mathbf{H}^{i}\overline{\mathbf{H}}^{i'}\right)^{-1}\left(\overline{\mathbf{H}}^{i}\mathbf{H}^{i'}\right)$
$\left(\mathbf{H}^{i}\mathbf{H}^{i'}+\overline{\mathbf{H}}^{i+1}\overline{\mathbf{H}}^{i+1'}+\sigma^2\mathbf{I}\right)^{-1}$,

$\mathbf{B21} = -\left(\mathbf{H}^{i}\mathbf{H}^{i'}+\overline{\mathbf{H}}^{i+1}\overline{\mathbf{H}}^{i+1'}+\sigma^2\mathbf{I}\right)^{-1}\mathbf{H}^{i}\overline{\mathbf{H}}^{i'}$
$\left(\overline{\mathbf{H}}^{i}\overline{\mathbf{H}}^{i'}+\sigma^2\mathbf{I}-\overline{\mathbf{H}}^{i}\mathbf{H}^{i'}\left(\mathbf{H}^{i}\mathbf{H}^{i'}+\overline{\mathbf{H}}^{i+1}\overline{\mathbf{H}}^{i+1'}+\sigma^2\mathbf{I}\right)^{-1}\mathbf{H}^{i}\overline{\mathbf{H}}^{i'}\right)^{-1}$, and

$\mathbf{B22} = \left(\mathbf{H}^{i}\mathbf{H}^{i'}+\overline{\mathbf{H}}^{i+1}\overline{\mathbf{H}}^{i+1'}+\sigma^2\mathbf{I}\right)^{-\mathbf{1}}+\left(\mathbf{H}^{i}\mathbf{H}^{i'}+\overline{\mathbf{H}}^{i+1}\overline{\mathbf{H}}^{i+1'}+\sigma^2\mathbf{I}\right)^{-\mathbf{1}}$
$\overline{\mathbf{H}}^{i}\mathbf{H}^{i'}\left(\overline{\mathbf{H}}^{i}\overline{\mathbf{H}}^{i'}+\sigma^2\mathbf{I}-\overline{\mathbf{H}}^{i}\mathbf{H}^{i'}\left(\mathbf{H}^{i}\mathbf{H}^{i'}+\overline{\mathbf{H}}^{i+1}\overline{\mathbf{H}}^{i+1'}+\sigma^2\mathbf{I}\right)^{-\mathbf{1}}\mathbf{H}^{i}\overline{\mathbf{H}}^{i'}\right)^{-1}\overline{\mathbf{H}}^{i}\mathbf{H}^{i'}$
$\left(\mathbf{H}^{i}\mathbf{H}^{i'}+\overline{\mathbf{H}}^{i+1}\overline{\mathbf{H}}^{i+1'}+\sigma^2\mathbf{I}\right)^{-\mathbf{1}}$

Using the $\mathbf{R}$ and $\mathbf{S}$ matrices from equation (6.23), it can be easily shown that

$$\mathbf{b^{i}_{MMSE}} = \mathbf{Rr_1}+\mathbf{Sr_2} \tag{6.25}$$

Further matrix manipulations of the result in (6.23) results in

$$\begin{aligned} \mathbf{b}^{i}_{MMSE} &= [\mathbf{I}-\sigma^2\overline{\mathbf{H}}^{i^{-1}}]\mathbf{Fr}_1 \\ &+ [\mathbf{H}^{i^H}[\mathbf{H}^{i}\mathbf{H}^{i^H}+\overline{\mathbf{H}}^{i+1}\overline{\mathbf{H}}^{i+1^H}+\sigma^2\mathbf{I}]^{-1}\sigma^2\mathbf{I}]^{-1} \\ &\quad [\mathbf{I}+\mathbf{H}^{i}]]\overline{\mathbf{H}}^{i}\mathbf{H}^{i'}[\mathbf{H}^{i}\mathbf{H}^{i^H}+\overline{\mathbf{H}}^{i+1}\overline{\mathbf{H}}^{i+1^H}+\sigma^2\mathbf{I}]^{-1}\mathbf{r}_2 \end{aligned} \tag{6.26}$$

where $\mathbf{F} = [\overline{\mathbf{H}}^{i}\overline{\mathbf{H}}^{i^H}+\sigma^2\mathbf{I}-\overline{\mathbf{H}}^{i}\mathbf{H}^{i^H}[\mathbf{H}^{i}\mathbf{H}^{i^H}+\overline{\mathbf{H}}^{i+1}\overline{\mathbf{H}}^{i+1^H}+\sigma^2\mathbf{I}]^{-1}\mathbf{H}^{i}\overline{\mathbf{H}}^{i^H}]$. Here, to perform the MMSE-MUD process we needed to invert three $N \times N$ matrices. In this way, we save more than half (57.14%) of the computation complexity of the MMSE-MUD as provided in equation 6.21.

6.4 Summary

Here, we present modified linear receivers for the extended observation window setting. Specifically, we analyze and adjust the decorrelator detector of Section 5.3.2 to better exploit the additional information made available by extending the observation window. The proposed adjustment have been shown capable of improving the Decorrelator MUD BER performance significantly. Moreover, we present a simplified MMSE-MUD that reduces the computational complexity of the MMSE-MUD of Section 5.3.3 without any degradation in its performance.

Chapter 7

Multicarrier Implementation of Single-carrier Systems

In this chapter, we propose a new multi-carrier platform to optimize the efficiency of wireless operators' licensed bands *and* to enable flexible sharing of licensed and unlicensed bands (in different spectral regions). This research supports a recent FCC proposal which goes beyond suggesting improved spectral efficiency, and instead suggests innovative spectrum management regulations. Specifically, this work presents a multi-carrier platform capable of (1) achieving high spectral efficiency by application of "narrow" orthogonal carriers; *and* (2) enables flexible spectral sharing across different licensed and unlicensed bands via operator borrowing/ lending. Moreover, For the first time, we apply the MUD idea to multicarrier implementation of single carrier systems incorporating the novel MUD schemes in Chapter 3 as a multi-symbol detection in CI-CDMA systems. This improvement in receiver design further illustrates the advantages of the proposed multicarrier platform.

The chapter is organized as follows. Section 7.2 provides a brief summary of the FCC recommendation in [96]. Section 7.3 introduces a novel spectrum allocation model that serves as an enabler to the FCC recommendations. And in Section 7.3 detail a multi-carrier platform that is capable of meeting the FCC requests. Moreover, in Section 7.3 we analyze the spectral

sharing capabilities of the new platform. Finally, Section 7.4 presents introductory performance results that demonstrate the potential of the proposed system and Section 7.5 concludes our work.

7.1 Introduction

In a recent proposal [96], the FCC (Federal Communications Commission) strongly suggests that a number of innovative regulations may soon be applied to manage the electromagnetic spectrum. These regulations will radically redefine the spectral landscape, allowing each operator far more freedom to operate in their own licensed bands, and requiring cooperation between operators (e.g., in adjacent bands) [96]. The aim of these future regulations is to improve spectral efficiency by removing rigid requirements on spectral allocation, ushering in a new era of "spectral freedom". The intention is that of increased cooperation among companies to (1) reduce resource wastage e.g., elimination of "white spaces" (unused or highly underused bands), and (2) to allow for faster and far more flexible spectral assignment.

It is the contention of the FCC itself that the current spectrum management structure is cumbersome and creates excessive delays in frequency allocation and re-assignment of bands to new operators. In short, the current regulations lead to high inefficiency. The FCC has focused on two main sources of the problems that it seeks to eliminate; the lack of freedom in employing licensed bands (e.g., the ability to introduce new and efficient techniques) and the rigid structure of spectral allocations which restrict both usage and time-sharing.

In this chapter, the authors introduce a multi-carrier platform based on our early research of [97], [98]-[99], which can serve as an important physical layer "enabler" to future FCC policy. Our multi-carrier platform is intended to: (1) provide high spectral efficiency (i.e., large bit/s/Hz) in each spectral band; (2) enable efficient sharing of wireless spectrum across different channels in the same band and/or across different bands; and (3) maintain low interference among adjacent systems.

Specifically, we propose a multi-carrier implementation of TDMA and DS-CDMA (similar to OFDM and MC-CDMA) using carrier interferometry ([97]-[99]) pulse shape and chip shape, respectively. We demonstrate that the CI approach not only enhances performance and capacity/throughput of DS-CDMA and TDMA systems, but also enables these systems to operate over non-contiguous spectral bands. Therefore, spectral sharing among CI-based TDMA or DS-CDMA systems is easily implemented via exchange of carriers constituting the CI pulse shape or chip shape. Using an example of two companies with different user loads, we demonstrate the improvement in Bit Error Rate (BER) performance and capacity achieved by employing different spectral sharing strategies. Furthermore, we also illustrate the ability of CI-based CDMA systems to support transmissions with different power levels in different sub bands within the total transmission bandwidth. This enables CI-based systems to maintain low interference while coexisting with other wireless systems in the same spectral band.

7.2 The FCC Spectrum Policy Report

In November 2002, the FCC released a report generated by the Spectrum Policy Task Force [96] in response to the growing demand for more up-to-date regulation – regulation that reshapes traditional models of spectral allocation and control. Operators were complaining about the ever-increasing time gap between filing and actual assignment of bandwidth. Moreover, engineers were pushing for technology upgrades that ensured increased resistance against RF (Radio Frequency) interference, while the FCC was assessing interference using out-dated techniques. Finally, measures of spectrum usage revealed the presence of various "white spaces", i.e. spectral regions that are underused or not used at all for long periods of time. All these factors motivated the creation of an FCC proposal that remodels spectral regulations.

Some key points of the new policy, at the physical layer, include:

1. *Flexibility*: Allow for maximum feasible flexibility of spectrum use by both licensed and unlicensed users;

2. *Metric:* Adopt a new quantitative metric that may be used to manage interference and set interference floors for distinct bands, geographical areas and services;

3. *Dimensionality:* Account for all potential dimensions of spectrum usage (frequency, power, space, and time);

4. *Grouping*: Encourage grouping of spectrum neighbors with technically compatible characteristics.

Regarding item (A) (*flexibility*), the proposed FCC approach will allow operators to:

1. Choose the services that will be provided on their own spectrum (e.g., commercial private use);

2. Choose the technology that is most appropriate for the desired spectrum environment (e.g., techniques that use low power in highly congested areas and higher power in rural areas);

3. Have the right to transfer, lease or subdivide spectrum (e.g., for narrow band services with short (in time) requests such as public safety, the excess capacity should be leased to other users via time sharing of the spectrum).

Concerning item (B) (*metric*), the FCC introduced the Interference Temperature [96], which refers to the RF power at the receive antenna per unit bandwidth. The Interference Temperature will be used to provide the following:

1. Licensed users will receive guarantees regarding the maximum permissible level of aggregate noise (interference) in their band;

2. Unlicensed users will be provided with a threshold, indicating the highest interference they are allowed to create in their environment (e.g., the interference temperature cannot exceed XdB in the Y_1 to Y_2 Hz band, as this would otherwise create harmful interference

to other operators; if the X dB threshold is exceeded, unlicensed user communication is terminated).

Regarding item (C) (*dimensionality*), the FCC will begin to request multiple dimensions of efficiency, summarized as follows:

1. Spectral Efficiency, i.e., a measure of the amount of information transmitted within the bandwidth, to ensure maximum data rate in minimum bandwidth;

2. Technical Efficiency, i.e., a measure of the operator equipment cost and operator financial investments, to ensure the highest output for the least cost to the operator;

3. Economic Efficiency, i.e., user's equipment cost, and user's financial investments, to generate the best consumer value.

Regarding item (D) (*grouping*), the FCC has proposed the following. First, the FCC has categorized spectral usage into three main groups or categories:

1. Command-and-control group: FCC assigned frequencies for specific government-defined uses.

2. Exclusive use group: FCC licensed bands where the operator (who purchases the license) has exclusive and *transferable* rights to the band with *flexible use rights*.

3. Commons or open access group: A virtually unlimited number of unlicensed users to share FCC designated frequencies, with usage rights governed by technical standards or "etiquette," but with no guarantee of protection from interference.

With regard to the spectral bands for these three groups, the FCC proposes the following:

1. The command and control group be located at low frequencies, and that groups be allocated as little bandwidth as possible for the shortest time possible, or this group does not permit spectral efficiency.

2. The exclusive model group is best suited for bands below $5GHz$, where congestion of services is the highest, and efficiency is ensured by the high level of competition among operators.

3. The commons group is strongly encouraged in regions where spectral scarcity is low and transactions cost may be high, i.e., bands over $50GHz$ (regions where narrowband services with low levels of mutual interference can be implemented).

In the remainder of this chapter, we present a spectral allocation and a physical layer technology capable of meeting the proposed spectral policy goals mentioned above.

7.3 Proposed Spectrum Allocation

We begin by suggesting a subdivision of the radio spectrum in four broad regions, namely:

(1) *Very Low Band*, frequencies below $1GHz$; (2)*Low Band,* frequencies in the range $1 - 3.5GHz$; (3) *Medium Band,* frequencies in the range $3.5 - 25GHz$; and (4) *High Band*, frequencies over $25GHz$. We propose this regionalization of spectrum for a number of reasons, both regulatory and technical.

First, from a regulatory stand point, we use this spectral allocation to accommodate unique groups as in the requirement of the FCC proposed spectral policy. Specifically, the Very Low Band region will be reserved to accommodate the command-and-control group. This is a likely choice because most public services (e.g., radio broadcasting, police and other emergency response communication) already exist at low frequencies; as such, we minimize any change to services that usually require lengthy governmental approval processes and large amounts of funding to accommodate equipment updates [96].

The Low Band region ($1 - 3.5GHz$) is reserved for the exclusive use group. This band is currently occupied by a variety of commercial services (e.g., 2G and 3G cellular systems) and the competition to acquire licensure in this bandwidth is already strong. It seems natural to

allow this region, already controlled by market demands, to fulfill the goals of the exclusive use policy.

The Medium and High Band regions are reserved for the commons use group. Specifically, in most of this broad range of frequencies, competition is already limited (due in part to high costs of RF devices) and transactions costs are high.

The four-region band is also selected based on technical considerations. First, at very high carrier frequencies, a LOS (Line-of-Sight) path is of utmost importance. A threshold between applications that require LOS and applications that can rely on N-LOS (Non LOS) may be set at a carrier frequency of approximately $3.5GHz$, although it is possible that technological improvement will enable the $3.5GHz$ threshold to be moved to higher frequencies in the future [100]. Because commercial services such as wireless mobile cellular systems must be able to operate without the assurance of LOS, we locate the exclusive use group in frequencies below $3.5GHz$. Additionally, the above four region characterization is well suited to the multi-carrier framework discussed next.

7.3.1 The CI Multi-Carrier Platform: A novel Physical layer

Multi-carrier technologies such as OFDM ([101],[102],[103]) and MC-CDMA ([104]-[105]) are attracting widespread interest in both industrial and academic communities. This growing interest is mainly due to the ability of multi-carrier systems to support high data rate communication, while maintaining good performance in severe multi-path channel [106]-[107]. Furthermore, with the development of OFDM-based wireless LANs and digital video broadcasting, the technological know-how of multi-carrier systems have significantly improved.

Recently, the authors have proposed multi-carrier implementations of TDMA ([108],[99]) and DS-CDMA [109] systems based on a multi-carrier chip shape (in DS-CDMA) and pulse shape (in TDMA). The starting point for both these implementations is the multi-carrier waveform:

$$h_{CI}(t) = \mathrm{Re}\left\{\sum_{n=0}^{N-1} e^{j2\pi n f_n t}\right\} \tag{7.1}$$

This multi-carrier signal corresponds to a linear combination of N "in-phase" carriers and results in the well known interferometery pattern. This signal h(t), referred to as the Carrier Interferometery (CI) signal [98]-[99] is shown in Figure 7.1(a); the corresponding frequency spectrum is illustrated in Figure 7.1(b).

It is evident from Figure 7.1(a) that the signal of equation (7.1) is similar to the classic sinc$(\cdot)$ pulse shape (viewed over one period). In fact, it is easy to show that the CI signal correspond to the truncated Fourier series approximation of a sinc$(\cdot)$ pulse shape [110]. Therefore, as N increases, the CI signal converges to a sinc$(\cdot)$ pulse shape. More generally, spectral sampling of any pulse shape can be used to create a multi-carrier implementation of that pulse shape.

The multi-carrier CI signal can be employed both as a chip shape at the DS-CDMA transmitter and a pulse shape at the TDMA transmitter. To demonstrate this concept, first consider a DS-CDMA system. Here, the sent signal corresponding to, user k's jth bit (in complex base-band notation) is

$$s^{(k)}(t) = b_j^{(k)} c^{(k)}(t - jT_s) \tag{7.2}$$

where $b_j^{(k)}$ $()\hat{I}$ {*-1,+1*} represents k^{th} user j^{th} modulated BPSK symbol, and $c^{(k)}(t)$ is user k's spreading code:

$$c^{(k)}(t) = \sum_{l=0}^{N-1} \beta_l^{(k)} h_{CI}(t - lT_c) \tag{7.3}$$

In (7.3), $\beta_l^{(k)}$refers to l^{th} element of the k^{th} user spreading sequence; T_c is chip duration, and $h_{CI}(t)$is the chip shape implemented using the CI signal of equation(7.1). In CI/DS-CDMA, HW codes are employed as the spreading sequence [111]. Alternately, the CI codes introduced in [98]-[99], may be employed as the spreading sequence in DS-CDMA. This modified CI/DS-CDMA scheme is referred to as CI-CDMA (see [112]).

We can rewrite the transmit signal as

$$s^{(k)}(t) = \sum_{i=0}^{N-1} \left(b_j^{(k)} \sum_{l=0}^{N-1} e^{-j2\pi(i)(j)\Delta f T_s} \beta_i^{(k)} e^{-j2\pi(i)(l)\Delta f T_c} \right) \cdot e^{j2\pi i \Delta f t} \tag{7.4}$$

From (7.4), it is clear that DS-CDMA transmissions employing CI chip shapes can be implemented using a weighted IFFT with the weights determined by the term in the parenthesis of

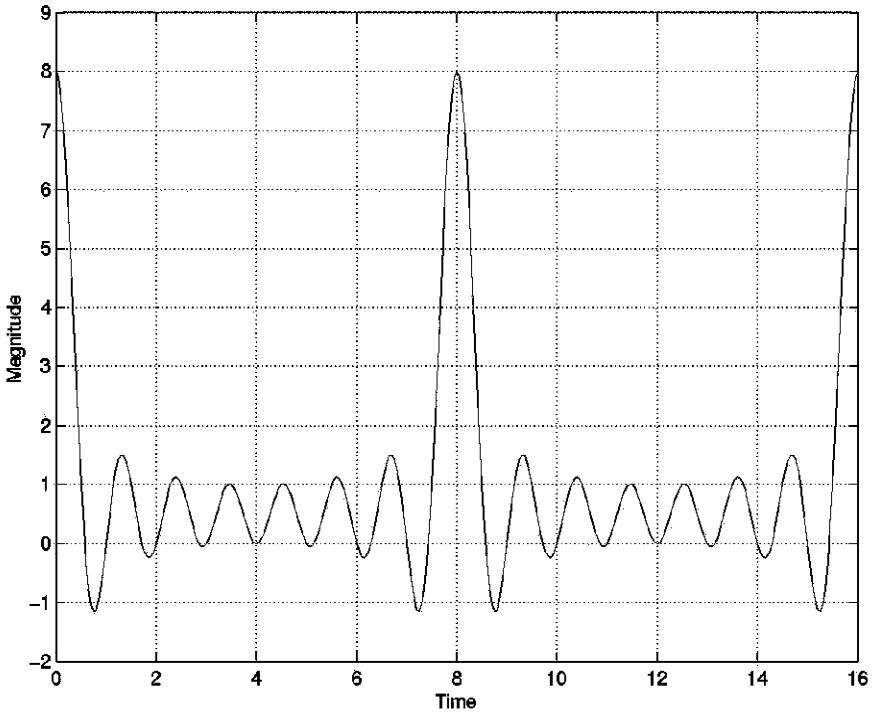

(a)

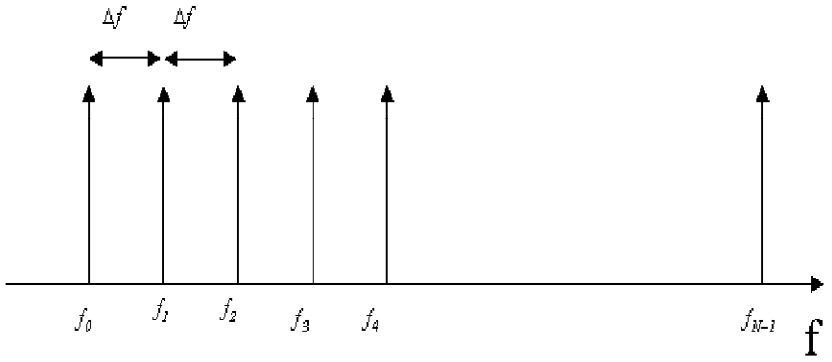

(b)

Figure 7.1: (a) Time domain representation of the CI signal. (b) Frequency domain conceptual representation of the CI signal.

equation(7.4). Additional details are available in [113]-[109].

Similarly, for TDMA, the kth user's transmission corresponds to (in complex baseband notation)

$$s^{(k)}(t) = \sum_{l=0}^{N-1} b_l^{(k)} h_{CI}(t - lT_s) \tag{7.5}$$

where $b_l^{(k)}$ represents the l^{th} BPSK symbol in user k's burst; and $h_{CI}(t)$ refers to the pulse shape implemented as the multi-carrier signal of equation(7.1). Combining equation (7.5) and equation (7.1), the transmit signal for user k can be expressed as

$$s^{(k)}(t) = \sum_{i=0}^{N-1} \left(\sum_{l=0}^{N-1} b_l^{(k)} e^{-j2\pi(i)(l)\Delta f T_s)} \right) \cdot e^{j2\pi i \Delta f t} \tag{7.6}$$

From (7.6), it is again evident that a TDMA system can be implemented by a weighted IFFT with weights determined by the term in the parenthesis of equation (7.6). As described above, much like OFDM and MC-CDMA, the CI-based DS-CDMA and TDMA transmitters can be constructed using appropriately weighted IFFT's.

CI signaling concepts may also be incorporated into traditional MC-CDMA architecture in the form of novel CI spreading codes [97],[98]. CI coded MC-CDMA systems (referred to as CI/MC-CDMA) outperform HW coded MC-CDMA systems in frequency selective channels and offer the flexibility of supporting twice the number of users relative to HW coded MC-CDMA systems. By coupling OFDM with CI spreading codes (referred to as CI-OFDM [98]-[101]), the authors demonstrated that it is possible to enhance the robustness of OFDM against frequency selective fading and reduce the PAPR of OFDM transmissions.

The multi-carrier pulse and chip shaping strategy not only enables a common transmitter design, but also enables a uniform receiver structure. Specifically, regardless of operating mode (MC-CDMA, OFDM, DS-CDMA, or TDMA mode), the receiver, upon input of the incoming signal, frequency decomposes the received signal into its N narrowband carrier components by use of an FFT and recombines across carriers. In MC-CDMA, cross carrier combining weights ensure that MAI (multi-access interference) and noise are minimized while maximizing the frequency diversity gain [97],[98]. In OFDM systems, cross carrier combining is not required since

each carrier contains a unique symbol (implemented using 0's and 1's as combining weights) [109]. In TDMA systems, cross carrier combining minimizes ISI (inter symbol interference) and noise while exploiting the available frequency diversity [108],[99]; and, in DS-CDMA, cross carrier combining minimizes the MAI, ICI (inter-chip interference), and noise and ensures an exploitable frequency diversity benefit [98]. Hence, we observe a single hardware platform supporting multi-mode reception, with transition from one mode to the next enabled by a shift of the cross carrier combining weights.

The CI based DS-CDMA, TDMA, OFDM and MC-CDMA systems not only offer a common multi-carrier hardware platform for software radio application, but also enhance the performance and capacity/throughput of these systems in hostile propagation environments (see [97]-[99]). Most importantly, the CI multi-carrier physical layer provides an ideal framework to implement spectral sharing and meet the requested FCC spectral policy regulations. This is detailed next.

7.3.2 The CI Multi-Carrier Platform: An Enabler of the FCC Spectral Policy on the Physical Layer

Traditionally, frequency division has been adopted to divide the electromagnetic spectrum between different wireless operators. In frequency division, portions of the spectrum are statically assigned to operators to support their customers' transmissions. This assignment has some inherent disadvantages with respect to spectral efficiency. For example, consider two Companies operating on their licensed bands (i.e., exclusive use model). It is possible that the first Company be fully loaded, while the second Company may have unused resources (or vice-versa). It would be profitable for both Companies if these unused resources are shared to allow more capacity for the fully loaded Company. This form of "spectral sharing" is much easier to accomplish if the underlying access technique in the two Company is multi-carrier based. Specifically, in this section we demonstrate how the CI multi-carrier platform enables the new FCC spectral policy regulation regarding "dimensionality."

In order to illustrate how the proposed CI multi-carrier platform implements efficient spectral sharing to improve spectral efficiency, we focus our discussion on CDMA systems ([114],[115]). However, as already mentioned, the CI multi-carrier platform can enable spectral sharing among systems based on different multiple access techniques (e.g., TDMA, MC-CDMA, etc.).

The CI-CDMA system (described in the previous section) provides two unique benefits (relative to traditional DS-CDMA) that makes it well equipped to support dynamic spectral allocation via spectral sharing.

First, the chip shape $h_{CI}(t)$ (equation (1)) is a multi-carrier signal, where the carriers are required to be orthogonal but not necessarily contiguous. As a direct consequence, the CI-CDMA chips (described in section 4.B) may be spread over non-contiguous bands if needed. In addition, CI-CDMA exploits the available frequency diversity over the entire transmit band. With noncontiguous transmission, the carriers are spread over a larger bandwidth resulting in enhanced diversity gains.

We propose two strategies for dynamically allocating spectrum (i.e., "sharing" strategies) to allow spectral sharing with the CI multi-carrier platform: (1) contiguous allocation and (2) non-contiguous allocation. Figure 7.2 illustrates the proposed approach for the case of two companies operating in the same spectral region. Figure 7.2(a) represents the spectral allocation for the case of no sharing. Here, both Companies employ the proposed multi-carrier CI -CDMA system, with N_1 and N_2 carriers respectively. Figure 7.2(b) illustrates a sharing strategy employing the contiguous approach, and Figure 7.2(c) demonstrates the non-contiguous approach. In the contiguous approach, Company 1 borrows a contiguous block of carriers from Company 2 (or vice-versa), while in the non-contiguous case the borrowed carriers (by Company 1) are evenly distributed over Company 2's entire spectrum. The contiguous approach is easier to implement, whereas the non-contiguous approach may result in improved system performance (for both systems) via increased frequency diversity. Figure 7.3 illustrates the sharing techniques for the case of two companies operating in different spectral regions. Figure 7.3(a) shows the case of no sharing; Figure 7.3(b) illustrates the sharing strategy with the contiguous approach, and Figure

7.3(c) presents the noncontiguous sharing strategy. It should be noted that companies operating in different spectrum regions may have different Δf between their sub-carriers. Details on the choice of carrier separation and the system representation of the spectral sharing follow.

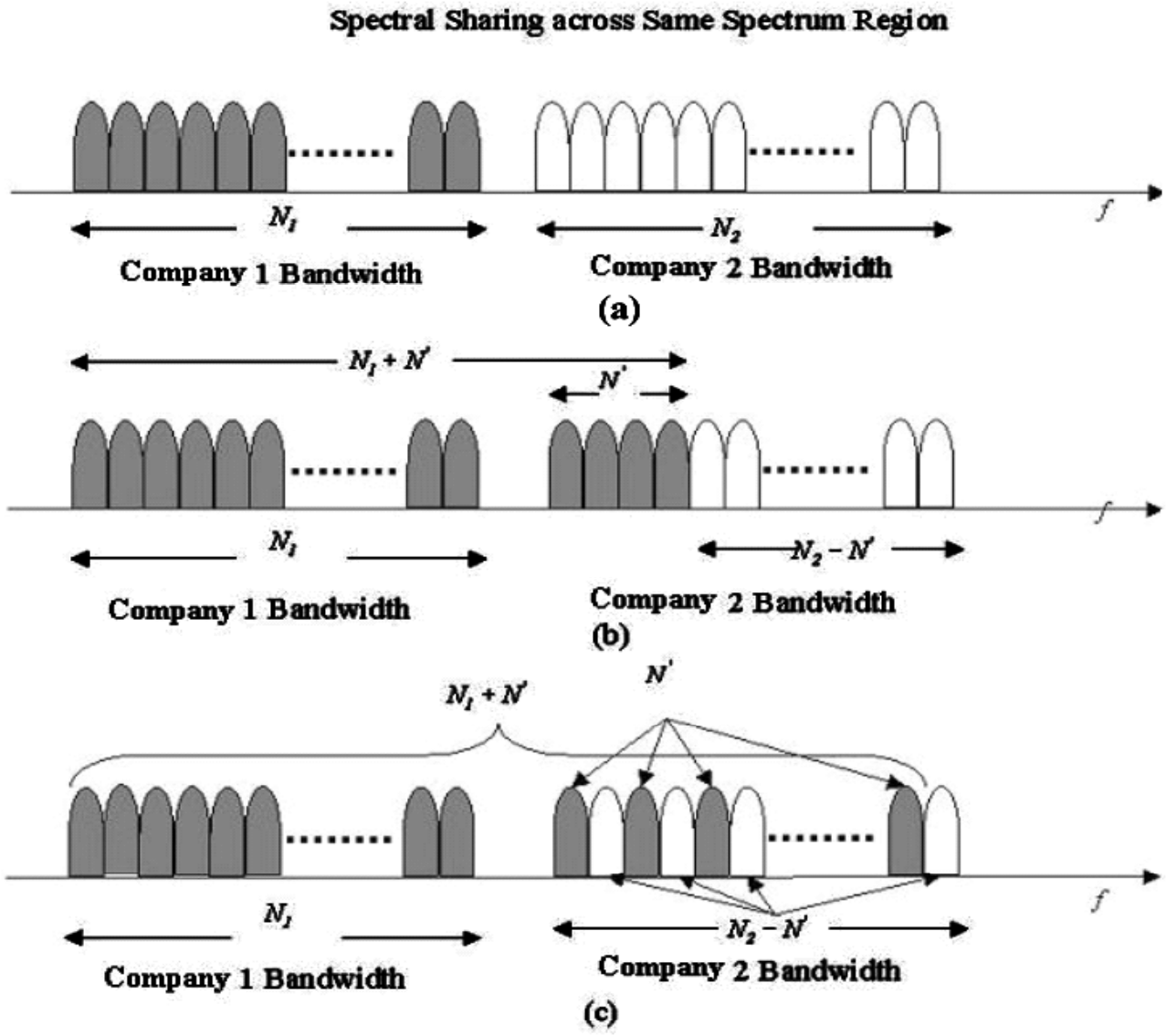

Figure 7.2: (b) Frequency domain conceptual representation of the CI signal.

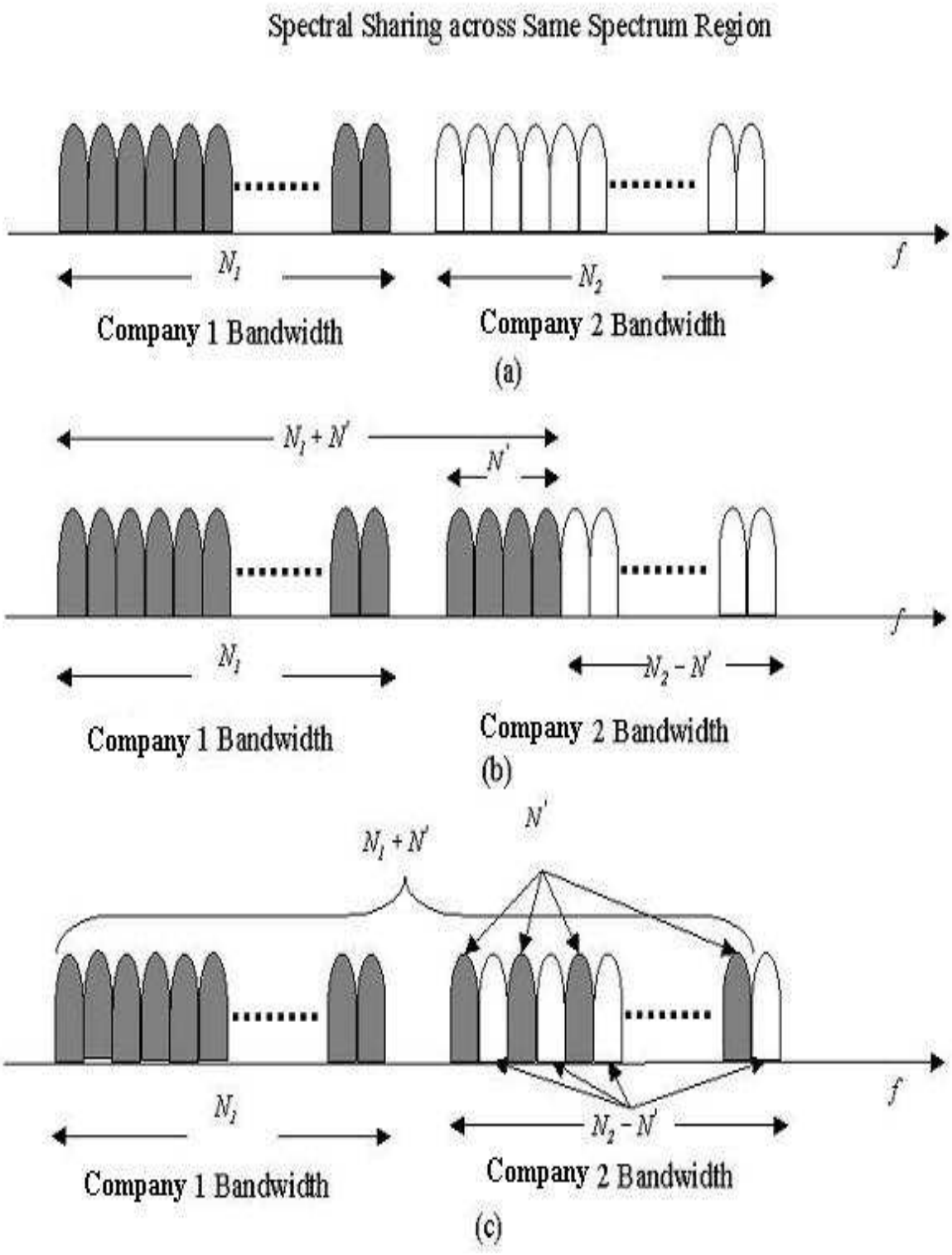

Figure 7.3: Illustration of the sharing process for Companies in different spectral regions (i.e., different values of Δf). (a) No sharing. (b) Contiguous sharing. (c) Non-contiguous sharing.

7.3.2.1 Harmonizing Spectral Sharing among Operators and across Spectral Regions

In order to allow operators to borrow/lend spectral bands from/to operators residing in the same or different spectral region, we first develop a strategy for selecting Δf (the frequency separation among carriers that constitute the CI chip-shape). We propose two different strategies to enable spectral sharing:

- Different Δf for different regions;
- Common Δf for all regions.

In the first strategy, different values of Δf are chosen for different spectral regions, based on the following practical considerations:

1. Δf is selected much smaller than the coherence bandwidth of the channel (to ensure that each carrier undergoes a flat fade).
2. Δf is selected big enough to prevent the use of large number of carriers (to allow practical implementation of the system via FFT/IFFT).

Therefore, we chose values of Δf that are proportional to the carrier frequency. This choice allows the system to maintain the transceiver complexity within reasonable levels. Specifically, we suggest the following sub-carrier spacing: (1) $\Delta f = 25\,kHz$ for the Low Band region; (2) $\Delta f = 100\,kHz$ for the Medium Band region; and (3) $\Delta f = 200\,kHz$ for the High Band region. These choices were made based on coherence bandwidth measurements for a typical indoor small office channel operating in the three different spectral bands (*65 kHz*, *232 kHz* and *678 kHz* are the measured coherence bandwidths for the low, mid and high band regions, respectively [115]). The suggested Δf values maintain the complexity of the FFT/IFFT within acceptable limits. For example, typical High Band region application may employ a bandwidth ranging from *400MHz* to $1GHz$ [100]; with a spacing $\Delta f = 200\,kHz$, the maximum size of

the FFT/IFFT (including guard bands) for this application is 5000 points. In this chapter, whenever we refer to CI-based systems operating in Region 1, 2 or 3, we implicitly assume an indoor small office channel and the corresponding Δf values suggested above.

Although we suggest that every operator use these Δf values, it should be noted that in the exclusive-use model, each operator is allowed to choose a different value for Δf. The major drawback in allowing this flexibility is that operators using different values of Δf will be unable to implement an "orthogonal spectral sharing", i.e., sharing orthogonal carriers among the CI platforms. Also, different channel characteristics (and therefore different Δfvalues) in different spectral regions prohibit the use of orthogonal sharing across different regions. For both the cases described above, the only alternative is to implement "frequency separable sharing", an FDM technique that separates the borrowed band from the remaining portion of the lender's band. Figure 7.4 shows the orthogonal and the frequency separable sharing strategies. Figure 7.4(a) and (b) show the contiguous and non-contiguous orthogonal approach. Figure 7.4(c) and (d), on the other hand, show frequency separable sharing with the contiguous and noncontiguous approach. In particular, Figure 7.4(c) and (d) demonstrate the need for highly selective filters to isolate the carriers that have been lent and those that remain assigned to the lender company. Furthermore, frequency separable sharing has lower spectral efficiency than orthogonal spectral sharing as illustrated in Figure 7.5. In this example, Company 1 borrows the same amount of bandwidth using both orthogonal and the frequency separable sharing strategies. In the case of orthogonal sharing, Company 1 is able to place three carriers in the borrowed bandwidth as shown in Figure 7.5(a). Figure 7.5(b) illustrates the frequency separable sharing strategy for the case of Company 1 and Company 2 having different Δf values. In this case, Company 1 has to allow guard bands around both ends of the borrowed spectrum in order to minimize interference with company 2's carriers (due to loss of orthogonality resulting from different Δf values). Consequently, company 1 is able to place not more than one carrier in the borrowed band. Due to its lower spectral efficiency, it is advisable to minimize the use of frequency separable sharing. The region boundary proposed in Section 3 minimizes the need of cross-

region sharing (since similar services are located in the same spectral region) which in turn reduces the need for implementing frequency separable sharing.

In the second strategy, we suggest the use of same carrier separation (e.g., $\Delta f = 25kHz$) across all regions. Even though this strategy facilitates orthogonal sharing across the entire bandwidth, it results in prohibitive complexity in IFFT/FFT implementation. For example, choosing $\Delta f = 25kHz$ for a $1GHz$ service in Region 3 requires a 40000 points IFFT.

7.3.2.2 System Model for Spectral Sharing via the CI Platform

When we integrate spectral sharing into CI-CDMA system model, the transmit signal correspond to:

$$s(t) = Re\left\{ \begin{array}{l} \sum_{k=0}^{K-1} A^{(k)} b^{(k)} \sum_{i=0}^{N_1+N'-1} \beta_i^{(k)} \left[\sum_{n=0}^{N_1-1} e^{j\ 2\pi n \Delta f t + \frac{2\pi i}{N_1+N'} n}\ e^{j2\pi f_c t} + \right. \\ \left. + \sum_{m=0}^{N'-1} e^{j\ 2\pi m \Delta f' P(m) t + \frac{2\pi i}{N_1+N'}(N_1+m)}\ e^{j2\pi f'_c t} \right] g(t) \end{array} \right\} \tag{7.7}$$

where N_1 is the number of carriers in the borrowing system (i.e., Company 1); N' is the number of borrowed carriers from the lending system (i.e. Company 2); Δf is the carrier frequency separation in the borrowing system's bandwidth; $\Delta f'$ is the carrier frequency separation in the lending system's bandwidth ($\Delta f' = \Delta f$in the case of orthogonal sharing); f_c is the carrier frequency in the borrowing system; f'_c denotes the transmit frequency of the lending system, and $P()$ is a vector that characterizes the location of borrowed carriers in the lending company spectrum. Specifically, in the contiguous sharing strategy,

$$P(m) = m \tag{7.8}$$

and, for the non-contiguous allocation strategy:

$$P(m) = \frac{m}{\lfloor N_2/N' \rfloor} \tag{7.9}$$

In (7.9), N_2 denotes the total number of carriers in the lending system (i.e., Company 2), and $\lfloor x \rfloor$ refers to the closest integer less than or equal to x.

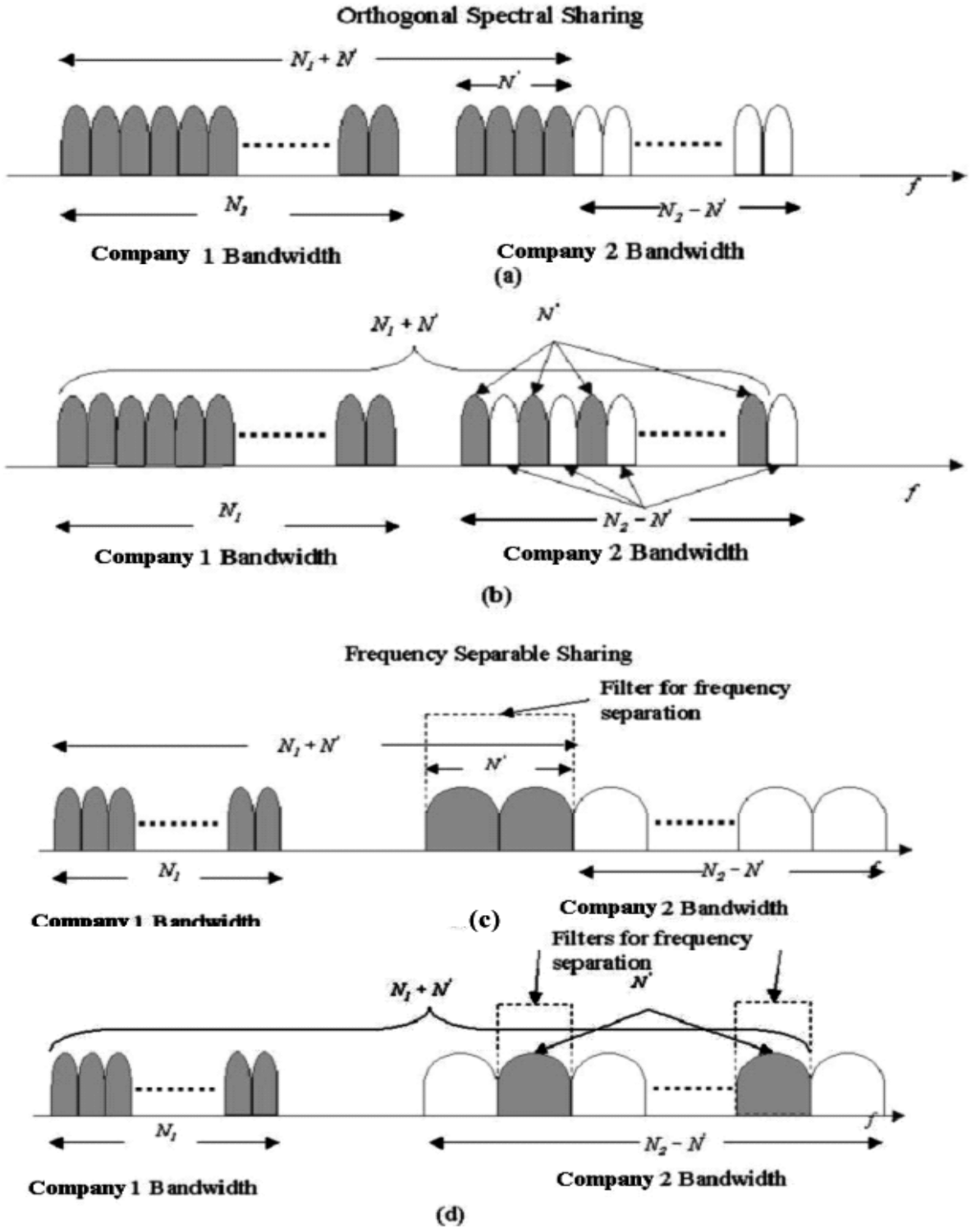

Figure 7.4: Illustration of the Orthogonal and Frequency Separable sharing. (a) Contiguous Orthogonal. (b) Non-contiguous Orthogonal. (c) Frequency Separable Contiguous. (d) Frequency Separable Non-Contiguous.

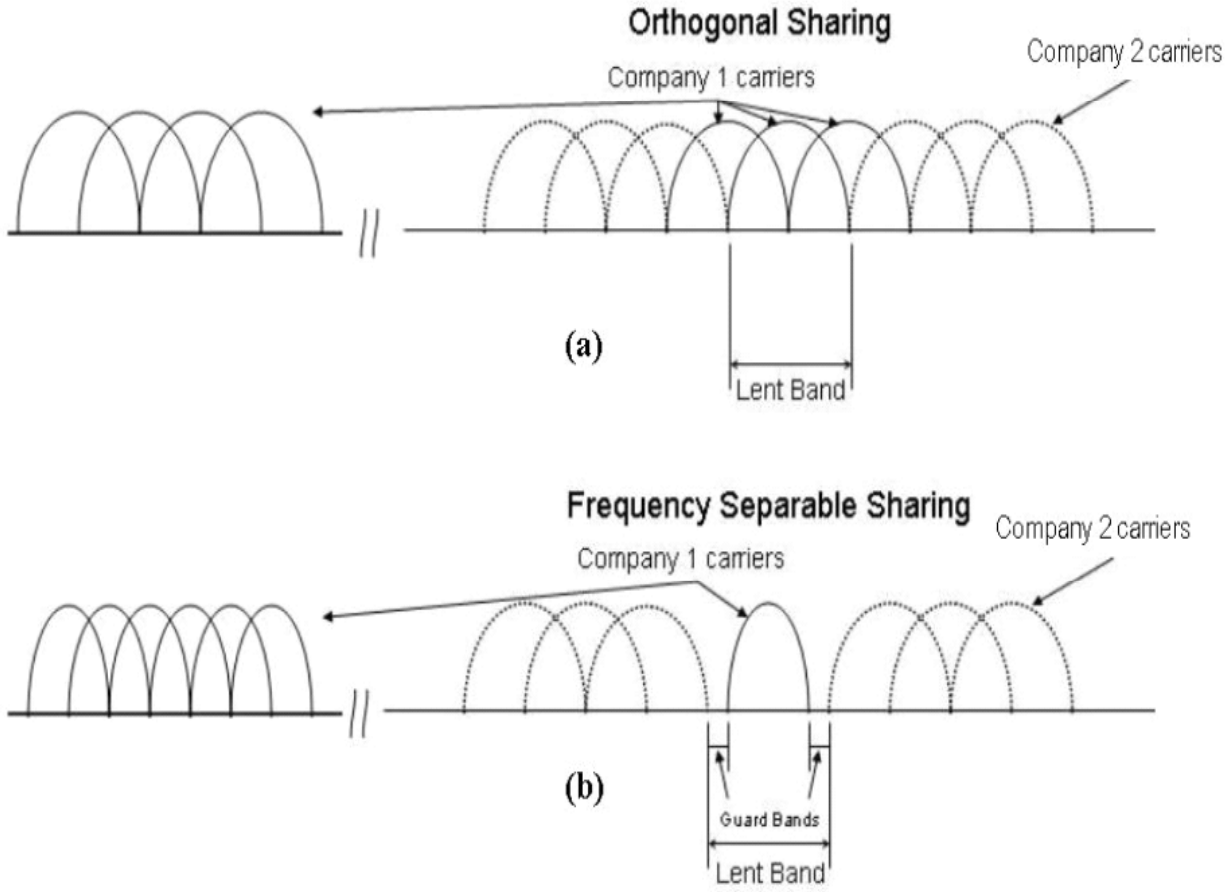

Figure 7.5: Spectral efficiency comparison. (a) Orthogonal Sharing. (b) Frequency Separable Sharing.

Similarly, the transmit signal in the lending system (i.e., Company 2 in our example) is modified according to:

$$s(t) = Re\left\{\sum_{k=0}^{K-1} A^{(k)} b^{(k)} \sum_{i=0}^{N_2-N'-1} w(k,i) \sum_{n=0}^{N_2-N'-1} e^{j\ 2\pi n \Delta f' \bar{P}(n) t + \frac{2\pi i}{N_2-N'} n}\ e^{j2\pi f_c' t} g(t)\right\} \qquad (7.10)$$

In (7.10), $\bar{P}()$ is a vector characterizing the location of the lending system carriers (the carriers that remain allocated to Company 2 upon lending N' carriers to Company 1).

It is important to note that in the non-contiguous approach, while the CI chip shape implemented for spectral sharing still satisfies the Nyquist criteria for zero ISI, this shape (in the time domain) no longer corresponds to a close approximation of the sinc$(\cdot)$ chip shape.

While with CI/DS-CDMA, spectral sharing is feasible, we propose CI-CDMA to make spectral sharing more flexible. If HW codes are employed the total number of carriers (the sum of original number of carriers and the borrowed carriers) is restricted to powers of 2. Therefore, we replace the HW codes with the proposed CI codes, and this allows (e.g., in the case of Company 1 in the previous example being fully loaded and Company 2 being scarcely loaded) Company 1 to borrow *as many* carriers as needed to increase capacity. By using orthogonal CI codes, it is possible to support N orthogonal users with N carriers (with no restriction on the choice of N). The flexibility in designing CI codes translates into the following benefit: (1) the sharing strategy provides flexible system capacity over noncontiguous bandwidth, (2) it is possible to dynamically update quantities of borrowed spectrum and borrowing duration, and (3) spectral efficiency as well revenues of both lender and borrower are optimized.

7.3.2.3 Accounting for "Interference Temperature" in Spectral Sharing

The interference temperature metric in the new FCC proposal mandates wireless operators to be able to operate under different power constraints on different parts of the spectrum [96]. For example, if a company utilizes several spectral regions, it should be able to transmit with different powers in different bands. The required power levels may be continuously updated through the MAC protocol that monitors signal transmissions within a spectral band.

Since CI based systems involve multi-carrier transmission, selective power control can be accomplished by controlling the amplitude of the individual carriers. Modulating the transmitted carriers with different powers at the transceiver end forces the MMSEC receiver to update the combining weights. With this minor modification to the transmitter structure, CI-based systems can operate under different power constraints over the electromagnetic spectrum.

Simulation results demonstrating the performance of CI-CDMA system with uneven power distribution are presented in the next section.

7.4 Numerical Results

In order to illustrate the ability of CI multi-carrier platform to improve spectral efficiency, we consider two companies (Company 1 and Company 2) that have an agreement on sharing their spectrum. Company 1 possesses 16 orthogonal carriers (i.e., it can accommodate 16 orthogonal users simultaneously), and is overwhelmed with users. Company 2 has a large number of carriers, and can lend part of its spectrum if required.

Figure 7.5 shows CI-CDMA BER vs. SNR performance curves when Company 1 borrows 9 carriers from Company 2 in the following manner:

1. At first, we consider the case of two companies utilize the same Δf (the bottom-most curve). Here, we assumes that Company 2's band is large enough to distribute the 9 borrowed carriers across its bandwidth. This assures independent fade among the 9 carriers, and guarantees maximum channel diversity gain.

2. The second set of simulations (the top three curves) present the "Frequency Separable Sharing," where Company 1 and Company 2 have different Δf values. Here, the borrowed spectrum consists of one contiguous band. Two examples are considered:

   (a) Company 1 and 2 are in the same region (Region 2 in our simulation) but operate with different Δf (the top-most curve)–Company 1's $\Delta f = 10\ kHz$ and Company 2's

$\Delta f = 25$ *kHz*. This is a legitimate assumption, because companies in the exclusive region are free to select their system parameters. For this scenario, we observe a 3dB degradation in performance relative to the orthogonal sharing case (the bottom-most curve). However, it is important to note that this non-orthogonal sharing strategy provides better performance as well as capacity relative to the CI-CDMA system with no sharing.

(b) Company 1 is in Region 2 with $\Delta f = 25$ kHz, while Company 2 is in Region 3. Two frequency separable sharing (FSS) procedures are considered:

i. The 9 borrowed carriers are allocated contiguously (the second curve from the top).

ii. The 9 borrowed carriers are allocated in 3 independent groups each consisting of 3 carriers (the third curve from the top).

It is evident from Figure 7.5 that noncontiguous FSS outperform contiguous FSS due to increased diversity gain.

The four examples discussed above, illustrate the various sharing strategies and Figure 7.6 presents a comparative performance analysis of these schemes.

Figure 7.6 presents four CI-CDMA BER performance curves for the case of Company 1 (that is operating in Region 2) borrowing increasing numbers of contiguous carriers to support increasing numbers of users. These curves demonstrate the relationship between the numbers of borrowed carriers and system performance. It is evident from Figure 7.6 that the BER performance of the CI-CDMA system improves with the increase in the number of borrowed carriers. The top-most curve, represents Company 1's performance utilizing it own 16 carriers, i.e., no spectral sharing is considered. The curves from top to bottom in Figure 7.6 represent BER performance with increasing numbers (5, 10, 16 and 32) of borrowed carriers. At BER of 10^{-3}, a 2dB improvement (relative to no sharing case) is observed when Company 1 borrows 32 carriers. This improvement in performance (due to increased diversity gain) is obtained alongside an increase in capacity. It is important to note that even though the bandwidth of

Company 1 increases with the number of borrowed carriers, the total bandwidth of Company 1 and Company 2 is still the same. In short, the sharing strategy provides a smarter way to utilize the total bandwidth in order to optimize capacity, performance and revenues. Similar observation is observed in Figure 7.7, where the MMSE MUD idea is utilized in detecting the transmitted symbols. Moreover, when the ML-MUD criterion is used instead, the benefits of the different sharing strategies are much more evident as can be seen from Figure 7.8.

Spectral sharing between CI-TDMA systems is illustrated via BER performance curves in Figure 7.9. These curves represent a CI-TDMA (operating in Region 2) BER performance with increasing numbers of borrowed carriers (i.e., 5, 10 and 16 carriers are borrowed in addition to the 16 carriers owned by Company 1). Similar to CI-CDMA, increasing the number of borrowed carriers, improves system BER performance (e.g., with 16 borrowed carriers, 3 dB improvement in system performance relative to the no sharing case is observed at a BER of 10^{-3}). In CI-TDMA, this gain in performance is achieved alongside an increase in throughput.

Simulations presented in Figure 7.10 demonstrate the ability of CI-based systems to transmit at different power levels in different spectral bands. Here, we consider a CI-CDMA system operating in Region 2. This system utilizes a total of 25 carriers which are divided into two groups: 16 carriers without any power constraint and 9 borrowed carriers with specific power restrictions. The BER performance for the following three cases are illustrated in Figure 7.10: (1) All 25 carriers transmit at the same power (bottom-most curve); (2) the power per carrier in the 9 borrowed carriers is 50% of the power per carrier in the 16-carrier set (middle curve), and (3) power per carrier in the 9-carrier set is 25% of the power per carrier in the 16-carrier set (top-most curve). From Figure 7.10 we observe that imposing power constraints on the CI-CDMA system in order to meet interference temperature metrics, degrades system performance. In this case, the degradation in performance worsens as the power constraint becomes more stringent (i.e., from 50% to 25%). The authors are currently exploring advanced reception techniques that can help reduce this degradation in performance.

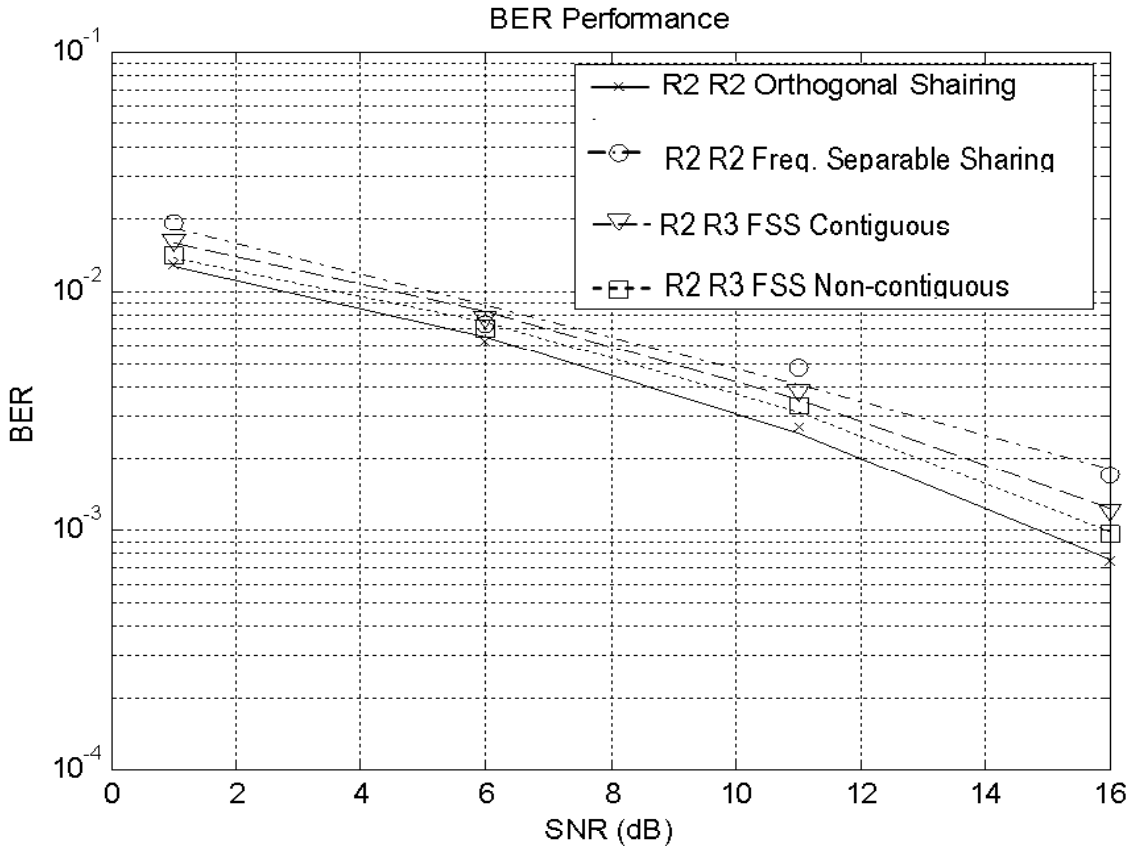

Figure 7.6: CI-CDMA BER performance curves for different sharing schemes.

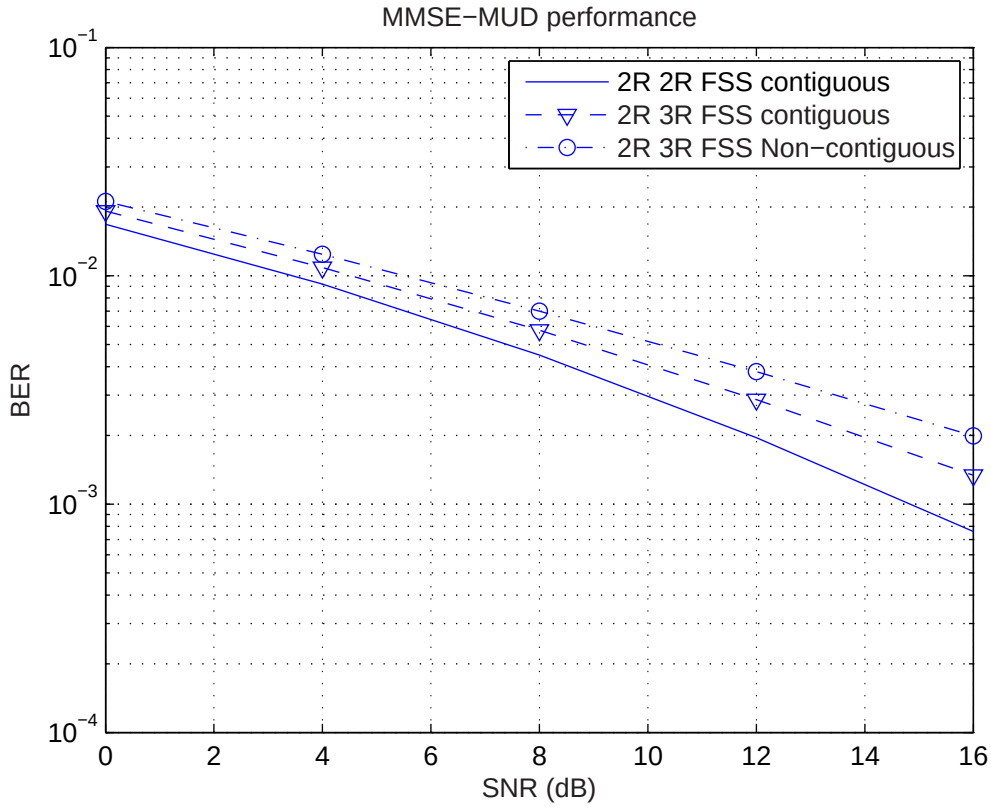

Figure 7.7: CI-CDMA BER performance curves for different sharing schemes with MMSE-MUD

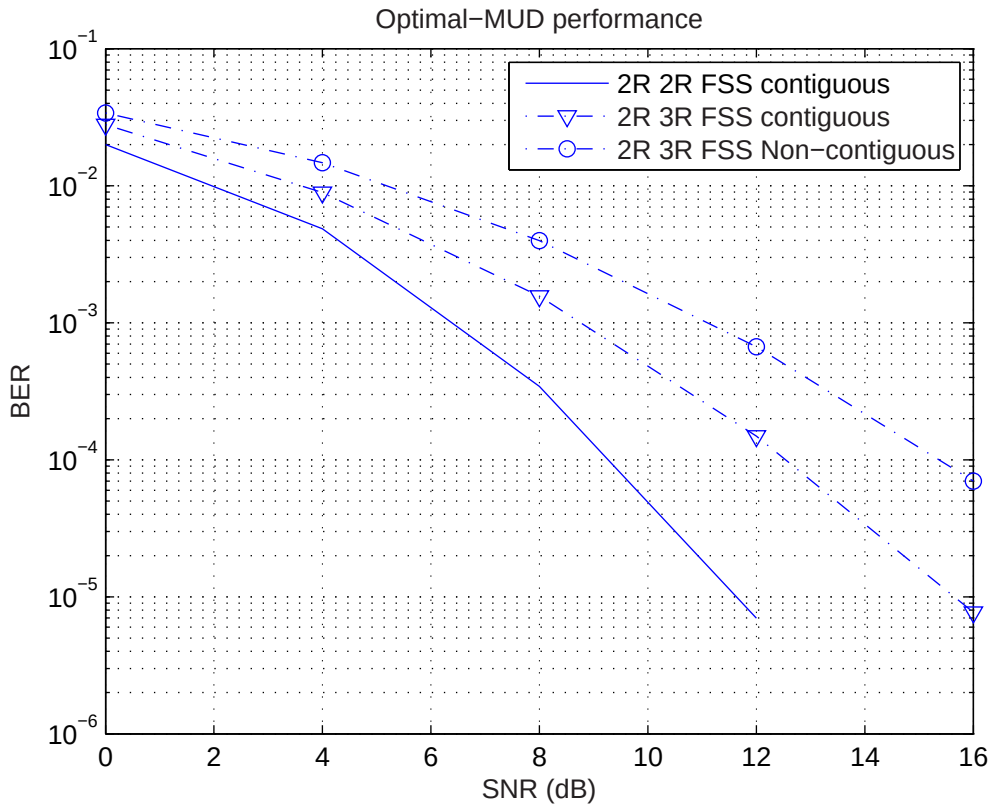

Figure 7.8: CI-CDMA BER performance curves for different sharing schemes with Optimal-MUD

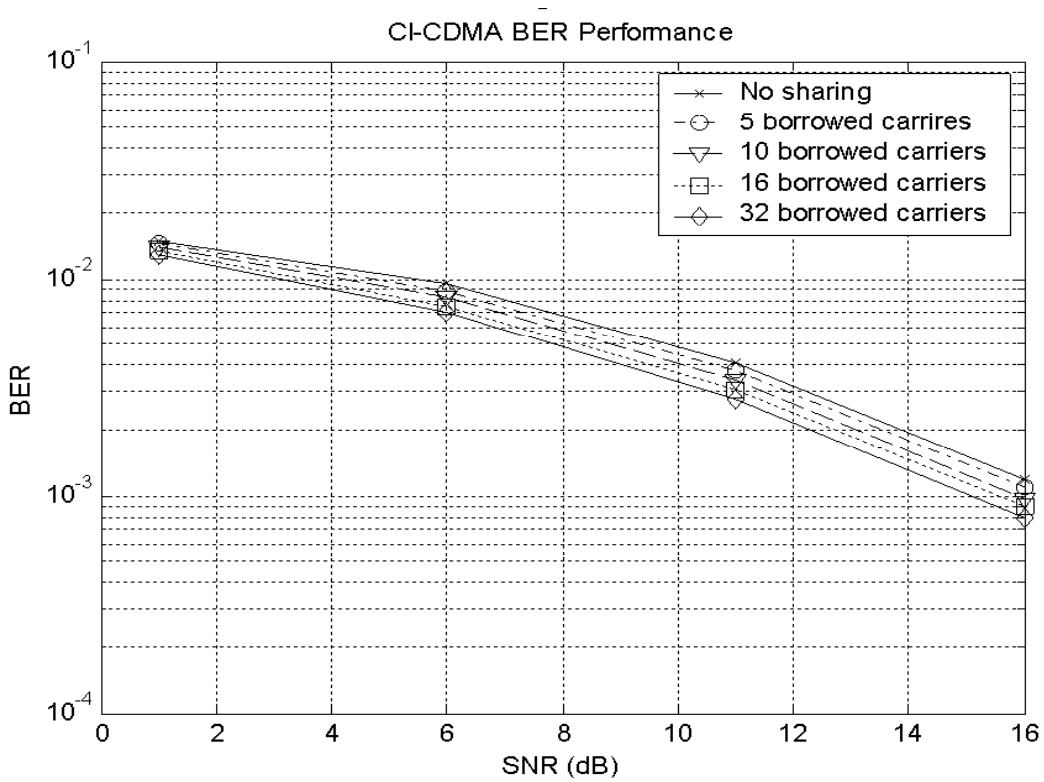

Figure 7.9: BER Performance as a function of borrowed carrier number in CI-CDMA system

7.5 Conclusion

With the rapid growth of wireless systems and services, there is a tremendous pressure to optimize spectral usage. The FCC has identified the main focus areas for better spectrum management in its latest spectral policy task force report. In this work, we suggest a CI-based multi-carrier platform to meet the new spectral policy requirements. Using CI-based DS-CDMA (CI-CDMA) as an example we demonstrate the ability of the proposed multi-carrier platform to: (1) provide high spectral efficiency (i.e., large bit/s/Hz) in each spectral band; (2) enable efficient sharing of wireless spectrum across different channels in the same band and/or across different bands; and (3) maintain low interference among adjacent systems. We also present a comparative analysis (in terms of BER performance) of different spectral sharing strategies for CI-based wireless systems. And for the first time, we apply the MUD idea to multicarrier implementation of single carrier systems incorporating the novel MUD schemes in Chapter 3 as a multi-symbol detection in CI-CDMA systems. From our simulations, we can see that

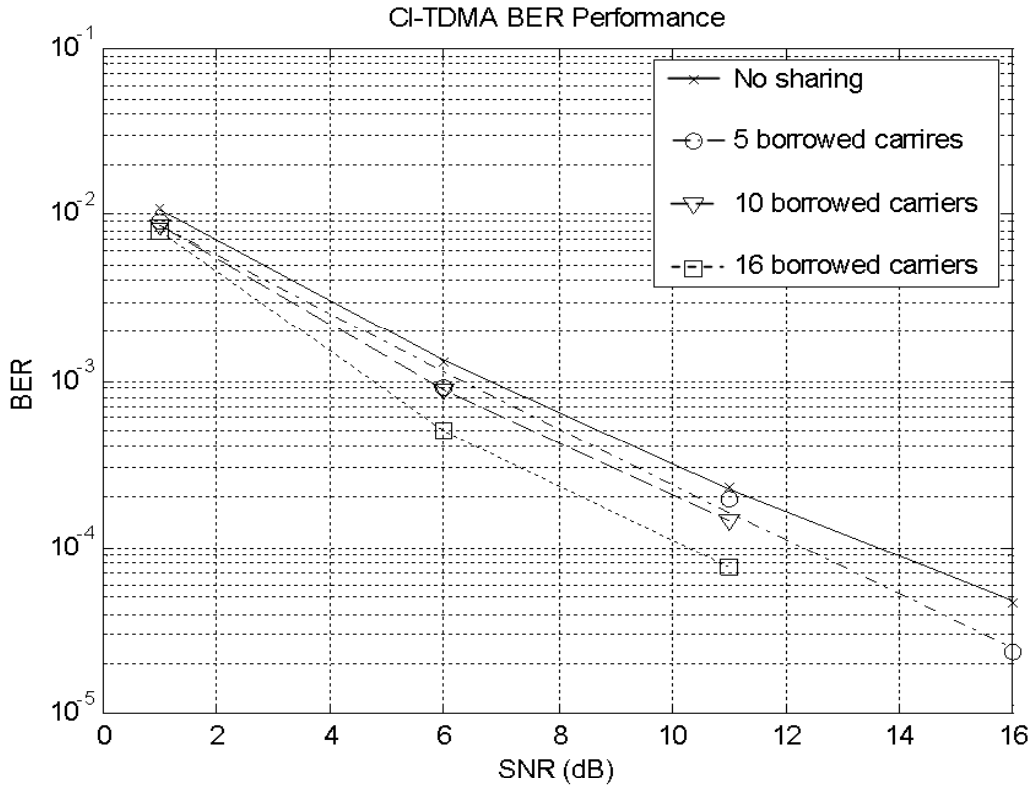

Figure 7.10: BER Performance as a function of borrowed carrier number in CI-TDMA system.

incorporating MUD algorithms in detecting transmitted results in significant BER performance gain.

To summarize, it is believed that the CI approach will pave the roadway for a wireless future where growth is not limited by spectral scarcity.

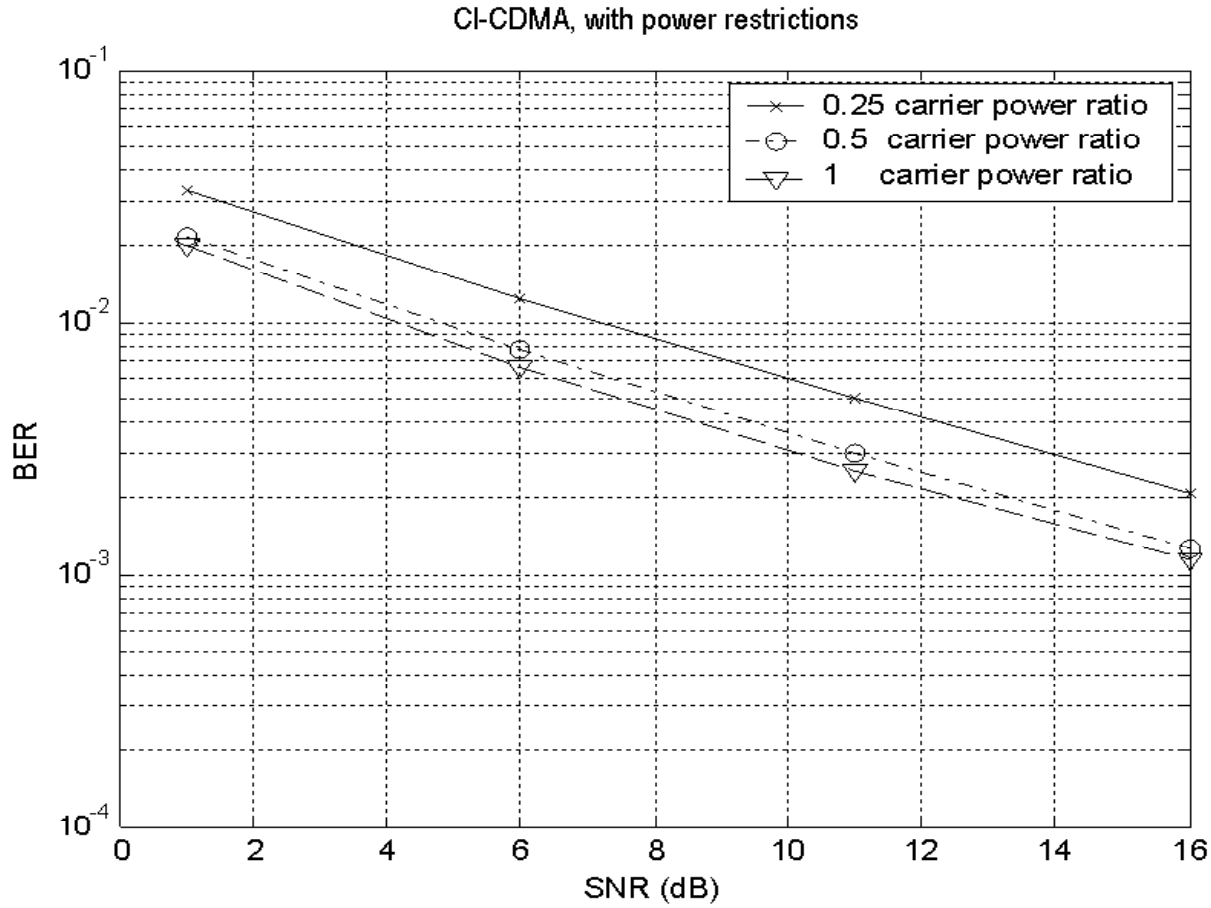

Figure 7.11: BER Performance as a function of borrowed carrier number in CI-TDMA system.

Chapter 8

Conclusions and Future Work

This chapter concludes this thesis by summarizing and highlighting the key contributions of this research. We also present areas of potential future work.

8.1 Key Results

MC-CDMA has a promising future for use in future wireless networks. Its use is likely to increase over the next 10 years, due to its high spectral efficiency and flexibility in spectrum utilization. In this thesis, we propose novel advanced receiver structures to enhance the performance of both synchronous and asynchronous MC-CDMA. Specifically, in Chapter 4, we employ the ACO approach to solve the optimal MUD problem in synchronous DS-CDMA and MC-CDMA up-link and present novel low complexity MUD with a close to optimal performance. We demonstrate that the ACO based MUD converges to the optimal BER performance in relatively few iterations providing 95% saving in computational complexity in synchronous DS-CDMA systems. This saving in complexity is retained even while considering users with unequal received powers. In synchronous MC-CDMA systems, our ACO-based MUD matches the BER performance of the optimal MUD with more than 98% savings in terms of computational complexity. Then, we show that if we decrease the number of iterations in the ACO based MUD by a factor of four, the receiver suffers only 1 dB performance loss relative to the optimal MUD.

Next we extend our investigation to asynchronous uplink MC-CDMA systems. We present a novel MUD for asynchronous MC-CDMA that detects all users' symbols simultaneously in one run. Unlike prior work, our proposed MUD for asynchronous MC-CDMA is not limited to a desired user scenario and consequently does not require multiple runs of the algorithm to detect all users' symbols. The proposed structure is based on extending the observation time of the receiver to $2T_s$. Doubling the integration window enables the receiver to fully recover the i^{th} symbols' energy for all users. Based on the extended observation window, we derive the optimal, decorrelator and MMSE MUDs and present their performances in multipath fading channel. Our simulations demonstrate that the doubling of the observation window reduces the computational complexity at the receiver while providing a comparable BER performance to that of a MUD employing a single T_s observation window. In Chapter 6, we further analyze the linear receivers based on the extended observation window setting. Specifically, we present an improved (in terms of its BER performance) decorrelator and modify the MMSE receiver to reduce its complexity while maintaining its BER performance.

Finally, we apply the MUD idea to multicarrier implementation of single carrier systems incorporating the novel MUD schemes in Chapter 3 as a multi-symbol detection in CI-CDMA systems. Specifically, we suggest a CI-based multi-carrier platform to meet new FCC demand for better spectrum management policy. Using CI-based DS-CDMA (CI-CDMA) and CI/TDMA as examples, we demonstrate the ability of the proposed multi-carrier platform to: (1) provide high spectral efficiency (i.e., large bit/s/Hz) in each spectral band; (2) enable efficient sharing of wireless spectrum across different channels in the same band and/or across different bands; and (3) maintain low interference among adjacent systems. We also present a comparative analysis (in terms of BER performance) of different spectral sharing strategies for CI-based wireless systems. From our simulations, we can see that incorporating MUD algorithms in detecting transmitted results in significant BER performance gain.

8.2 Future Work

The work in this thesis can serve a launch pad for a number of future research topics. The future work presented below is subdivided into three categories: Incorporating multiple transmitting and receiving antennas, channel estimation analysis, and blind MUD.

8.2.1 Incorporating Multiple Transmitting and Receiving Antennas

The use of multiple antennas on both transmitter and receiver ends is referred to as a multiple input multiple output (MIMO) system [116]. MIMO exploits phenomena such as multipath propagation to increase throughput, or reduce bit error rates, rather than attempting to eliminate the multipath effect. In the past decade, MIMO has be the focus of attention of several researchers and has been added as an optional feature in the IEEE802.16 and the emerging IEEE802.11n standards. That is to say, future MC-CDMA systems may very well employ multiple transmit and multiple receive antennas. Therefore, it is important to investigate the impact of utilizing MIMO on MUD design. In our current research, we assume a single antennas at both ends. Hence, utilizing multiple antennas may be considered as a superposition of several single antenna systems, and consequently changes the nature of the wireless channel. In designing a MUD for a MIMO based an MC-CDMA system, special attention has to be given to the correlation among the channels formed between the various transmit-receive antennas pairs.

8.2.2 Channel Estimation Analysis

In this work, we assume that the receiver has perfect knowledge about the channel (i.e., fading parameters, delay and noise power). In practice this assumption is not valid, and instead the receiver has to estimate the channel characteristics. There are several ways for the receiver to estimate channel's state information (e.g., pilot-assisted channel estimation and decision directed channel estimation). However, regardless of the method used in estimating the channel

conditions, there is an error associated with this estimate. The error between the actual channel matrix **H** and the estimated channel matrix can degrade the MUD performance. Therefore, it is important to study the effect of imperfect channel estimates on our MUD performance.

8.2.3 Blind MUD

It is important to note that although the ML-MUD provides the optimal performance in MC-CDMA, this performance depends on a receiver's perfect knowledge of channels' fading parameters and users' transmission delays. The users' timing and channel estimation are usually evaluated utilizing bandwidth-consuming training sequences [117]. To avoid this wastage of resources, a blind MUD for MC-CDMA systems is needed. Specifically, a subspace based blind MUD receiver like the one presented in [118] is a feasible option. In [118], the authors present a subspace blind MUD for asynchronous MC-CDMA. However, in their design they limit the observation window to one T_s. Furthermore, unlike in [118], it would be logical to address the subspace problem in the frequency domain. The design of blind MUDs for asynchronous MC-CDMA is a topic that requires further investigation.

Bibliography

[1] S. Verdu, "Wireless bandwidth in the making," *IEEE Communications Magazine*, pp. 53–58, July 2000.

[2] A. J. Viterbi, *CDMA : Principles of Spread Spectrum Communication (Addison-Wesley Wireless Communications)*. Pearson Education, 1995.

[3] R. B. Ash, *Information Theory*. Courier Dover Publications, 1990.

[4] S. G. .Glisic, S. Gilsic, and P. A. Leppanen, *Wireless Communications: TDMA Versus CDMA*. Kluwer Academic Publishers, 2004.

[5] J.G.Proakis, *Digital Communications*, 3rd ed. McGraw-Hill, 1995.

[6] R. Bekkers, *Mobile Telecommunications Standards: GSM, UMTS, Tetra, and Ermes*. Artech House, Incorporated, 2001.

[7] B. H. Walke, P. Seidenberg, M. P. Althoff, P. Seidenberg, and M. P. Althoff, *UMTS: The Fundamentals*. Wiley, John and Sons, Incorporated, 2001.

[8] L. Korowajczuk, C. Korowajczuk, L. A. DaSilva, A. M. F. Filho, and L. Z. Ribeiro, *Designing CDMA 2000 Systems*. Wiley, John and Sons, Incorporated, 2004.

[9] L. J. Harte, D. McLaughlin, R. Kikta, and M. Hoenig, *CDMA IS-95 for Cellular and PCs: Technology, Applications, and Resource Guide*. McGraw-Hill Companies, 2000.

[10] J. Wang and T.-S. Ng, *Advances in 3G Enhanced Technologies for Wireless Communications.* Artech House, 2002.

[11] A. J. Viterbi, "Error bounds for convolutional codes and an asymptotically optimum decoding algorithm," *IEEE Trans. Inform. Theory*, vol. IT-13, pp. 260–269, Apr. 1967.

[12] W. Hoeg and T. Lauterbach, *Digital Audio Broadcasting: Principles and Applications of Digital Radio.* Wiley, John and Sons, Incorporated, 2003.

[13] U. Reimers, *Digital Video Broadcasting.* Springer-Verlag New York, LLC, 2004.

[14] L. Hanzo, M. Munster, B. J. Choi, and T. Keller, *OFDM and MC-CDMA for Broadband Multi-User Communications, WLANs and Broadcasting.* John Wiley and IEEE Press, 2003.

[15] J. Bingham, "Multicarrier modulation for data transmission: An idea whose time has come," *IEEE Commun. Mag.*, pp. 5–14, May 1990.

[16] S. Weinstein and P. Ebert, "Data transmission by frequency-division multiplexing using the discrete fourier transform," *IEEE Transcations on Communications Technology*, vol. 19, pp. 628–634, Oct. 1971.

[17] D. Richard, van Nee, and R. Prasad, *OFDM for Wireless Multimedia Communications*, 1st ed. Artech House Publishers, 2000.

[18] S. Hara, R. Prasad, and R. K. Wysocki, *Multicarrier Techniques for 4G Mobile Communications.* Artech House, Incorporated, 2003.

[19] S. Hara and R. Prasad, "Overview of multicarrier CDMA," *IEEE Communications Magazine*, vol. 35, pp. 126–133, Dec. 1997.

[20] J. Korhonen, *Introduction to 3G Mobile Communications.* Artech House, Incorporated, 2003.

[21] B.Natarajan and C.R.Nassar, "Multi-carrier implementation of single-carrier wireless systems for enhanced performance and throughput," *CIIT*, Nov. 2003.

[22] S. Verdu, *Multiser Detection*, 1st ed. Cambridge University Press, 1998.

[23] L. Brunel, "Multiuser detection techniques using maximum likelihood sphere decoding in multicarrier CDMA systems," *IEEE Transactions on Wireless Communications*, pp. 949–957, May 2004.

[24] Y. Bar-Ness, J.-P. Linnartz, , and X. Liu, "Synchronous multi-user multicarrier cdma communication system with decorrelating interference canceler," *in Proc. of IEEE Personal Indoor and Mobile Radio Communications Conference*, pp. 184–188, 1994.

[25] H. V. Poor and S. Verdu, "Single-user detectors for multiuser channels," *IEEE Trans. Comm.*, vol. 36, no. 1, pp. 50–60, Jan 1998.

[26] R. Lupas and S. Verdu, "Linear multiuser detectors for synchronous code-division multiple-access channels," *IEEE Trans. Information Theory*, vol. 35, no. 1, pp. 123–136, Jan 1989.

[27] ——, "Near-far resistance of multiuser detectors in asynchronous channels," *IEEE Trans. Comm.*, vol. 38, no. 4, pp. 496–508, April 1990.

[28] Duel-Hallen, J. Holtzman, and Z. Zvonar, "Multiuser detection for CDMA systems," *IEEE Personal Communications*, pp. 46–58, April 1995.

[29] M. Honig, U. Madhow, and S. Verdu, "Blind adaptive multiuser detection," *IEEE Trans. Info. Theory*, vol. 41, no. 4, pp. 944–960, July 1995.

[30] M. Honig and M. K. Tsatsanis, "Adaptive techniques for multiuser CDMA receivers," *IEEE Signal Processing Magazine*, no. May, pp. 49–61, 2000.

[31] X. Wang and H. V. Poor, "Blind multiuser detection: a subspace approach," *IEEE Transactions on Information Theory*, vol. 44, no. 2, pp. 677–690, March 1998.

[32] X. Wang and H. Poor, "Space-time multiuser detection in multipath CDMA channels," *IEEE Transactions on Signal Processing*, vol. 47, no. 9, Sep 1999.

[33] X. Wang and H. V. Poor, "Iterative (turbo) soft interference cancellation and decoding for coded CDMA," *IEEE Transactions on Communications*, vol. 47, no. 7, pp. 1046–1061, July 1999.

[34] S.L.Hijazi, A. Best, B.Natarajan, and S. Das, "Novel low-complixity MC-CDMA multiuser detector based on ant colony optimization," *IEEE International Conference on Wireless and Mobile Computing, Networking and Communications (WiMob2005)*, Aug. 2005.

[35] M. Valenti, "Iterative detection and decoding for wireless communications," Ph.D. dissertation, Virginia Polytechnic Institute and State University, July 1999.

[36] P. Jung and M. Nasshan, "Results on turbo-codes for speech transmission in a joint detection cdma mobile radio system with coherent receiver antenna diversity," *IEEE Trans. Vehic. Tech*, vol. 46, no. 4, pp. 862–870, Apr 1997.

[37] M. C. Reed, "Iterative multiuser detection for CDMA with FEC: Near single user performance," *IEEE Trans. Commun.*, vol. 46, no. 12, pp. 1693–1699, Dec 1998.

[38] P. D. Alexander, "Iterative multiuser interference reduction: Turbo CDMA," *IEEE Trans. Commun.*, vol. 47, no. 7, pp. 1008–1014, July 1999.

[39] X. Wang and H. Poor, "Iterative (turbo) soft interference cancellation and decoding for coded CDMA," *IEEE Trans. Commun.*, vol. 47, no. 7, pp. 1046–1061, 1999.

[40] M. M. P.W. Baier, "Advanced CDMA transmission concepts for 3g and 4g mobile radio communications," *IEEE International Symposium on Spread Spectrum ISSSTA2004*, Aug 2004.

[41] Z. Wu and C. R. Nassar, "Mmse combiner for CI/DS-CDMA," *Proc. of 2000 IEEE Radio and Wireless Conference, Denver, CO*, pp. 103–106, Sept. 2000.

[42] P. Zong, K. Wang, and Y. Bar-Ness, "Partial sampling MMSE interference suppression in asynchronous multicarrier CDMA system," *IEEE Journal on Selected Areas in Communications*, vol. 19, pp. 1605 – 1613, 2001.

[43] Z. Xie, R. T. Short, and C. K. Rushforth, "A family of suboptimum detectors for coherent multi-user communications," *IEEE JSAC*, vol. 8, no. 4, pp. 683–690, May 1990.

[44] M. Dangl, J. Egle, W. Teich, and J. Lindner, "Multiuser detection in ds-cdma systems based on a lattice code decoder," *IEEE Seventh International Symposium on Spread Spectrum Techniques and Applications*, vol. 2, pp. 500–505, 2002.

[45] L.Hanzo, L-L.Yang, E-L.Kuan, and K.Yen, *Single and Multi-Carrier [DS-CDMA]: Multi-User Detection, Space-Time Spreading, Synchronisation*, 1st ed. John Wiley and Sons, Inc, 2003.

[46] M. J. Juntti, T. Schlsser, and J. O. Lilleberg, "Results on turbo-codes for speech transmission in a joint detection cdma mobile radio system with coherent receiver antenna diversity," *IEEE Trans. Vehic. Tech*, pp. 492–498, 1997.

[47] X. F. Wang, W.-S. Lu, and A. Antoniou, "A genetic-algorithm-based multiuser detector for multiple-access communications," *Proc. IEEE Int. Symp. on Circuits and Systems, ISCAS 98*, pp. 534–537, 1998.

[48] H. Wei and L.Hanzo, "Genetic algorithms assisted MUD for asynchronous MC-CDMA," *IEEE Transactions on Wireless Communications*, vol. 53, pp. 1413–1422, 2004.

[49] T. Fogarty, "Using the genetic algorithm to adapt intelligent systems," *IEE Colloquium onjsac Symbols Versus Neurons*, vol. 12, pp. 4/1–4/4, Oct. 1990.

[50] D. Fogel, "What is evolutionary computation?" *IEEE Spectrum*, vol. 37, pp. 28–32, Feb. 2000.

[51] J. Kennedy and R. Eberhart, "Particle swarm optimization," *IEEE International Conference on Neural Networks*, vol. 4, pp. 1942–1948, Dec. 1995.

[52] M. Dorigo, L. Gambardella, M. Middendorf, , and T. Stutzle, "Guest editorial: special section on ant colony optimization," *IEEE Transactions on Evolutionary Computation*, vol. 6, pp. 317–319, Aug. 2002.

[53] M. Dorigo and L. Gambardella, "Ant colony system: a cooperative learning approach to the traveling salesman problem," *IEEE Transactions on Evolutionary Computation*, vol. 1, no. 1, pp. 53–66, Apr. 1997.

[54] S. L. Hijazi and B. Natarajan, "Optimal multi-user detection in asynchronous MC-CDMA via the ant colony approach," *Submitted for publication in IEEE GLOBCOM*, 2005.

[55] S. Sigdel, K. Ahmed, and R. Rajatheva, "Performance evaluation of MC-CDMA uplink system with diversity reception and multiuser detection," *IEEE 5th International Symposium on Wireless Personal Multimedia Communications*, vol. 2, pp. 650 – 654, Oct. 2002.

[56] R. Liu, E. Chester, and B. Sharif, "Performance of asynchronous multicarrier CDMA multiuser receiver over frequency selective multipath fading channels," *IEEE Electronics Letters*, vol. 40, pp. 48 – 49, Jan. 2004.

[57] S. Haykin and M. Moher, *Modern wireless communications*. Upper Saddle River, N.J.: Prentice Hall, 2005.

[58] B. Salzberg, "Performance of an efficient parallel data transmission system," *IEEE Trans. Commun. Technol.*, vol. COM-15, pp. 805–813, Dec 1967.

[59] T.S.Rappaport, *Wireless Communications: Principles and Practice*, 1st ed. Prentice Hall, 1996.

[60] L. L. Scharf, *Statistical signal processing : detection, estimation, and time series analysis.* Reading, MA: Addison-Wesley, 1991.

[61] S. Weinstein and P. Ebert, "Data transmission by frequency-division multiplexing using the discrete fourier transform," *IEEE Trans. Commun. Technol.*, vol. COM-19, pp. 628–634, Oct 1971.

[62] T. Keller and L. Hanzo, "Adaptive modulation techniques for duplex ofdm transmission," *IEEE Trans. on Vehicular Technologies Commun.*, vol. 49, pp. 1893–1905, Sep. 2000.

[63] M. B. T.Pollet and M.Moeneclaey, "Sensitivity of OFDM systems to carrier freuency offset and wiener phase noise," *IEEE Transaction on Communications*, vol. 43, pp. 191–193, Apr 1995.

[64] S. Haykin, *Adaptive Filter Theory.* Upper Saddle River, NJ: Prentice-Hall, 1996.

[65] P. J. Green, "On the use of the em algorithm for penalized likelihood estimation," *Journal of the Royal Statistical Society*, vol. 52, pp. 443–452, 1990.

[66] R.Lupas and S.Verdu, " Linear multiuser detectors for synchronous code-division multiple-access channels," *IEEE Transactions on Information Theory*, vol. 35, pp. 123–136, Jan. 1989.

[67] D. J. Sakrison, "Stochastic approximation: A recursive method for solving regression problems," *Advances in Communication Systems*, no. 2, pp. 51–106, 1966.

[68] K. . Schneider, "Optimum detection of code division multiplexed signals," *IEEE Trans. Aerospace Nett. Sys.*, vol. AES-15, pp. 181–185, Jan. 1979.

[69] R. Kohno, M. Hatori, , and H. Imai, "Cancellation techniques of co-channe1 interference in asynchronous spread spectrum multiple access systems," *Elect. and Commun. in Japan*, vol. 66-A, no. 5, pp. 20–29, 1983.

[70] R. Lupas and S. Verdu, "Near-far resistance of multi-user detectors inasynchronous channels," *IEEE Trans. Commun*, vol. 38, no. 4, pp. 496–508, Apr 1990.

[71] ——, "Linear multi-user detectors for synchronous code-division multiple-access channels," *IEEE Trans. Info. Theory*, vol. 35, no. 1, pp. 123–136, Jan 1989.

[72] R. Lupas-Golaszewski and S. Verdu, "Asymptotic efficiency of linear multi-user detectors," *Proc. 25th Conf. on Decision and Control, Athens, Greece*, pp. 2094–2100, Dec. 1986.

[73] F. Zheng and S. K. Barton, "Near far resistant detection of CDMA signals via isolation bit insertion," *IEEE Trans. Commun.*, vol. 43, no. 2/3/4, pp. 1313–1317, Feb./Mar./Apr. 1995.

[74] S. Krishnan and B. Petersen, "Spatial-temporal decorrelating decision-feedback multiuser detector for synchronous code-division multiple-access channels," *IEEE Pacific Rim Conference on Communications, Computers and Signal Processing*, vol. 1, pp. 22–27, Aug 1997.

[75] B. Petersen and D. Falconer, "Suppression of adjacent-channel, cochannel, and intersymbol interference by equalizers and linear combiners," *IEEE Transactions on Communications*, vol. 42, pp. 3109 – 3118, Dec 1994.

[76] R.Fantacci, S.Morosi, and F.Panchetti, "One-shot multi-user cancellation receiver for wireless CDMA communication systems," *IEEE Transactions on Vehicular Technology*, pp. 1134 – 1138, 1999.

[77] Y. Li and R.Steele, "Serial interference cancellation method for cdma," *IEEE Electronics Letters*, vol. 30, pp. 1581 – 1583, 1994.

[78] J. M.Holtzman, "Successive interference cancellation for direct sequence code division multiple access," *IEEE Military Communications Conference*, vol. 3, pp. 997 – 1001, 1994.

[79] S. W. Kim and Y.-J. Hong, "Log-likelihood ratio based successive interference cancellation in CDMA systems," *The 57th IEEE Semiannual Vehicular Technology Conference*, vol. 4, pp. 2390 – 2393, 2003.

[80] P.S.Guinand, R.W.Kerr, and M.Moher, "Serial interference cancellation for highly correlated users," *IEEE trans. Communications*, pp. 133 – 136, 1999.

[81] D. Hong, Y. You, and C. Kang, "Pipelined successive interference cancellation scheme for a DS-CDMA system," *IEEE Commun letter*, vol. 3, pp. 2045 – 2048, 1997.

[82] T. Kim, D. Hong, C. Kang, and D. Hong, "Adaptive pipelined successive interference cancellation scheme for a DS-CDMA system," *IEEE 49th Vehicular Technology Conf.*, vol. 3, pp. 740 – 743, 2000.

[83] H.K.Park, Eung.BaeKim, Y.Lee, and K.HyonTchah, "Multi-carrier CDMA system with parallel interference cancellation for multipath fading channels," *IEEE trans. Communications*, pp. 513 – 517, 1998.

[84] D. Divsalar and M. Simon, "New approach to parallel interference cancellation for CDMA," *Global Telecommunications Conference*, vol. 3, pp. 1452–1457, 1996.

[85] R.M.Buehrer and S.P.Nicoloso, "Comments on partial parallel interference cancellation for CDMA," *IEEE Transactions on Communications*, vol. 47, pp. 658–661, 1999.

[86] F.Petre, P.Vandenameele, A.Bourdoux, B. M. M.Moonen, and H.DeMan, "Combined MMSE/pcPIC multiuser detection for MC-CDMA," *IEEE Transactions on Vehicular Technology*, pp. 770–774, June 2000.

[87] M. D.Divsalar and D.Raphaeli, "Improved parallel interference cancellation for CDMA," *IEEE Transactions on Communications*, vol. 46, pp. 258–268, 1998.

[88] F.Bader, S.Zazo, and I.Raos, "Improvement on the multi-user detection decorrelator of a mc-cdma used in the reverse link," *IEEE Transactions on Personal, Indoor and Mobile Radio Communications*, vol. 1, pp. 409 – 413, 2002.

[89] W. H. Press, B. P. Flannery, S. A. Teukolsky, and W. T. Vetterling, *Optimal (Wiener) Filtering with the FFT*, 2nd ed. Cambridge University Press, 1992.

[90] V. Thippavajjula and B. Natarajan, "MC-CDMA uplink ananlysis with interference cancelation," *M.S. Thesis at Kansas State University*, Dec. 2004.

[91] F. Glover and M. Laguna, *Tabu Search*. Kluwer Academic Publishers, 2004.

[92] M. Dorigo, M. Birattari, C. Blum, and L. M. Gambardella, *Ant Colony Optimization and Swarm Intelligence*. Springer-Verlag New York, LLC, 2004.

[93] X. Gui and T. S. Ng, "Performance of asynchronous orthogonal multicarrier CDMA system in frequency selective fading channel," *IEEE Trans. Commun.*, vol. 47, pp. 1084 – 1091, 1999.

[94] Q. Shi and M. Latva-aho, "Performance analysis of MC-CDMA in Rayleigh fading channels with correlated envelopes and phases," *IEE Proceedings Communications*, vol. 150, pp. 214 – 220, 2003.

[95] W. S. Levine and W. S. Levine, *Control System Fundamentals*. Hardcover, Pub., January 1999.

[96] R. ET, "Fcc spectrum policy task force," FCC, Tech. Rep. 02-1935, 2002.

[97] B. Natarajan, C. R. Nassar, S. Shattil, M. Michelini, and Z. Wu, "High-performance MC-CDMA via carrier interferometry codes," *IEEE Trans. on Veh. Tech.*, vol. 50, no. 6, pp. 1344–1353, 2001.

[98] B. Natarajan, C. R. Nassar, and S. Shattil, "Innovative pulse shaping for high-performance wireless TDMA," *IEEE Comm. Letters*, vol. 5, no. 9, pp. 372–374, Sept. 2001.

[99] W. Webb, *The Future of Wireless Communications*, 1st ed. Boston, MA: Artech House Publishers, 2002.

[100] R. V. Nee and R. Prasad, *OFDM for Wireless Multimedia Communications*. Boston, MA: Artech House Publishers, 2000.

[101] Z. Wu, C. R. Nassar, and S. Shattil, "Capacity enhanced DS-CDMA via carrier interferometry chip shaping," *Proc.of 2001 Intl. Symp. on Advanced Radio Technologies*, 2001.

[102] W. Y. Zhou and Y. Wu, "COFDM: an overview," *IEEE Trans. Broadc.*, vol. COM-19, pp. 1–8, March 1995.

[103] R. Prasad, *CDMA for Wireless Personal Communications*. Boston, MA: Artech House Publishers, 1996.

[104] S. Hara and R. Prasad, "Overview of multicarrier CDMA," *IEEE Comm. Mag.*, vol. 94, no. 12, pp. 126–133, Dec. 1997.

[105] S. Verdu, *MultiUser Detection*. Cambridge, NY: Cambridge University Press, 1998.

[106] T. S. Rappaport, *Wireless Communications-Principles and Practice*. Upper Saddle River, N.J., London: Prentice Hall PTR, 2002.

[107] W. H. Steel, *Interferometry*, 1st ed. Cambridge, NY: Cambridge University Press, 1967.

[108] D. A. Wiegandt and C. R. Nassar, "High-throughput, high-performance OFDM via pseudo-orthogonal carrier interferometry coding," *Proc. IEEE PIRMC 2001*, vol. 2, pp. G–98–G–102, Sept. 2001.

[109] B. Natarajan, C. R. Nassar, and S. Shattil, "Throughput enhancement in TDMA through carrier interferometry pulse shaping," *IEEE VTS-Fall VTC 2000 conferance*, vol. 4, pp. 1799–1803, Sept. 2000.

[110] S. L. Hijazi, C. R. Nassar, and Z. Wu, "Spectral sharing in DS-CDMA systems: A multi-carrier approach," *IEEE GLOBECOM2003*, 2003.

[111] M. Michelini, S. L. Hijazi, C. R. Nassar, and Z. Wu, "Spectral sharing across 2G/3G systems," *IEEE VTC fall 2003*, 2003.

[112] L. Harte, *CDMA IS-95 for Cellular and PCS Applications.* New York, NY: McGraw-Hill, 1999.

[113] Z. Wu and C. R. Nassar, "Novel orthogonal codes for DS-CDMA with improved cross-correlation characteristics in multipath fading channels," *Proc. of IEEE WPMC2002, Honolulu, HW*, vol. 3, pp. 1128–1132, Oct. 2002.

[114] H. Holma and A. Toskala, *WCDMA for UMTS: Radio Access for Third Generation Mobile Communications*, 2ed ed. Hoboken, NJ: John Wiley & Sons, 2002.

[115] I. U. &. I. P. P. Wireless Valley Communications, "available on line at: http://www.wirelessvalley.com/products/smrcim/smrcim.asp," 2003.

[116] H. J. Bessai, *MIMO Signals and Systems.* Springer-Verlag New York, LLC, Jan 2005.

[117] Z. Yuanjin, "A novel chnnel estimation and tracking methods for wirless ofdm systems based on pilots and kalman filtering," *IEEE Transactions on Consumer Electronics*, vol. 49, pp. 275–283, May 2003.

[118] G. Zhang, G. Bi, and L. Zhang, "Blind multiuser detection for asynchronous mc-cdma systems without channel estimation," *IEEE Transactions on Vehicular Technology*, vol. 53, pp. 1001 – 1013, 2004.